Development of chitosan-based nanocomposite enriched with essential oil as antifungal coating for fresh fruit application

アタ, アディタヤ, ワルダナ

https://hdl.handle.net/2324/5068267

Development of chitosan-based nanocomposite enriched with essential oil as antifungal coating for fresh fruit application

Ata Aditya Wardana

2022

Development of chitosan-based nanocomposite enriched with essential oil as antifungal coating for fresh fruit application

by

Ata Aditya Wardana

A dissertation submitted to the Laboratory of Postharvest Science in fulfillment of the requirements for the degree of

DOCTOR OF PHILOSOPHY

Graduate School of Bioresource and Bioenvironmental Sciences

Kyushu University

Japan

June 2022

Acknowledgements

I would like to express the sincerest gratitude for Bina Nusantara University for always supporting me to find and start this PhD journey.

I would like to thank all faculty members and staffs, especially Kanae Iwasaki San and Masami Morita San for their kindness, patience, and support during my study.

These acknowledgements would not complete without mentioning to all my friends from the University for their support and help throughout my research project and particularly to Laras Putri Wigati, Dr. Eng. Wahyu Ramadhan, Dr. Eng. Adroit T. N Fajar, Dr. Passakorn Kingwascharapong, Arisa Koga who taught me many things about analytical instruments.

Lastly, the scholarship from JICA, is also acknowledged. This of my highest education degree may not happen without by this scholarship schemes, Innovative Asia Program.

Ata Aditya Wardana

Fukuoka, August 2022

ABSTRACT

Edible packaging (coatings and films) has been used to improve the shelf life of fresh fruit products. The preparation process for edible packaging depends on the properties of the ingredients and the application end use. The objective of this study were to 1) develop antifungal nanocomposite coating formulated from Chi, Indonesia-origined EO, and nanoparticles; 2) characterize the functional properties of the coating film. This was done by optimizing the raw material dosage selection, and blending sequence.

In the first work, the properties of an antifungal coating film made from chitosan (Chi) combined with zinc oxide nanoparticles (ZNPs) and Indonesian sandalwood essential oil (SEO) were investigated. Incorporation of 0.5% SEO or 0.025% ZNPs plus 0.5% SEO into 0.8% CH coating solution showed outstanding effects on the inhibition of both mycelium growth and spore germination of *Penicillium italicum*. The antifungal mechanism was explained by measuring the loss of membrane integrity of spores. The antifungal effectiveness was confirmed in vivo by carrying out tests on tangerine fruit. The biocompatibility of these coatings was analyzed using Fourier transform infrared spectroscopy, scanning electron microscopy, atomic force microscopy, and fluorescence microscopy. Significant increases in pH, appearance viscosity, and transparency and a decrease in light transmittance were found with 0.8% Chi plus 0.025% ZNPs and 0.5% SEO compared with the control. Chi films incorporating SEO and ZNPs can be used as an edible film and coating to reduce chemical use.

Further work, a novel formulation of composite coating comprising 0.8% chitosan (Chi) incorporating 0.025% CuO nanoparticles (CuO) and 0.5% Indonesian cedarwood essential oil

(CEO) was fabricated by casting method. FTIR, CLSM, and SEM analyses were employed to characterize the biocompatibility of each formulation. Additionally, the physico-chemically properties of the composite coatings were characterized. The colour ($L*$), light transmission, zeta potential, and roughness of Chi were significantly ($P < 0.05$) altered negatively by the presence of CuO or CEO; the colour ($a*$, $b*$, and ΔE), apparent viscosity, and transparency also changed positively as a consequence of CuO and CEO incorporation. The antifungal features of a pure Chi coating against *Penicillium italicum* and *Penicillium digitatum* were improved synergistically by CuO and CEO, confirmed by *in vitro* and *in vivo* assays. Composite coatings obtained in this work may have potential applications for active primary food packaging, particularly for fresh postharvest commodities.

Lastly, A novel composite edible coating film was developed from 0.8% chitosan (Chi) and 0.5% sandalwood oil (SEO). Cellulose nanofibers (CNFs) were used as a stabilizer agent of oil-in-water Pickering emulsion. We found four typical groups of CNF level-dependent emulsion stabilization, including (1) unstable emulsion in the absence of CNFs; (2) unstable emulsion (0.006–0.21% CNFs); (3) stable emulsion (0.24–0.31% CNFs); and (4) regular emulsion with the addition of surfactant. Confocal laser scanning microscopy was performed to reveal the characteristics of droplet diameter and morphology. Antifungal tests against *Botrytis cinerea* and *Penicillium digitatum*, between emulsion coating stabilized with CNFs (Chi/SEOpick) and Chi or Chi/SEO was tested. The effective concentration of CNFs (0.24%) may improve the performance of Chi coating and maintain Chi/SEO antifungal activity synergistically confirmed with a series of assays (in vitro, in vivo, and membrane integrity changes). The incorporation of CNFs contributed to improve the functional properties of CS and SEO-loaded Chi including light transmission at UV and visible light wavelengths and tensile strength. AFM and SEM were

employed to characterize the biocompatibility of each coating film formulation. Emulsion-CNF stabilized coating may have potential applications for active coating for fresh fruit commodities.

CONTENTS

LIST OF FIGURES

LIST OF TABLES

CHAPTER 1

INTRODUCTION

1.1. Background

Quality has been considered as the most essential parameters in the selection of fresh fruit and vegetable produce. However, perishability of these commodities is a major challenge in the food industry because of their high moisture content (75–95%) allowing to rapid deterioration and undesirable appearance (Otoni et al., 2017). The consequent cost incurred due to injury and damage during marketing is believed higher than during the production phase. Fungal decay is the most extensive cause in a wide range, about 30%, of fruit loss during postharvest handling (Okawa, 2015). Hence, the development of strategies to control fungal decay on fruit during storage and distribution is essential to achieve reasonable shelf life.

Edible coating and film have emerged as a potential alternative as a safe active packaging against fungal growth on fruits and vegetables. Food coating and film could delay food product deterioration by presenting external protective thin layer and barrier from adverse environmental exposure. This type of layer are fabricated mainly from any or a combination biopolymers including polysaccharides (carbohydrates and gums), proteins, and lipids, and from food-grade

additives (Nesic et al., 2017). Edible coatings and film are required to have acceptable organoleptic and functional characteristics for the particular food involved (Saha et al., 2017).

Chitosan (Chi)-based coatings or films have been gaining intensive research attention due to its biocompatibility and antimicrobial performance (Zeng et al., 2010; Panebianco et al., 2014; Shao et al., 2015). Chi consists of linear cationic D-glucosamine and N-acetyl-D-glucosamine, which is commonly derived from crustacean exoskeletons. Several studies have been done to investigate the potential of chitosan coatings for maintaining the quality from microbial decay on strawberry (Romanazzi et al., 2013), mango (Khalil et al., 2021), pineapple (Basumatary et al., 2021), and citrus fruit (El Guilli et al., 2016). Despite the benefits have been offered, the use of pure chitosan has been documented to be relatively unsatisfactory particularly for antifungal feature (Kong et al., 2010).

A promising strategy to increase chitosan-based functional properties is the incorporation of essential oil. Previous works revealed more effective antimicrobial action when Chi matrix was loaded with one of various natural oils including tea tree (Cháfer et al., 2012), lemongrass or cloves (Shao et al., 2015), and *Mentha* essential oil (EO) (Braga et al., 2019). Among the essential oils reported as having inhibitory performances against fungi, the use of Indonesia-origined EO has not been documented yet. Papua sandalwood and cedarwood essential oil are some of the possible sources as possessing antifungal activities which are corresponded to their terpenoid compounds (Jeong et al., 2014; Powers et al., 2018). Moreover, these essential oils have been permitted by the United States Food and Drug Administration (FDA) and Flavor and Extract Manufacturers Association (FEMA) for direct addition to food for human consumption (Burdock and Carabin, 2008).

Today, nanotechnology offers an area of opportunity for developing vehicles to transport certain substance for improving functional properties of edible film or coating. The implementation of this emerging technology has included various nanosystems, including polymeric nanoparticles, nanoemulsions and nanocomposites (Zambrano-Zaragoza et al., 2018). There has been increasing interest of the incorporation of organic or inorganic nanoparticles into polymeric matrices to improve antifungal activities of biofilm. Metal oxides have been offering the prospective nano fillers in the development of nanocomposite in the food industry because of their beneficial properties including biocompatibility, UV protection ability, low toxicity and cost, and antimicrobial activity (Reddy et al., 2007; El Shafei and Abou-Okeil, 2011). One of the potential fields in the use of organic nanoparticle is to enhance the stability of the emulsion system, namely Pickering, instead of surfactants. In this regard, nanocellulose has been gaining interest as stabilizer. The most appealing feature of nanocellulose is its anisotropic fiber structure, allowing for stabilization of the oil-water interface at very low loading levels (Lu et al., 2021; Seo et al., 2021). In this work, to maximize coating treatment efficacy, the development of nanocomposite coating film based on combination of chitosan, essential oils, and nanoparticles has been proposed.

1.2. Objectives

Based on above-explained fact, therefore, the objectives of this study were to 1) develop antifungal nanocomposite coating formulated from Chi, Indonesia-origined EO, and nanoparticles; 2) characterize the functional properties of the coating film. The finding are expected that it may facilitate the development of food-grade nanocomposite coating film suitable for fresh fruit applications.

1.3. Thesis layout

- Chapter 1 presents the background, objectives, thesis layout, and list of publication and conferences.

- Chapter 2 exhibits the antifungal effect against *Penicillium italicum* and characterization of fruit coating from chitosan/ZnO nanoparticle/Indonesian sandalwood essential oil composites.

- Chapter 3 demonstrates the CuO nanoparticles/Indonesian cedarwood essential oil-loaded chitosan coating film: Characterization and antifungal improvement against *Penicillium* spp.

- Chapter 4 focuses on the antifungal features and properties of chitosan/sandalwood oil Pickering emulsion coating stabilized by appropriate cellulose nanofiber dosage for fresh fruit application.

- Chapter 5 summarizes the contents of all chapters presented in this this paper and presents an outlook.

1.4. Publications and conferences

Peer-reviewed journal publication:

- Wardana, A.A., Kingwascharapong, P., Wigati, L.P., Tanaka, F. and Tanaka, F. 2021. The antifungal effect against *Penicillium italicum* and characterization of fruit coating from chitosan/ZnO nanoparticle/Indonesian sandalwood essential oil composites. *Food Packaging and Shelf Life,* 32: 100849.

- Wardana, A.A., Kingwascharapong, P., Tanaka, F. and Tanaka, F. 2021. CuO nanoparticles/Indonesian cedarwood essential oil-loaded chitosan coating film: characterisation and antifungal improvement against Penicillium spp. *International Journal of Food Science and Technology,* 56 (9): 4224-4238.

- Wardana, A.A., Koga, A., Tanaka, F. and Tanaka, F. 2021. Antifungal features and properties of chitosan/sandalwood oil Pickering emulsion coating stabilized by appropriate cellulose nanofiber dosage for fresh fruit application. *Scientific Reports,* 11:18412.

Conferences publication:

- Wardana, A.A., Tanaka, F., and Tanaka. 2020. Surface microstructure of nanocomposite from chitosan loaded with ZnO nanoparticle by atomic force microscopy. *Key Engineering Materials,* 862: 83-87.

- Wardana, A.A., Tanaka, F., and Tanaka. 2021. Inhibition of *Botrytis cinerea* by alginate/cajuput essential oil and the composite's surface properties as potential antifungal coating. *Materials Today: Proceedings*, 45: 5263–5268.

- Wardana, A.A., Van, T.T., Mohammadi, L., Tanaka, F., and Tanaka. 2022. Combination of chitosan and peppermint essential oil as potential active coating Against *Penicillium digitatum* and *Botrytis cinerea*. *Macromolecular Symposia*, 401: 2100315.

1.5.   References

Basumatary, I. B., Mukherjee, A., Katiyar, V., Kumar, S., & Dutta, J. (2021). Chitosan-based antimicrobial coating for improving postharvest shelf life of pineapple. *Coatings*, *11*(11), 1–12.

Braga, P., Alencar, G., Alves, S., Fechine, J., Anderson, W., Paz, M., Câmara, S., Leite, E., & Souza, D. (2019). Application of coatings formed by chitosan and *Mentha* essential oils to control anthracnose caused by *Colletotrichum gloesporioides* and *C . brevisporum* in papaya (*Carica papaya* L .) fruit. *International Journal of Biological Macromolecules*, *139*, 631–639.

Burdock, G. A., & Carabin, I. G. (2008). Safety assessment of sandalwood oil (*Santalum album* L.). *Food and Chemical Toxicology*, *46*(2), 421–432.

Cháfer, M., Sánchez-González, L., González-Martínez, C., & Chiralt, A. (2012). Fungal decay and shelf life of oranges coated with chitosan and bergamot, thyme, and tea tree essential oils. *Journal of Food Science*, *77*(8), 182–187.

El Guilli, M., Hamza, A., Clément, C., Ibriz, M., & Barka, E. A. (2016). Effectiveness of postharvest treatment with chitosan to control citrus green mold. *Agriculture (Switzerland)*, *6*(2).

El.shafei, A., & Abou-Okeil, A. (2011). ZnO/carboxymethyl chitosan bionano-composite to impart antibacterial and UV protection for cotton fabric. *Carbohydrate Polymers*, *83*(2), 920–925.

Jeong, H.-U., Kwon, S.-S., Kong, T. Y., Kim, J. H., & Lee, H. S. (2014). Inhibitory Effects of Cedrol, β-Cedrene, and Thujopsene on Cytochrome P450 Enzyme Activities in Human

Liver Microsomes. *Journal of Toxicology and Environmental Health, Part A*, *77*(22–24), 1522–1532.

Khalil, H. A., Abdelkader, M. F. M., Lo'ay, A. A., El-Ansary, D. O., Shaaban, F. K. M., Osman, S. O., Shenawy, I. E., Osman, H. E. H., Limam, S. A., Abdein, M. A., & Abdelgawad, Z. A. (2022). The combined effect of hot water treatment and chitosan coating on mango (*Mangifera indica* L. cv. Kent) fruits to control postharvest deterioration and increase fruit quality. *Coatings*, *12*(1).

Kong, M., Chen, X. G., Xing, K., & Park, H. J. (2010). Antimicrobial properties of chitosan and mode of action: A state of the art review. *International Journal of Food Microbiology*, *144*(1), 51–63.

Lu, Y., Li, J., Ge, L., Xie, W., & Wu, D. (2021). Pickering emulsion stabilized with fibrous nanocelluloses: Insight into fiber flexibility-emulsifying capacity relations. *Carbohydrate Polymers*, *255*.

Nesic, A. R., & Seslija, S. I. (2017). *19 - The influence of nanofillers on physical–chemical properties of polysaccharide-based film intended for food packaging* (A. M. B. T.-F. P. Grumezescu (ed.); pp. 637–697). Academic Press. https://doi.org/https://doi.org/10.1016/B978-0-12-804302-8.00019-4

Okawa, K. (2015). Market and trade impacts of food loss and waste reduction, OECD food, agriculture and fisheries papers, no. 75, OECD Publishing, Paris.

Otoni, C. G., Avena-bustillos, R. J., Azeredo, H. M. C., Lorevice, M. V, Mchugh, T. H., & Mattoso, L. H. C. (2017). Recent advances on edible films based on fruits and vegetables - a review. *Comprehensive Reviews in Food Science and Food Safety,16*, 1151–1169.

Panebianco, S., Vitale, A., Platania, C., Restuccia, C., Polizzi, G., & Cirvilleri, G. (2014). Postharvest efficacy of resistance inducers for the control of green mold on important Sicilian citrus varieties. *Journal of Plant Diseases and Protection*, *121*(4), 177–183.

Powers, C. N., Osier, J. L., Mcfeeters, R. L., Brazell, C. B., Olsen, E. L., Moriarity, D. M., Satyal, P., & Setzer, W. N. (2018). Antifungal and cytotoxic activities of sixty commercially - available essential oils. *Molecules, 23*, 1-13.

Reddy, K. M., Feris, K., Bell, J., Wingett, D. G., Hanley, C., & Punnoose, A. (2007). Selective toxicity of zinc oxide nanoparticles to prokaryotic and eukaryotic systems. *Applied Physics Letters*, *90*(21), 10–13.

Romanazzi, G., Feliziani, E., Santini, M., & Landi, L. (2013). Effectiveness of postharvest treatment with chitosan and other resistance inducers in the control of storage decay of strawberry. *Postharvest Biology and Technology*, *75*, 24–27.

Saha, A., Tyagi, S., Gupta, R. K., & Tyagi, Y. K. (2017). Natural gums of plant origin as edible coatings for food industry applications. *Critical Reviews in Biotechnology, 37*(8), 959–973.

Seo, S.-M., Lee, J.-W., Shin, J., Tak, J.-H., Hyun, J., & Park, I.-K. (2021). Development of cellulose nanocrystal-stabilized Pickering emulsions of massoia and nutmeg essential oils for the control of Aedes albopictus. *Scientific Reports*, *11*(1), 1–12.

Shao, X., Cao, B., Xu, F., Xie, S., Yu, D., & Wang, H. (2015). Effect of postharvest application of chitosan combined with clove oil against citrus green mold. *Postharvest Biology and Technology*, *99*, 37–43.

Zambrano-Zaragoza, M. L., González-Reza, R., Mendoza-Muñoz, N., Miranda-Linares, V., Bernal-Couoh, T. F., Mendoza-Elvira, S., & Quintanar-Guerrero, D. (2018).

Nanosystems in edible coatings: A novel strategy for food preservation. *International Journal of Molecular Sciences*, *19*(3).

Zeng, K., Deng, Y., Ming, J., & Deng, L. (2010). Induction of disease resistance and ROS metabolism in navel oranges by chitosan. *Scientia Horticulturae*, *126*(2), 223–228.

CHAPTER 2

The antifungal effect against *Penicillium italicum* and characterization of fruit coating from chitosan/ZnO nanoparticle/Indonesian sandalwood essential oil composites

2.1. Introduction

The development of strategies to control fungal decay caused by *Penicillium italicum* on fruit is essential to reduce food loss. Synthetic fungicides sprayed on the fruit surface have been used widely to control postharvest disease. However, excessive use of these agents is associated with increased resistance in harmful fungi (de Oliveira et al., 2014). Moreover, due to increased health and environmental awareness, the development of alternative treatments utilizing eco-friendly and generally recognized as safe (GRAS) materials is necessary. Edible coatings have emerged as a potential alternative as antifungal active packaging.

Chitosan (Chi)-based coatings have been considered as a promising edible matrix and developed to improve antimicrobial performance for fruit treatment (Zeng et al., 2010; Panebianco et al., 2014; Shao et al., 2015). Chi is composed of linear cationic D-glucosamine and N-acetyl-D-glucosamine, which is commonly extracted from crustacean exoskeletons. This unique positively charged polysaccharide can interact naturally with negatively charges on microbial cell membranes. Despite the benefits that have been demonstrated using Chi films and coatings, the use of pure Chi has been found to be relatively unsatisfactory due to its limited antifungal action (Kong et al., 2010).

Previous studies found more effective antifungal activity when an essential oil (EO) was entrapped into Chi. *P. italicum* CECT 2294 growth on oranges (cv. Navel Powell) was effectively reduced by 50% using a Chi coating containing tea tree EO compared with uncoated oranges (Cháfer et al., 2012). In addition, EO from lemongrass or cloves incorporated in Chi showed synergistic effects against the phytopathogenic fungi *P. digitatum* and *P. italicum* infected artificially onto citrus fruits (Shao et al., 2015). Even though several studies of Chi-EO

have been carried out and found positive effects, investigations of Chi incorporated with other EOs are ongoing.

Indonesian sandalwood essential oil (SEO), obtained from *Santalum album* plants found in the Papua area, is a potential compound to improve the antifungal activity of Chi-based coatings. α- and β-santalol are the principal components of SEO that inhibit fungal growth. Reports have demonstrated the antifungal activities of SEO against *Trichophyton mentagrophytes* (Inouye et al., 2006), *Microsporum canis* (Nardoni et al., 2015), and *Trichophyton rubrum* (Kim et al., 2017). In the context of safety, SEO has been approved for food application by the United States Food and Drug Administration (FDA), Flavor and Extract Manufacturers Association (FEMA), and the Council of Europe (CoE) (Burdock and Carabin, 2008). This volatile oil is commonly utilized as a food flavoring and adjuvant agent.

Recently, the utilization of nanoparticles has been developed to improve nanocomposite performance. ZnO nanoparticles (ZNPs) have received great attention as nano fillers in the food industry due to its GRAS status. In the field of food processing and agriculture, ZNPs have been used because of their beneficial properties including biocompatibility, low toxicity and antimicrobial activity (Reddy et al., 2007). ZNPs also show some advantages compared with other metal oxides, including lower cost, lack of color, and UV protection ability (El Shafei and Abou-Okeil, 2011). A previous study found new possibilities for ZnO against *Botrytis cinerea* and *Penicillium expansum* (He et al., 2011). However, antifungal additive approaches with Chi/ZNP/SEO formulations have not been documented.

In this study, the application of edible coatings comprised of Chi/ZNP/SEO composites was investigated against *P. italicum*. *In vitro* and *in vivo* tests on tangerine fruit were performed. Harvested tangerines are easily affected by fungal decay, such as green mold (*P. digitatum*) and

blue mold (*P. italicum)*, during storage due to their rich nutritional content and tender peel (Chen et al., 2016). In addition, to increase understanding of the coating properties, the physico-chemical characteristics of the composites were also studied.

2.2. Materials and methods

2.2.1. Coating and film preparation

Coating solutions composed of Chi solution (Chis) were made by gelatinizing 1% (w/v) Chi flakes with a deacetylation degree of 80% (FUJIFILM Wako Pure Chemical Corporation, Japan) in 1% (v/v) acetic acid (FUJIFILM Wako Pure Chemical Corporation, Japan) followed by adding 2 N NaOH FUJIFILM Wako Pure Chemical Corporation, Japan) solution until pH 5.8. A 0.25% (w/v) ZnO powder, with particle size less than 50 nm (Sigma Aldrich, USA) was dispersed in distilled water using an ultrasonicator (Dual Frequency, ASU-10D Series) at a temperature 27 ± 2°C and frequency 43 kHz for 60 min to produce ZnO solution (i.e. ZNPs). A 5% (v/v) Papua SEO (Aromindo CV, Indonesia) with the two main contents, α-santalol (19.36%) and β-santalol (16.48%), was emulsified by adding 2.5% (w/v) Tween 80 (FUJIFILM Wako Pure Chemical Corporation, Japan) in distilled water and mixed using a homogenizer (T 25 digital ULTRA-TURRAX® - IKA, Germany) at 20,000 rpm for 3 min to produce SEO solution (i.e. SEOs). Chi, Chi/ZNP, CH/SEO, and Chi/ZNP/SEO solutions were prepared by adding 20% (v/v) distilled water, 10% (v/v) distilled water + 10% (v/v) ZNPs, 10% (v/v) distilled water + 10% (v/v) SEOs, and 10% ZNPs + 10% SEOs, respectively, in 80% (v/v) Chis and blended using homogenizer at 20,000 rpm for 3 min then degassed in a vacuum oven (ADP300, Yamato Scientific Co, Ltd, Japan). The films were cast by pouring 5 mL of coating

solution onto a plate (50 mm diameter), dehydrated in an oven at 40°C for 20 h, peeled, and stored at 25°C and 50% relative humidity (RH) until examination.

2.2.2. Coating material characterization

ZNP particle size and morphology analyses were performed using an atomic force microscopy (AFM) method (Hitachi 5200S, Japan) equipped with micro-cantilever type SI-DF20. ZNP powder (0.1%) was first dispersed in acetone and ultrasonicated for 60 min before deposited and dried on mica. The scan area of $10 \, \mu$m $\times 10 \, \mu$m were set at frequency of 0.7–0.84 Hz. Furthermore, particle size distribution and polydispersity index of ZNP were carried out using a dynamic light scattering method with a Zetasizer (Nano, Malvern Instruments, UK). For fourier transform infrared (FTIR) spectroscopy analysis, the potassium bromide (KBr) pellet method was carried out using an FTIR spectrometer (Jasco, FTIR-620, Japan). ZNP and SEO pellets were prepared by attaching them to plates of cut KBr crystals followed by pressured pulverizing. The pellets were placed in a sample holder and measured using spectra transmittance mode at wave numbers of 375–4000 cm^{-1}.

2.2.3. Antifungal assays

The antifungal effectiveness of each material was evaluated using spore germination and germ tube elongation. *P. italicum* Wehmer obtained from the National Institute of Technology and Evaluation, Biological Resource center, Tokyo, Japan, was first cultured on potato dextrose agar (PDA) (Nissui Pharmaceutical Co., Ltd., Japan) for 7 days before harvesting. Then, 1 mL of spore solution with 2×10^5 spores/mL was mixed with 1 mL of treatment solution, and 1 mL of potato dextrose broth (Difco™, USA) and incubated on a shaker (100 rpm) at 25°C prior to analysis. After incubation for 24 h, spore germination was inspected using confocal laser

scanning microscopy (CLSM) (Olympus IX71, Japan) with a 50× objective lens. Moreover, germ tube elongation was measured with the aid of *ImageJ* software.

The additive effect of materials against mycelial growth of *P. italicum* was determined in solid medium. Culture media (7.5 mL) were prepared by mixing each coating solution and PDA medium with ratio of 1:2 and immediately poured into sterilized petri dishes (50 mm in diameter). A 8-mm-agar disc of the mycelium of fungi, obtained from 5-day-old cultures, was deposited in the center of each petri dish, incubated at 25°C for 6 days. Afterwards, the diameter of the colony zone was measured using *ImageJ* software. The result was also expressed as a percentage inhibition (*PI*) following this equation:

$$PI \% = \frac{A-B}{A} x \ 100$$

where *A* is the maximum value of the mycelium diameter (control plate) and *B* is the mycelium diameter obtained from each treatment. All of the samples were analyzed in triplicate.

Membrane permeability changes of *P. italicum* were investigated by observing the uptake of propidium iodide (Sigma Aldrich, USA). Briefly, spore solution of the control and coating treated samples after 4 h incubation were stained with 50 (mg L^{-1}) propidium iodide and incubated for 15 min. Then, the samples were examined using a CLSM with excitation and emission wavelengths of 543 nm and 585 nm.

2.2.4. Application on fruit

The effects of coating treatments on physicochemical properties and lesion diameter on tangerines were determined using a previously reported method with slight modifications (Chen et al., 2020). The selected tangerines purchased from the Japan Agricultural Cooperatives group in Fukuoka, Japan, were washed with 1% sodium hypochlorite for 10 min and air dried before

coating treatment by immersing method for ± 5 s. Uncoated (control) and coated fruits were then packed with perforated polyethylene terephthalate and stored at 25°C and 80% RH. Total soluble solid (TSS) measurement, fruits were sliced and pressed with a hand press. The resulting tangerine juice was dropped and read by busing a digital refractometer (PR-101α, Atago Co., Ltd., Japan). The percentage of fruit weight loss was calculated by comparing weight change of each uncoated (day 0) and coated tangerine during storage time. The fruit color was measured referring to the CIELab (*Commision international de l'éclairage*, *L**, *a**, and *b**) color method to obtain *L** (lightness), *a** (green to red), and *b** values by using a color reader (Konica Minolta CR-20, Japan). The color was measured at 4 points on each fruit surface. For antifungal *in vivo* analysis, each fruit was pierced (2 mm deep) using a sterile tip on the equatorial side. About 2.5 µL of spore solution (2×10^6 spores/mL) was injected in each wound. After air drying for 5 h, the whole surfaces of tangerines were immersed in coating solution and dried. The lesion diameters from triplicate analyses of fungal decay were recorded in millimeters with the aid of *ImageJ* software.

2.2.5. Apparent viscosity

The apparent viscosity of the coating solution was measured using a rotational viscometer (Brookfield DV2T, USA) with three replications. About 90 mL of solution was placed into the sample cell. A rotor speed of 50 rpm, spindle LV-01 (61), temperature of 18 ± 1°C were employed for 30 s per sample.

2.2.6. *Zeta potential and pH*

Zeta potential analysis was carried out using a Zetasizer with five replications. The pH measurement was performed using a manual pH meter (Horiba LAQUAtwin, Japan) with three replications.

2.2.7. *Oil droplet*

Emulsion droplets of SEO in the coating solution were observed using a CLSM with a 20× objective lens in accordance with the previously described method (Kingwascharapong et al., 2020). Samples (1 mL) were mixed with 100 μL of Nile red (FUJIFILM Wako Pure Chemical Corporation, Japan) solution (1 mg/mL in ethanol) to dye the oil phase. After homogenization, 6 μL of dyed samples were dropped gently on to a microscope glass slide (Toshinriko, Japan) and covered with a glass coverslip with the thickness $\approx$ 170 μm (Matsunami, Japan). Monodisperse emulsions were scanned using x / y series.

2.2.8. *Color*

A film specimen was placed on a white plate and measured using a color reader (Konica Minolta CR-20, Japan). A measurement of five different spots per sample was performed followed by ΔE (color difference) calculation referring to the following equation.

$$\Delta E = \sqrt{(L_0 * -L *)^2 + (a_0 * -a *)^2 + (b_0 * -b *)^2}$$

Where the letters followed by a subscript are the standard white plate value ($L_0* = 94.8$, $a* = -0.1$, and $b_0* = 4.1$), and letters without a subscript are the values of the films.

2.2.9. Light transmission and transparency

Referring to the modified method from Tongnuanchan et al. (2012), the light transmission of the samples was determined using a UV-Vis spectrophotometer (Jasco, V-530, Japan) at wavelength ranges of 300–800 nm. The transparency of the film specimens was determined using its fractional transmittance at 600 nm in accordance with Bonilla and Sobral (2016). Each thin film was cut into a rectangular shape and attached on the cell side. Three replications were used for each film specimen using this equation:

$$\text{Transparency} = \frac{(-log\ T600)}{x}$$

Where $T600$ represents the fractional value of transmittance at 600 nm and x is the film thickness (mm). The lower transparency, the higher opacity of the sample.

2.2.10. FTIR

The transmittance of thin coating films was measured using the attenuated total reflectance ATR method using an FTIR spectrometer (Jasco, FTIR-620, Japan). The thin film was attached into sample holder and the spectrum was run at wave numbers of 500–4000 cm^{-1}.

2.2.11. Surface roughness

Each 10 μL of coating sample was deposited on mica and dried in the desiccator at 25°C for 24 h before observation under AFM. The scan area of 5 μm × 5 μm was set at frequency of 0.7–0.84 Hz. Roughness parameters were calculated as root mean square deviation from the mean (Rq) and arithmetical mean deviation from the mean (Ra) following below equations and with the aid of the Nano Navi Application program.

$$Rq = \sqrt{\frac{1}{n} \sum_{i=1}^{n} Zi^2}$$

$$Ra = \frac{1}{n} \sum_{i=1}^{n} |Zi|$$

where Zi was the height deviation of i-th from the mean of heights and n was the number of data points. All of the samples were examined using ten replications.

2.2.12. Cross-section morphology

The thin coating films were previously conditioned in a desiccator (53 ± 1% RH) containing $Mg_2(NO_3)_2$ at 25°C. Prior to visualization, film specimens were fixed on the specimen stub using double-sided adhesive tape and coated in vacuum condition with the aid of osmium coater. Then, microstructure observations of cross-section were carried out using a scanning electron microscopy (SEM) method (SU3500, Hitachi, Japan) at 15 kV.

2.2.13. Statistical analysis

The experimental data were expressed as mean ± SD. The mean comparisons were then analyzed through analysis of variance (ANOVA) at a significance level of P-value < 0.05 according to Duncan's multiple range test (DMRT) with the aid of Statistical Package for Social Science software (SPSS 17.0, SPSS Inc., USA).

2.3. Results and discussion

2.3.1. Coating material characterization

ZNP powder was characterized using AFM, as shown in Fig. 2.1a, to observe the 3D morphologies of ZNPs. ZNP had sharp features and displayed to be slender in shape with the Z axis (height) of 0.25–33.33 nm and the width of 13–177 nm. Small nanoclusters were easily detectable due to agglomerations between individual ZNP occurred in some regions. Furthermore, the particle size distribution, 154.42 ± 0.29 nm and 0.136 ± 0.01 for each diameter

and polydispersity index, was confirmed using a dynamic light scattering technique, as shown in Fig. 2.1b. The value of PDI represented the distribution of uniform monodisperse sample with respect to the particle size of ZNP.

(a)

(b)

(c)
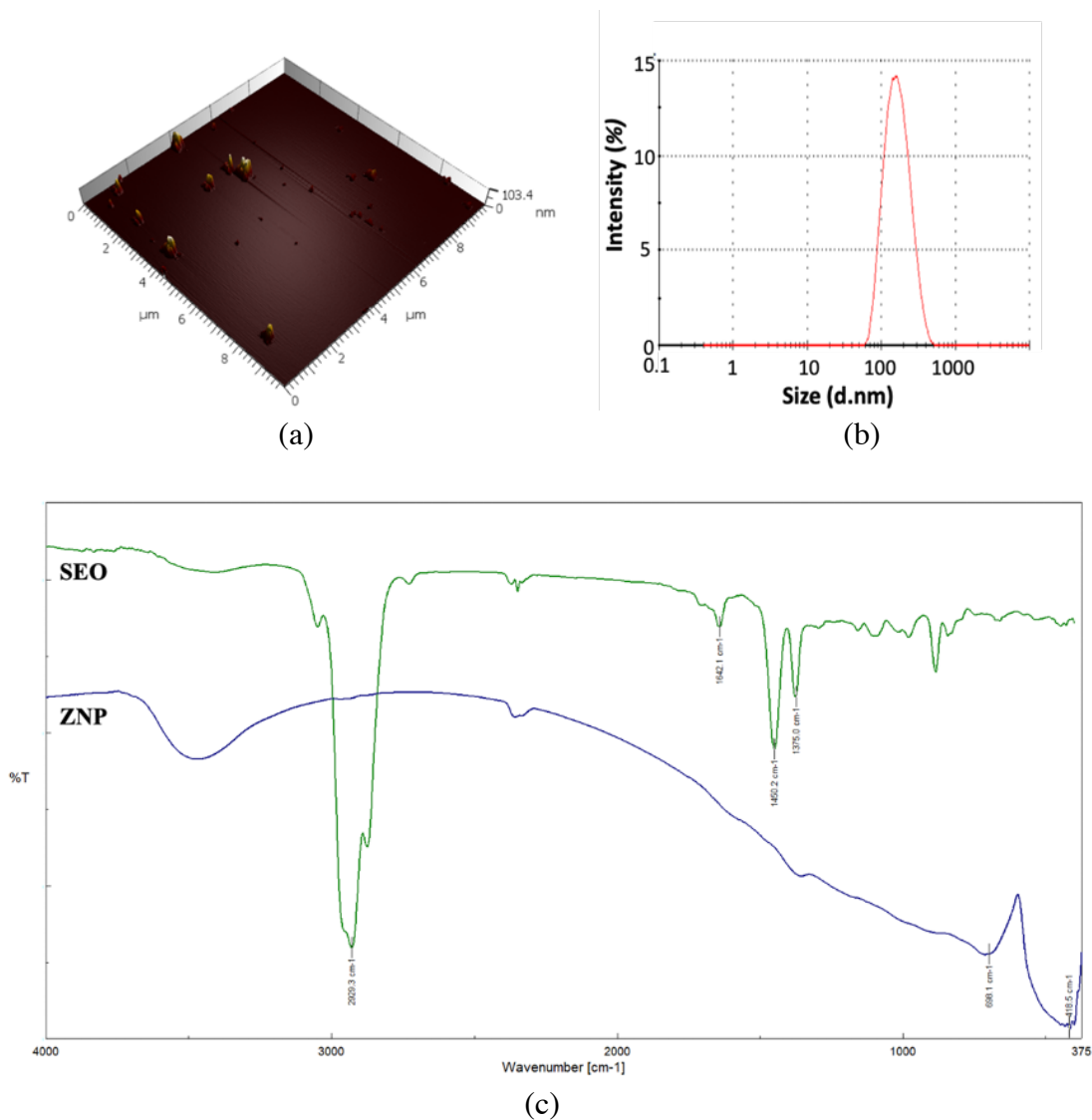
Fig. 2.1. (a) AFM topography image of ZNP, (b) ZNP particle size distribution, and (c) FTIR spectra.

The potassium bromide (KBr) pellet method was employed to measure the infrared spectra of ZNP powder and SEO (Fig. 2.1c). Peaks at 418.5 cm^{-1} and 698.1 cm^{-1} clearly indicated the Zn-O vibration bond. Those peaks showed similar general features with most of the peak

attributes found by Mitra et al. (2012). FTIR spectra of SEO exhibited a characteristic absorption peak, which was in agreement with previous studies (Baker et al., 2014; Worzakowska, 2017; Kala et al., 2020). The presence of absorption band for peaks at 1375 cm^{-1} and 1450.2 cm^{-1} were attributed to the methyl, methylene, and C-H stretch from SEO terpenes. The peak at 1642.1 cm^{-1} and 2923.3 cm^{-1} were respectively due to vibration of the aromatic ring C=C skeleton (aromatic substance) and C-H stretching band of fatty acids.

2.3.2. *Spore germination and germ tube elongation treated with Chi, ZNP, and SEO*

Determination of the optimal dosage was intended to produce an efficient coating formulation while maintaining good performance. The assay was performed in broth media considering a higher accuracy could be confirmed (Negi et al., 2012). Fig. 2.2 depicts that *P. italicum* growth inhibition was concentration level dependent. 0.8% Chi/0.025% ZNPs were found to completely suppress spore germination. Previous work on *P. digitatum* inhibition also found a similar trend that the effectiveness of Chi was highly correlated with its dose (El Guilli et al., 2016). Possible mechanisms were considered to explain Chi antifungal activities including interactions between positively charged Chi molecules and negatively charged fungal cell walls allowing ionic imbalance (Liu et al., 2007; Jayaraj et al., 2009), intracellular interaction of Chi and DNA leading the mRNA inhibition, and protein synthesis disruption (Avadi et al., 2005; Zhang et al., 2011), and the chelating effect of Chi on metals that are essential as nutrients (Torres et al., 2006; Jiang et al., 2012). In agreement with the current study, ZNPs were found to possess antifungal activity against *Penicillium* (Jamdagni et al., 2016). ZNP antimicrobial mechanisms have been documented, including i) intracellular ZNP accumulation, ii) destruction of cell membranes, iii) H_2O_2 generation, and iv) release of Zn^{2+} ions (Kumar et al., 2016;

21

Dananjaya et al., 2018). Additionally, spore germination and germ tube elongation of *P. italicum* were also delayed in the presence of 0.5% SEO. Although the antifungal action of SEO has not been thoroughly documented, the proposed effects might be partly because of fungal cell wall disturbance. Further elucidation that α-and ß-santalol, the antifungal agents in SEO, induced the detrimental effects on fungal cell wall synthesis of essential components including Chi and thereby abnormal morphology, swelling and curling, of terminal hyphae appeared (Kim et al., 2017). Finally, these results were considered in selecting coating formulation of CH 0.8%/ZNPs 0.025%/SEO 0.5%.
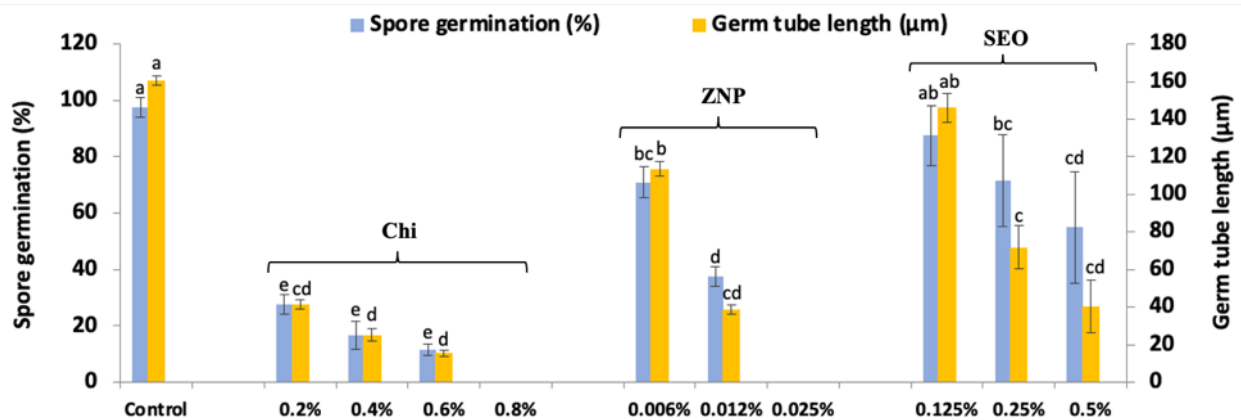
Fig. 2.2. Inhibitory effects of Chi, ZNP, and SEO at various concentrations on spore germination and germ tube elongation of *P. italicum*. Data followed by different letters indicates statistically different by DMRT ($P < 0.05$).

2.3.3. Mycelium growth after treatment with coating solutions

Mycelial growth tests in solid medium have many benefits over other antimicrobial assays including simplicity, inexpensive, and the possibility to test a high number of microorganisms and antimicrobial agents (de Souza et al., 2019). There was a coherent efficacy referring to the results on spore germination and mycelial growth inhibition. Fig. 2.3 shows that the use of combination approach with Chi/ZNP/SEO was found to control the growth of *P. italicum* significantly ($P < 0.05$) compared with the control.
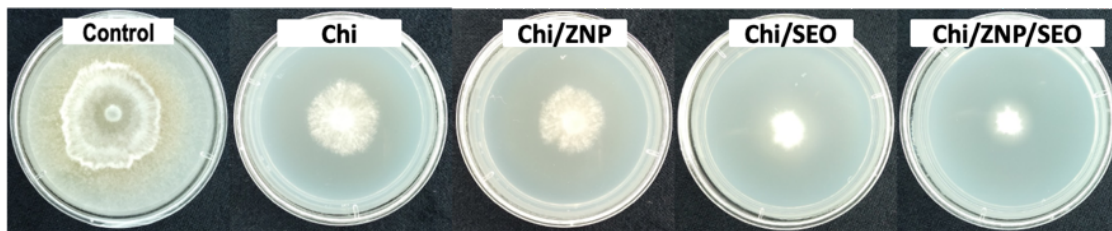
(a)
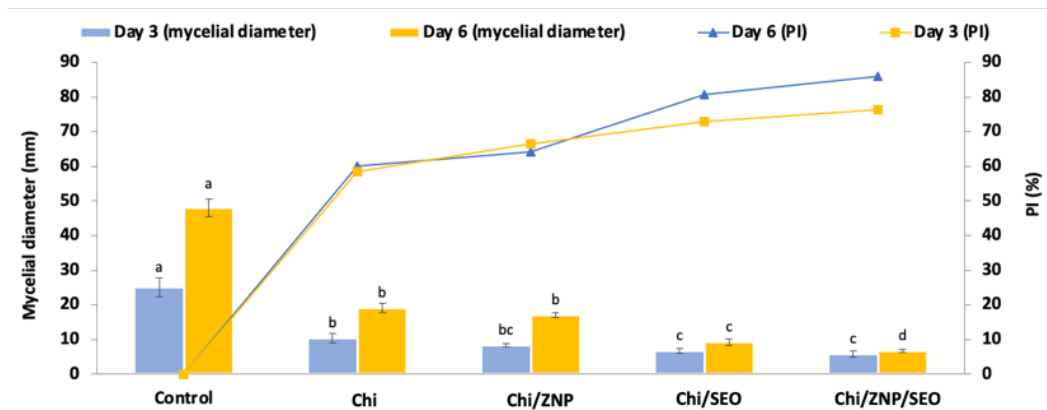
(b)

Fig. 2.3. Coating solution significantly suppressed *P. italicum* mycelial extension. (a) Visual image of mycelium diameter in the end of incubation. (b) Statistical analysis after 3 days and 6 days incubation. Data followed by different letters indicates statistically different by DMRT ($P < 0.05$).

In the end of incubation, mycelial samples treated with Chi/ZNP/SEO demonstrated the greatest inhibition effect on colony diameter extension. Of note, the antifungal activity with the addition SEO into Chi was higher than ZNPs, contrary to the spore germination in the previous results (Fig. 2.2), which was probably due to the penetration of ZNPs into microbial cells. The possibility of nanoparticle-microbial interaction was lower in the solid phase than in the liquid phase (Negi et al., 2012). The distribution of ZNPs into the media might be restrained resulting in lower efficacy.

2.3.4. *Spore germination and membrane integrity of spores treated with coating solution*

Spores germinated well in the absence of treatment, whereas treated spores began to germinate partially, as indicated with a blue arrow (Fig. 2.4a). Fungal spore germination was inhibited significantly in the presence of coating solutions with Chi and Chi/ZNP ($P < 0.05$). Surprisingly, a significantly higher level of inhibition was ($P < 0.05$) shown by Chi/SEO compared with Chi/ZNP coating solutions, as well as Chi, in contrast with previous data (Fig. 2.2). This finding might be ascribed to the release of ZNPs as either metal oxide or zinc ions as a consequence of environmental *pH* (Table 2.1). At this *pH*, the partial dissolution of ZNPs may have occurred (Chanakul et al., 2014). Although the mechanism has not been fully explained, the antimicrobial action of nanoparticles appeared to be more potent than their ions due to the greater uptake efficiency of the particles (Yan et al., 2018). Furthermore, the incorporation of ZNPs and SEO into the CH matrix demonstrated a significant effect ($P < 0.05$) in controlling spore germination (Fig. 2.4d).
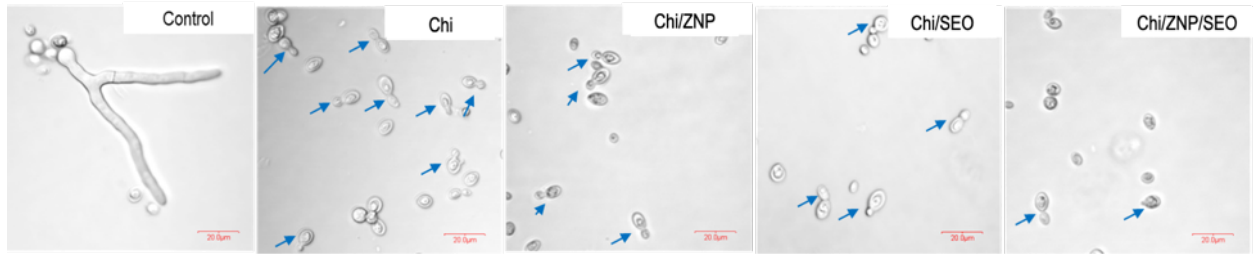
(a)
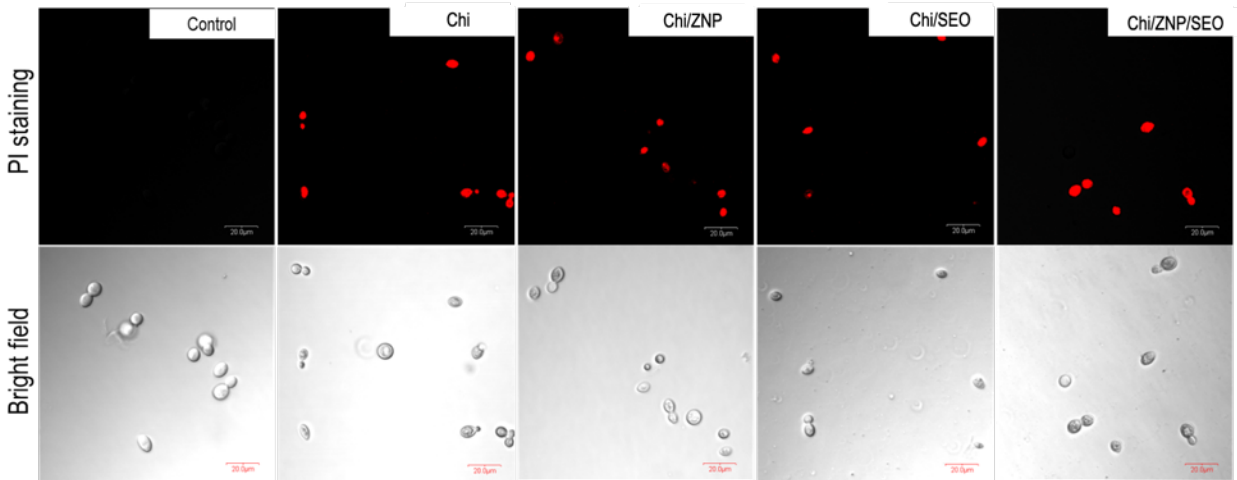
(b)
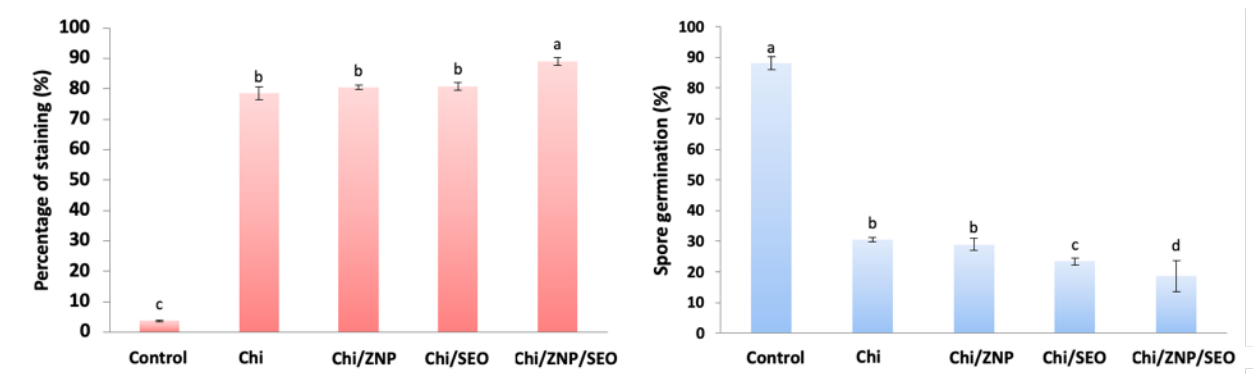
(c)

(d)

Fig. 2.4. Inhibitory effects of coating solutions on spore germination of *P*. *italicum* (a) visually and (d) statistically; and CLSM image representing the cell membrane permeability, (b) visually and (c) statistically. Data followed by different letters indicates statistically different by DMRT ($P < 0.05$).

In order to investigate the immediate effects of treatment, propidium iodide staining was performed to check for the loss of membrane integrity in *P. italicum*. Propidium iodide is a unique fluorescent molecule that is able to bind DNA and exhibits red fluorescence but it is incapable of entering healthy spores due to the membrane barrier (membrane impermeable) (Suzuki et al., 1997). As a result, untreated spores (control) were not stained, as depicted in Fig. 2.4b, whereas treated spores were readily stained. However, there were no significant differences ($P < 0.05$) among those with Chi alone or Chi/ZNP/SEO. The cells spores exposed to Chi/ZNP/SEO showed a significantly increased level of red fluorescence (Fig. 2.4c) in comparison with other coating solution treatments, indicating better antifungal action. This phenomena indicated that the spores with red fluorescence were dead. The data obtained proved that coating treatments interfered with the membrane integrity of spores, which led to metabolic disruption and the death of fungi.

2.3.5. *Antifungal (in vivo) study: efficacy of coating treatment in controlling blue mold on tangerine fruit*

To confirm the antifungal efficacy of the coating solutions, *in vivo* tests on tangerine fruit infected with *P. italicum* were performed. Fig. 2.5a shows the appearance of tangerines inoculated with *P. italicum*, in which the blue mold symptoms and growth increased during storage. The control and coated fruits exhibited similar appearances on storage day 3. On day 5, hyphae appeared on the surface of control fruit, and minor symptoms appeared on Chi and Chi/ZNP samples. Furthermore, mold incidence increased with storage time, and blue mold were clearly observed on control and Chi samples. Although almost no hyphal fragments were found

visually on Chi/ZNP, Chi/SEO, and Chi/ZNP/SEO surfaces, expanding internal lesions appeared on day 7. Likewise, through observing cross-sections of inoculated tangerines, fungal decay showed higher penetration in control fruit than Chi Chi/ZNP, and the growth internal decay of Chi/SEO and Chi/ZNP/SEO were the lowest. It can be assumed that Chi/SEO and Chi/ZNP/SEO had acceptable visual quality during the first 5 days of storage prior to mold deterioration beginning. Statistically, as shown in Fig. 2.5b, the incidence diameter of tangerines coated with Chi (29.21 mm and 35.23 mm at 5 and 7 days, respectively) and Chi/ZNP (27.48 mm and 33.73 mm at 5 and 7 days, respectively) were significantly inhibited ($P < 0.05$) compared with the control (38.67 mm and 42.87 mm at 5 and 7 days, respectively). Moreover, a smaller diameter ($P < 0.05$) was shown in samples coated with Chi/SEO (13.20 mm and 29.37 mm at 5 and 7 days, respectively) and the highest inhibition level ($P < 0.05$) was found in Chi/ZNP/SEO treatment (7.79 mm and 25.1 mm at 5 and 7 days, respectively), suggesting the most effective antifungal effect. Of note, the diameter growth inhibition of blue mold infection at day 5 was higher than at day 7, as shown in Fig. 2.5c. This might be associated with the availability of intrinsic carbon in plant hosts (Ji et al., 2018). At the end of storage, a higher carbon source might be found in coated fruit, while fungi had a higher adaptability to the host environment. Overall, the addition of ZNP and SEO together improved the antifungal activity of Chi, because they act as antimicrobial agents.
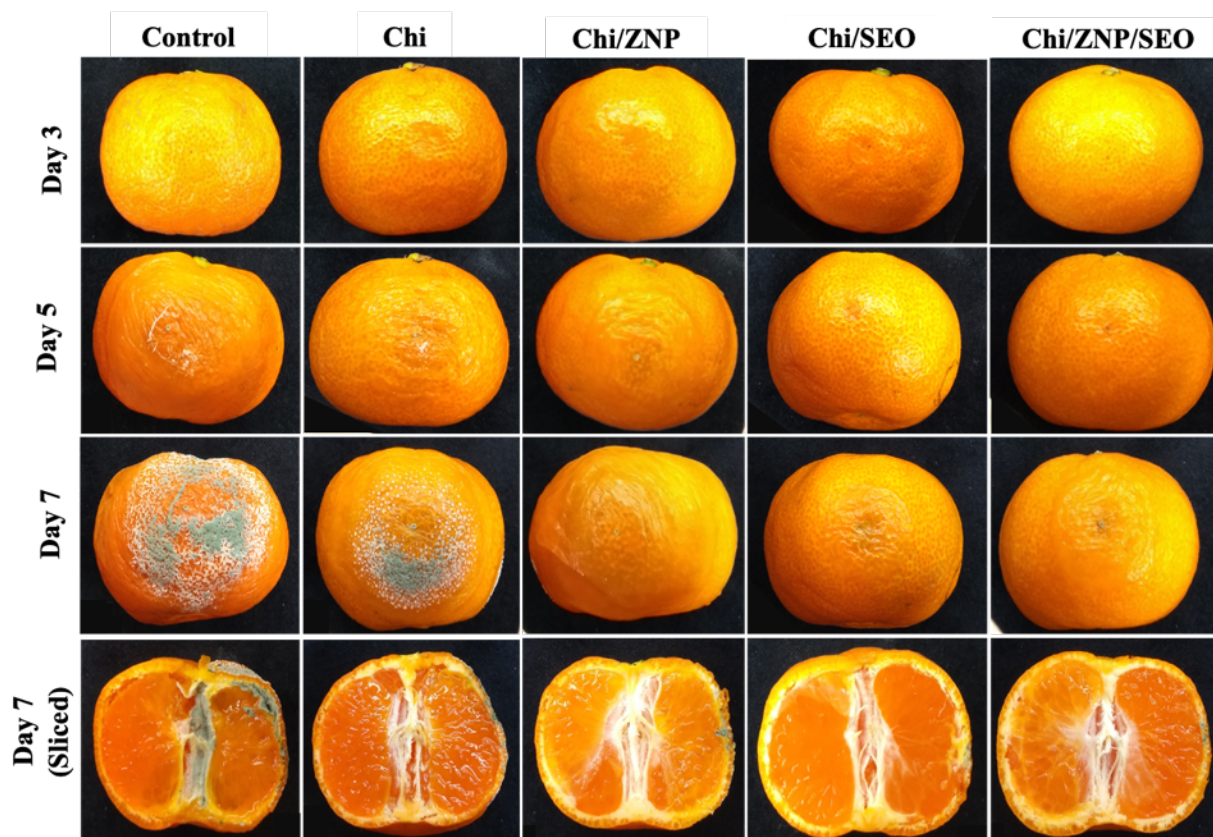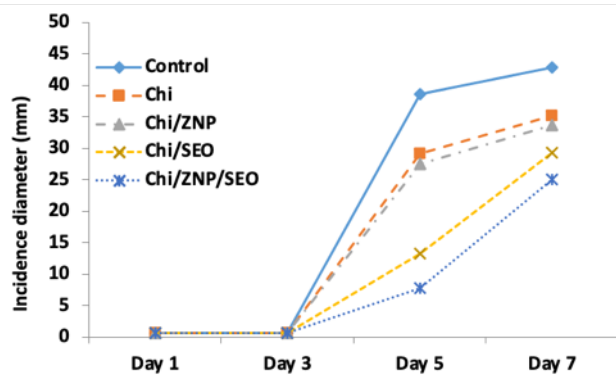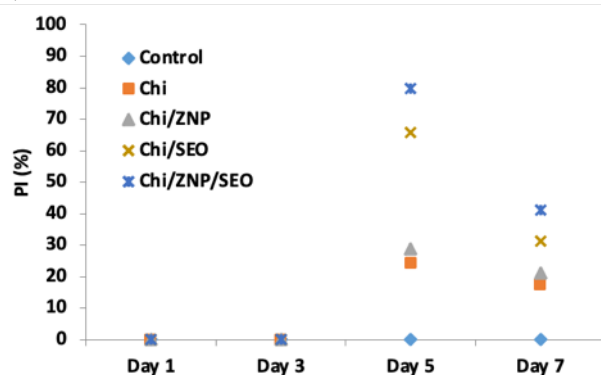
Fig. 2.5. Efficacy of various coating treatment on disease severity caused by *P. italicum* on tangerines. (a) visual appearance of representative sample and (b, c) statistical analysis during storage. Data followed by different letters indicates statistically different by DMRT (*P* < 0.05).

2.3.6. *Effect of coating treatment on physicochemical properties of tangerine fruit*

The characterization of the physicochemical properties was analyzed to indirectly reflect the efficacy of coating treatment in controlling blue mold on tangerine fruit. The TSS of uncoated and coated fruits tended to increase over the storage period, as seen in Fig. 2.6a. The increase in TSS level was significantly higher in control fruit $(P < 0.05)$ compared to coated fruits.

(a)

(b)

(c)
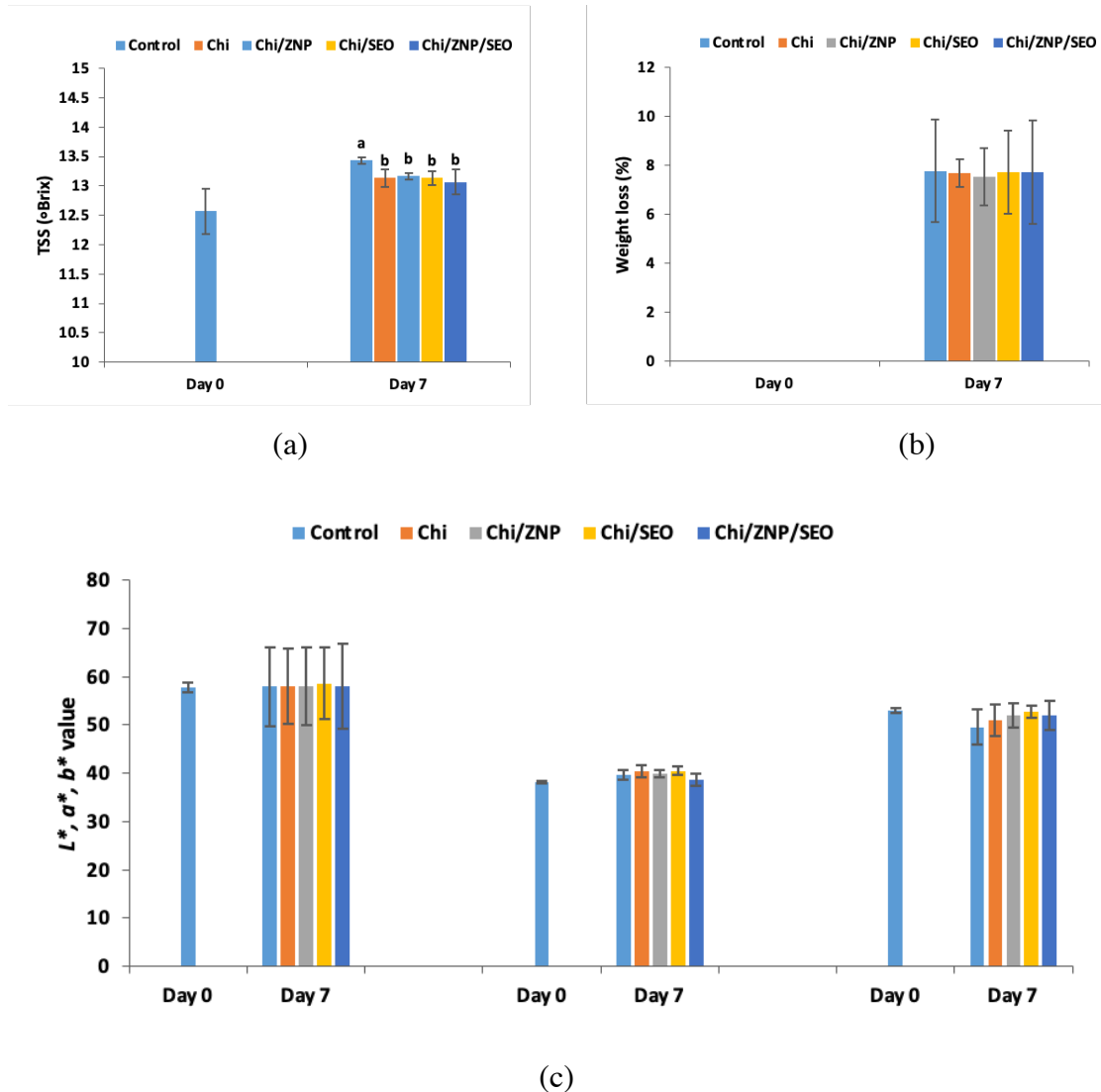
Fig. 2.6. Efficacy of various coating treatment on physicochemical properties of tangerines. (a) Total soluble solid, (b) weight loss, and (c) color changes. Data followed by different letters indicates statistically different by DMRT ($P < 0.05$).

Edible coatings may inhibit the metabolic rate by lowering the internal respiration, therefore preventing hydrolytic changes from starch to sugar (Klangmuang and Sothornvit, 2018; Naeem et al., 2018). Weight loss is one of important parameters of postharvest shelf-life for fresh fruit commodities (Klangmuang and Sothornvit, 2018). All samples demonstrated increasing trend (Fig. 2.6b), and there were no significantly difference among the fruits *(P > 0.05)* during storage. The weight loss of fruits and vegetables is mainly due to the loss of moisture as the result of transpiration and respiration (Chen et al., 2019). Moreover, as seen in Fig. 2.6c, the color parameter of tangerine fruit, *L** and *a** value, slightly increased, whereas *b** value slightly decreased. Over the storage time, no significantly difference was exhibited among the samples *(P > 0.05)* in color parameters.

2.3.7. *Apparent viscosity*

The apparent viscosity of the coating solutions, ranging from 30.06 to 34.74 cP, was affected by the incorporation of SEO (Table 2.1). The apparent viscosity in both Chi/SEO and Chi/ZNP/SEO increased significantly with respect to pure Chi and Chi/ZNP. In addition, the presence of oil droplets tend to enhance viscosity (Bonilla et al., 2012), and a possible mechanism was that the Chi matrix may stabilize SEO droplets using an amphiphilic action in the emulsion system.

2.3.8. *Zeta potential and pH*

Zeta potential characteristic of the samples showed positively charged surfaces varying between 29.70 and 34.44 mV. These values implied a good interaction among the components and good stability of the suspended colloidal dispersion for potential functionality with the

exception of Chi blended with ZNP and SEO. A higher zeta potential of ±30 mV (negative or positive) showed the physically stable dispersions as a consequence of electrostatic repulsion (Kringel et al., 2019).

Table 2.1. Physicochemical characteristics of the coating or film

Characteristic	Chi	Chi/ZNP	Chi/SEO	Chi/ZNP/SEO
Apparent viscosity (cP)	30.06 ± 0.08^b	30.66 ± 0.42^b	34.44 ± 0.84^a	34.74 ± 1.10^a
pH	5.65 ± 0.03^c	5.82 ± 0.02^a	5.65 ± 0.01^c	5.78 ± 0.01^b
Zeta potential (mV)	$+43.72 \pm 2.81^a$	$+43.68 \pm 2.32^a$	$+36.18 \pm 2.71^b$	$+29.70 \pm 1.86^c$
Color				
$L*$	91.7 ± 0.30^a	92.5 ± 0.48^a	88.6 ± 1.34^b	91.9 ± 0.43^a
$a*$	0.44 ± 0.15^b	-0.24 ± 0.54^b	1.78 ± 1.50^a	-1.38 ± 0.04^c
$b*$	16.86 ± 1.58^b	14.62 ± 1.73^b	27.2 ± 5.34^a	18.36 ± 1.28^b
ΔE	13.14 ± 1.44^b	10.82 ± 1.58^b	23.99 ± 4.96^a	14.55 ± 1.18^b
Light transmission at various wavelength (%)				
300	40.73 ± 0.81^b	49.43 ± 1.79^a	10.18 ± 0.03^d	34.97 ± 1.78^c
350	55.41 ± 0.11^b	66.89 ± 0.51^a	22.23 ± 0.13^c	34.97 ± 1.78^b
450	75.58 ± 0.09^c	92.81 ± 0.01^a	41.54 ± 0.02^d	78.5 ± 0.11^b
600	89.95 ± 0.06^b	97.35 ± 0.06^a	51.09 ± 0.02^d	78.5 ± 0.11^c
800	89.91 ± 014^b	97.87 ± 0.01^a	54.37 ± 002^d	87.02 ± 0.03^c
Transparency	1.27 ± 0.01^c	0.20 ± 0.01^d	3.17 ± 0.01^a	1.39 ± 0.01^b
Roughness (nm)				
Ra	6.57 ± 3.20^a	7.31 ± 2.29^a	4.14 ± 2.09^b	4.36 ± 1.60^b
Rq	4.42 ± 0.50^{3ab}	4.97 ± 1.32^a	3.26 ± 1.45^b	3.37 ± 1.59^b

Data followed by different letters indicates statistically different by DMRT ($P < 0.05$).

Noticeably, with the addition of SEO, lower zeta potential values were observed. This was because -NH$_3$$^+$ of the Chi material was less available as a consequence of interactions

between the amino group of Chi and the terpenoid group of SEO (Sotelo-Boyás, et al., 2017; Barrera-Ruiz et al., 2020). Likewise, it could be assumed that the pH of all the coating solutions (5.65–5.82) were below the isoelectric point of Chi (pI = 6.3) (Popat et al., 2012) and at these ranges of pH, ZnO was partly dissociated (Chanakul et al., 2014).

2.3.9. Optical properties

In this study, edible coatings were applied on the fruit surfaces forming a thin layer film; therefore, the thin film was also characterized. The color of a film is an essential parameter due to its effect on consumer acceptance of food commodities (Adilah et al., 2018). The L^* value decreased significantly ($P < 0.05$), whereas the a^*, b^*, and ΔE values increased when 0.5% SEO was added, as shown in Table 4.1. It was believed that an SEO-enriched edible film may increase brightness, indicating lower L^* value, greater ΔE and higher film opacity, which was in agreement with previously reports on color parameters as a consequence of adding an EO (Escamilla-García et al., 2017; Yao et al., 2017). Table 3.1 also shows that the addition of SEO can reduce film transparency and light transmission significantly ($P < 0.05$) at various UV and visible wavelengths. This phenomenon might be ascribed to the presence of oil droplets in the film matrix, which can scatter light and increase opacity (Yao et al., 2017). The results indicated that the thin films loaded with SEO had better light barrier properties for UV and visible light. Furthermore, ZNP incorporation decreased the opacity of the samples ($P < 0.05$), which was similar to a previous study, in which undoped ZnO film had a lower transparency than the film prepared with ZnO (Jiamprasertboon et al., 2019). In the application as fruit coating, the benefits of optical properties might be neglectable for mold-infected fruit due to the appearance of hyphae, as seen in antifungal *in vivo* test (Fig. 2.5a).

2.3.10. Oil droplet

CLSM has played an invaluable role as a method for confirming particle distribution and the interactions of lipid droplets in emulsion systems (Li et al., 2019). The microstructure of emulsions was dyed using the fluorescent dye Nile Red. CLSM images for each coating solution are presented qualitatively in Fig. 2.7. The prevalent continuous red coloration exhibited in the scanned area was a positive indication of the oil-in-water emulsion type. Furthermore, the small sized oil droplets were not easily distinguished on the photograph. Similar findings were reported where emulsion droplets were not easily perceptible once they were present at sizes lower than 2 μm (Colucci et al., 2020).
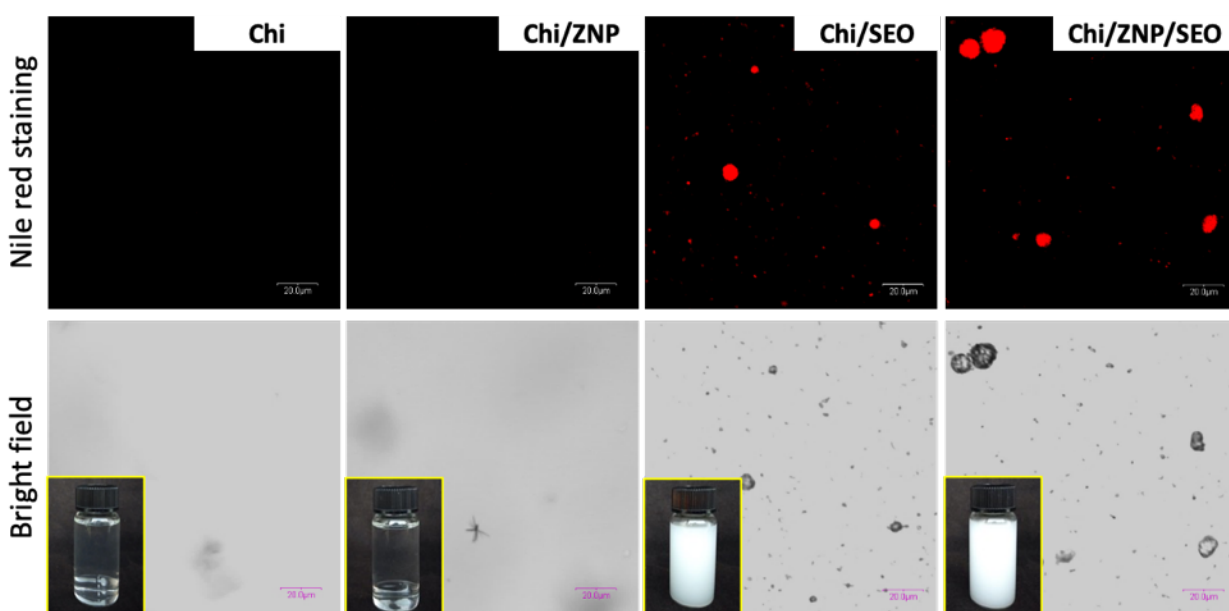
Fig. 2.7. CLSM photographs to confirm distribution and emulsion droplets of SEO.

2.3.11. FTIR

To know the interaction of each material, the characteristic absorption band of the coating film was analyzed by using FTIR, depicted in Fig. 2.8. The broad bands at 3283.2–3358.4 cm^{-1} found in all samples represented stretching vibrations of O–H. The typical bands at 1645 cm^{-1},

1552.4 cm^{-1}, 1408.7 cm^{-1}, and 1020.2 cm^{-1} in all samples were due to the stretching vibration of O–H and N–H bonds, N–H bending (amide II), C=O (amide I), C-N, and C-O-C, respectively, of Chi. There was stronger intensity particularly at 1552.4 cm^{-1}, 1408.7 cm^{-1}, and 1020.2 cm^{-1} when ZNP was inserted into Chi, indicating to the strong attachment of ZnO to the amide groups of Chi molecules. Moreover, there were decreased trend of intensity when SEO or ZNP/SEO were loaded into Chi matrix. It indicated that the existence of hydrogen bonding between the Chi and SEO emulsion may disrupt the molecular networking between individual d-glucosamine (deacetylated unit) and N-acetyl-d-glucosamine (acetylated unit). The absence of more prominent characteristic peaks of SEO and ZNP might be corresponded to the overlap of these bands with the typical characteristic peak of Chi.
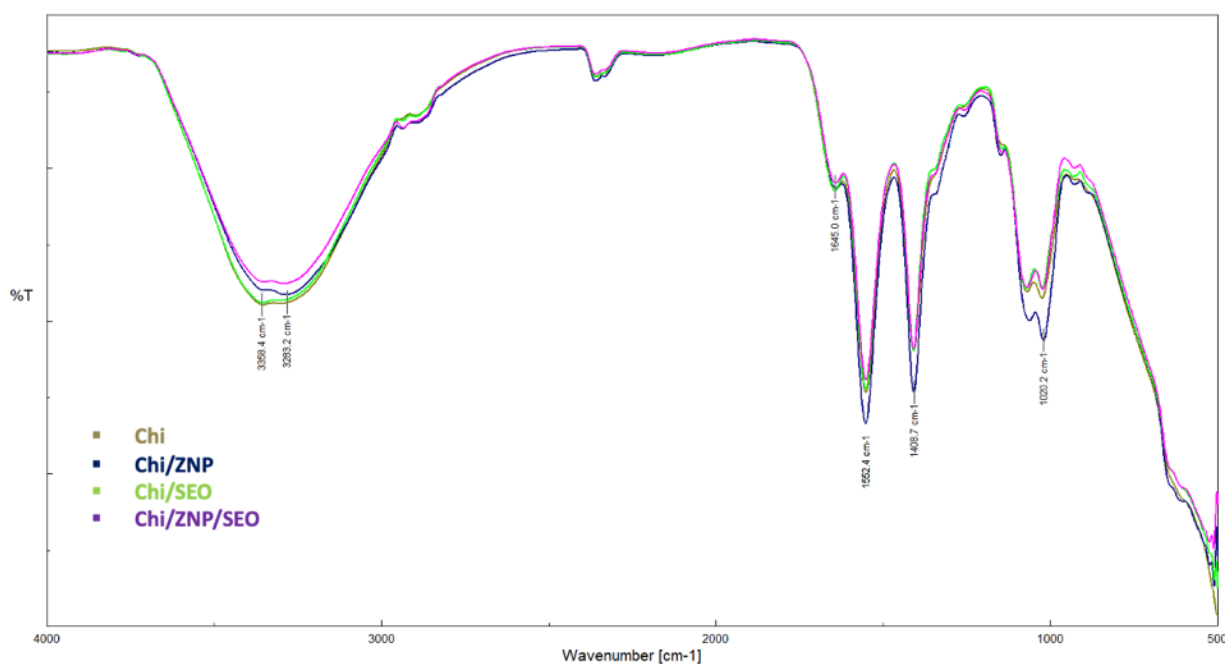
Fig. 2.8. FTIR spectra.

2.3.12. Surface roughness

AFM analysis was performed to observe the influence of ZNPs and SEO incorporation on the surface topography. 2D and 3D AFM images (Fig. 2.9a) clearly displayed the different morphologies of the dried coating solutions. Although there were no significant differences, there was a tendency of increasing *Ra* and *Rq* values as the ZNPs were loaded. Previous work noted that by adding ZNPs, matrix with clavate units in microscale particles occurred resulting in increased roughness (Ni et al., 2018). In addition, the composite film generated a smoother surface when SEO droplets were inserted. Even though the opposite results have been found (Alexandre et al., 2016; Pérez-Córdoba et al., 2017), other studies demonstrated similar findings that the film prepared without an EO tended to have the formation of *Z* agglomerates (Escamilla-García et al., 2017). Moreover, the stabilizing effect of the emulsifier and EO on the biopolymer matrix film allowed the formation of smoother of surface films (Jahed et al., 2017).

2.3.13. Cross-section morphology

Cross-section analysis was carried out to observe the microstructural arrangement of the different components in the film matrix. As shown in Fig. 2.9b, the Chi and Chi/ZNP films had a compact, continuous structure, and almost no obvious separation was detected. Moreover, the oil droplets were homogenously distributed, with oval shapes and various sizes, across the film which implied that flocculation and coalescence occurred as a consequence of the drying process (Peng and Li., 2013). The addition of ZNP into the Chi/SEO emulsion system influenced the shape formation of SEO droplets resulting in shrinkage to form oval-shaped droplets. Although in several reports, ZNPs were utilized as stabilizing agent for the Pickering emulsion system; however, this was not exhibited in a recent study (Chen et al., 2010; Tian et al., 2021). The

phenomena was possibly associated with the flocculation and coagulation of dispersed particles. It can be related to the lowest zeta potential value of Chi/ZNP/SEO (Table 3.1) among the coating samples leading to poor physical stability. In general, for a higher zeta potential in an emulsion system, the repulsive forces exceed the attractive forces, the more relatively stable.

(a)   (b)
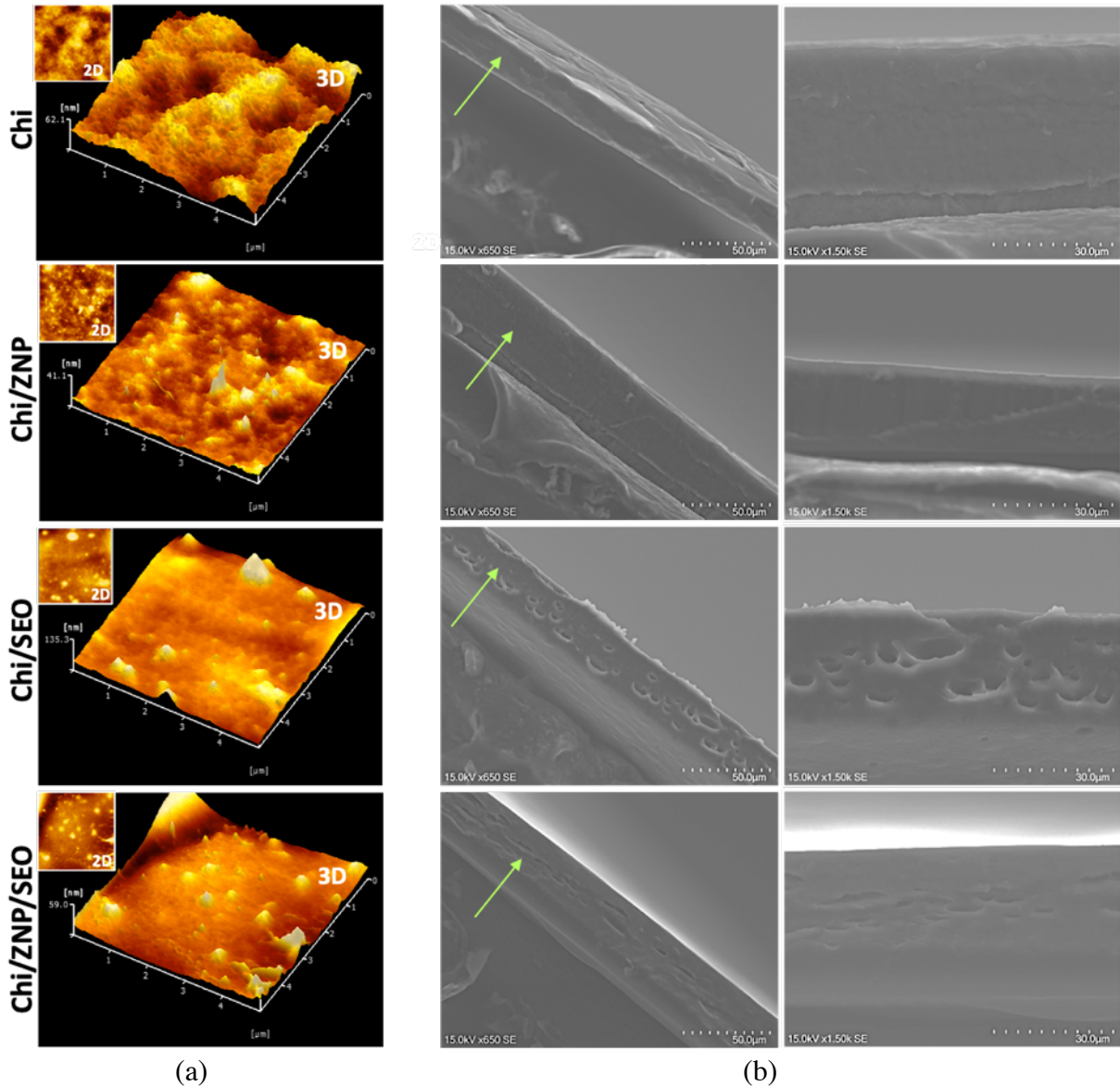
Fig. 2.9. (a) AFM images (2D and 3D) of surface roughness and (b) longitudinal cross section of

SEM images.

2.4.   References

Adilah, M. Z. A., Jamilah, B., & Nur Hanani, Z. A. (2018). Functional and antioxidant properties of protein-based films incorporated with mango kernel extract for active packaging. *Food Hydrocolloids*, *74*, 207–218.

Alexandre, E. M. C., Lourenço, R. V., Bittante, A. M. Q. B., Moraes, I. C. F., & Sobral, P. J. do A. (2016). Gelatin-based films reinforced with montmorillonite and activated with nanoemulsion of ginger essential oil for food packaging applications. *Food Packaging and Shelf Life*, *10*, 87–96.

Avadi, M. R., Jalali, A., Mir Mohammad Sadeghi, A., Shamimi, K., Bayati, K. H., Nahid, E., Dehpour, A. R., & Rafiee-Tehrani, M. (2005). Diethyl methyl chitosan as an intestinal paracellular enhancer: Ex vivo and in vivo studies. *International Journal of Pharmaceutics*, *293*(1–2), 83–89.

Barrera-Ruiz, D. G., Cuestas-Rosas, G. C., Sánchez-Mariñez, R. I., Álvarez-Ainza, M. L., Moreno-Ibarra, G. M., López-Meneses, A. K., Plascencia-Jatomea, M., & Cortez-Rocha, M. O. (2020). Antibacterial activity of essential oils encapsulated in chitosan nanoparticles. *Food Science and Technology*, *40,* 568-573.

Baker, M. J., Trevisan, J., Bassan, P., Bhargava, R., Butler, H. J., Dorling, K. M., Fielden, P. R., Fogarty, S. W., Fullwood, N. J., Heys, K. A., Hughes, C., Lasch, P., Martin-Hirsch, P. L., Obinaju, B., Sockalingum, G. D., Sulé-Suso, J., Strong, R. J., Walsh, M. J., Wood, B. R., Martin, F. L. (2014). Using Fourier transform IR spectroscopy to analyze biological materials. *Nature Protocols*, *9*(8), 1771–1791.

Bonilla, J., Atarés, L., Vargas, M., & Chiralt, A. (2012). Effect of essential oils and homogenization conditions on properties of chitosan-based films. *Food Hydrocolloids*, *26*(1), 9–16.

Bonilla, J., & Sobral, P. J. A. (2016). Investigation of the physicochemical, antimicrobial and antioxidant properties of gelatin-chitosan edible film mixed with plant ethanolic extracts. *Food Bioscience*, *16*, 17–25.

Burdock, G. A., and Carabin, I. G. (2008). Safety assessment of sandalwood oil (*Santalum album* L.). *Food and Chemical Toxicology, 46*(2), 421-432.

Cháfer, M., Sánchez-González, L., González-Martínez, C., & Chiralt, A. (2012). Fungal decay and shelf life of oranges coated with chitosan and bergamot, thyme, and tea tree essential oils. *Journal of Food Science*, *77*(8), 182–187.

Chanakul, A., Traiphol, N., Faisadcha, K., & Traiphol, R. (2014). Dual colorimetric response of polydiacetylene/Zinc oxide nanocomposites to low and high pH. *Journal of Colloid and Interface Science*, *418*, 43–51.

Chen, W., Liu, X., Liu, Y., & Kim, H. Il. (2010). Synthesis of microcapsules with polystyrene/ZnO hybrid shell by pickering emulsion polymerization. *Colloid and Polymer Science*, *288*(14–15), 1393–1399.

Chen, C. Y., Zheng, J. P., Wan, C. P., Chen, M., & Chen, J. Y. (2016). Effect of carboxymethyl cellulose coating enriched with clove oil on postharvest quality of "Xinyu" Mandarin oranges. *Fruits*, *71*(5), 319–327.

Chen, H., Sun, Z., and Yang, H. (2019). Effect of carnauba wax-based coating containing glycerol monolaurate on the quality maintenance and shelf-life of Indian jujube (*Zizyphus mauritiana* Lamk.) fruit during storage. *Scientia Horticulturae, 244*, 157–164.

Chen, C., Chen, J., & Wan, C. (2020). Pinocembrin-7-Glucoside (P7G) reduced postharvest blue mold of navel orange by suppressing *Penicillium italicum* growth. *Microorganisms*, *8*(4).

Colucci, G., Santamaria-Echart, A., Silva, S. C., Fernandes, I. P. M., Sipoli, C. C., & Barreiro, M. F. (2020). Development of water-in-oil emulsions as delivery vehicles and testing with a natural antimicrobial extract. *Molecules*, *25*(9), 5–7.

Dananjaya, S. H. S., Kumar, R. S., Yang, M., Nikapitiya, C., Lee, J., & De Zoysa, M. (2018). Synthesis, characterization of ZnO-chitosan nanocomposites and evaluation of its antifungal activity against pathogenic *Candida albicans*. *International Journal of Biological Macromolecules*, *108*, 1281–1288.

de Oliveira, C. E. V., Magnani, M., de Sales, C. V., de Souza Pontes, A. L., Campos-Takaki, G. M., Stamford, T. C. M., & de Souza, E. L. (2014). Effects of chitosan from *Cunninghamella elegans* on virulence of post-harvest pathogenic fungi in table grapes (*Vitis labrusca* L.). *International Journal of Food Microbiology*, *171*, 54–61.

de Souza, R. C., Haberbeck, L. U., Riella, H. G., Ribeiro, D. H. B., & Carciofi, B. A. M. (2019). Antibacterial activity of zinc oxide nanoparticles synthesized by solochemical process. *Brazilian Journal of Chemical Engineering*, *36*(2), 885–893.

El Guilli, M., Hamza, A., Clément, C., Ibriz, M., & Barka, E. A. (2016). Effectiveness of postharvest treatment with chitosan to control citrus green mold. *Agriculture*, *6*(12), 1-15.

El Shafei, A., & Abou-Okeil, A. (2011). ZnO/carboxymethyl chitosan bionano-composite to impart antibacterial and UV protection for cotton fabric. *Carbohydrate Polymers*, *83*(2), 920–925.

Escamilla-García, M., Calderón-Domínguez, G., Chanona-Pérez, J. J., Mendoza-Madrigal, A. G., Di Pierro, P., García-Almendárez, B. E., Amaro-Reyes, A., & Regalado-González, C.

(2017). Physical, structural, barrier, and antifungal characterization of chitosan-zein edible films with added essential oils. *International Journal of Molecular Sciences*, *18*(11).

He, L., Liu, Y., Mustapha, A., & Lin, M. (2011). Antifungal activity of zinc oxide nanoparticles against *Botrytis cinerea* and *Penicillium expansum*. *Microbiological Research*, *166*(3), 207–215.

Inouye, S., Uchida, K., & Abe, S. (2006). Vapor activity of 72 essential oils against a Trichophyton mentagrophytes. *Journal of Infection and Chemotherapy*, *12*(4), 210–216.

Jahed, E., Khaledabad, M. A., Bari, M. R., & Almasi, H. (2017). Effect of cellulose and lignocellulose nanofibers on the properties of *Origanum vulgare* ssp. *gracile* essential oil-loaded chitosan films. *Reactive and Functional Polymers*, *117*, 70–80.

Jamdagni, P., Khatri, P., & Rana, J. S. (2018). Green synthesis of zinc oxide nanoparticles using flower extract of *Nyctanthes arbor-tristis* and their antifungal activity. *Journal of King Saud University - Science*, *30*(2), 168–175.

Jayaraj, J., Rahman, M., Wan, A., & Punja, Z. K. (2009). Enhanced resistance to foliar fungal pathogens in carrot by application of elicitors. *Annals of Applied Biology*, *155*(1), 71–80.

Ji, D., Chen, T., Ma, D., Liu, J., Xu, Y., & Tian, S. (2018). Inhibitory effects of methyl thujate on mycelial growth of *Botrytis cinerea* and possible mechanisms. *Postharvest Biology and Technology*, *142*, 46–54.

Jiamprasertboon, A., Dixon, S. C., Sathasivam, S., Powell, M. J., Lu, Y., Siritanon, T., & Carmalt, C. J. (2019). Low-cost one-step fabrication of highly conductive ZnO:Cl transparent thin films with tunable photocatalytic properties via aerosol-assisted chemical vapor deposition. *ACS Applied Electronic Materials*, *1*(8), 1408–1417.

Jiang, R., Zhu, H., Yao, J., Fu, Y., & Guan, Y. (2012). Chitosan hydrogel films as a template for mild biosynthesis of CdS quantum dots with highly efficient photocatalytic activity. *Applied Surface Science*, *258*(8), 3513–3518.

Kala, S., Sogan, N., Naik, S. N., Agarwal, A., & Kumar, J. (2020). Impregnation of pectin-cedarwood essential oil nanocapsules onto mini cotton bag improves larvicidal performances. *Scientific Reports*, *10*(1), 1–12.

Kim, T. H., Hatano, T., Okamoto, K., Yoshida, T., Kanzaki, H., Arita, M., & Ito, H. (2017). Antifungal and ichthyotoxic sesquiterpenoids from *Santalum album* heartwood. *Molecules*, *22*(7), 1–8.

Kingwascharapong, P., Arisa, K., Karnjanapratum, S., Tanaka, F., & Tanaka, F. (2020). Effect of gelatin-based coating containing frog skin oil on the quality of persimmon and its characteristics. *Scientia Horticulturae*, *260*, 1-9.

Klangmuang, P. & Sothornvit, R. (2018). Active coating from hydroxypropyl methylcellulose-based nanocomposite incorporated with Thai essential oils on mango (cv. *Namdokmai Sithong*). *Food Bioscience, 23*, 9–15.

Kringel, D. H., da Silva, W. M. F., Biduski, B., Waller, S. B., Lim, L. T., Dias, A. R. G., & Zavareze, E. da R. (2020). Free and encapsulated orange essential oil into a β-cyclodextrin inclusion complex and zein to delay fungal spoilage in cakes. *Journal of Food Processing and Preservation*, *44*(5), 1–10.

Kong, M., Chen, X. G., Xing, K., & Park, H. J. (2010). Antimicrobial properties of chitosan and mode of action: a state of the art review. *International Journal of Food Microbiology, 144*(1), 51-63.

Kumar, R. S., Dananjaya, S. H. S., De Zoysa, M., & Yang, M. (2016). Enhanced antifungal activity of Ni-doped ZnO nanostructures under dark conditions. *RSC Advances*, *6*(110), 108468–

Li, Y., Liu, H., Liu, Q., Kong, B., & Diao, X. (2019). Effects of zein hydrolysates coupled with sage (*salvia officinalis*) extract on the emulsifying and oxidative stability of myofibrillar protein prepared oil-in-water emulsions. *Food Hydrocolloids*, *87*, 149–157.

Liu, J., Tian, S., Meng, X., & Xu, Y. (2007). Effects of chitosan on control of postharvest diseases and physiological responses of tomato fruit. *Postharvest Biology and Technology*, *44*(3), 300–306.

Mitra, S., Patra, P., Chandra, S., Pramanik, P., & Goswami, A. (2012). Efficacy of highly water-dispersed fabricated nano ZnO against clinically isolated bacterial strains. *Applied Nanoscience*, *2*(3), 231–238.

Naeem, A., Abbas, T., Ali, T.M., & Hasnain, A. (2018). Effect of guar gum coatings containing essential oils on shelf life and nutritional quality of green-unripe mangoes during low temperature storage. *International Journal of Biological Macromolecules, 113*, 403–410.

Nardoni, S., Giovanelli, S., Pistelli, L., Mugnaini, L., Profili, G., Pisseri, F., & Mancianti, F. (2015). *In vitro* activity of twenty commercially available, plant-derived essential oils against selected dermatophyte species. *Natural Product Communications, 10*(8), 1473-1478.

Negi, H., Agarwal, T., Zaidi, M. G. H., & Goel, R. (2012). Comparative antibacterial efficacy of metal oxide nanoparticles against Gram negative bacteria. *Annals of Microbiology*, *62*(2), 765–772.

Ni, S., Zhang, H., Dai, H., & Xiao, H. (2018). Starch-based flexible coating for food packaging paper with exceptional hydrophobicity and antimicrobial activity. *Polymers*, *10*(11).

Panebianco, S., Vitale, A., Platania, C., Restuccia, C., Polizzi, G., & Cirvilleri, G. (2014). Postharvest efficacy of resistance inducers for the control of green mold on important Sicilian citrus varieties. *Journal of Plant Diseases and Protection*, *121*(4), 177–183.

Peng, Y., & Li, Y. (2014). Combined effects of two kinds of essential oils on physical, mechanical and structural properties of chitosan films. *Food Hydrocolloids*, *36*, 287–293.

Pérez-Córdoba, L. J., Norton, I. T., Batchelor, H. K., Gkatzionis, K., Spyropoulos, F., & Sobral, P. J. A. (2018). Physico-chemical, antimicrobial and antioxidant properties of gelatin-chitosan based films loaded with nanoemulsions encapsulating active compounds. *Food Hydrocolloids*, *79*, 544–559.

Popat, A., Liu, J., Lu, G. Q. (Max), & Qiao, S. Z. (2012). A pH-responsive drug delivery system based on chitosan coated mesoporous silica nanoparticles. *Journal of Materials Chemistry*, *22*(22), 11173–11178.

Reddy, K. M., Feris, K., Bell, J., Wingett, D. G., Hanley, C., & Punnoose, A. (2007). Selective toxicity of zinc oxide nanoparticles to prokaryotic and eukaryotic systems. *Applied Physics Letters*, *90*(21), 10–13.

Shao, X., Cao, B., Xu, F., Xie, S., Yu, D., & Wang, H. (2015). Effect of postharvest application of chitosan combined with clove oil against citrus green mold. *Postharvest Biology and Technology*, *99*, 37–43.

Sotelo-Boyás, M. E., Correa-Pacheco, Z. N., Bautista-Baños, S., & Corona-Rangel, M. L. (2017). Physicochemical characterization of chitosan nanoparticles and nanocapsules incorporated with lime essential oil and their antibacterial activity against food-borne pathogens. *LWT - Food Science and Technology*, *77*, 15–20.

Suzuki, T., Fujikura, K., Higashiyama, T., & Takata, K. (1997). DNA staining for fluorescence and laser confocal microscopy. *Journal of Histochemistry and Cytochemistry*, *45*(1), 49–53.

Tian, X., Ge, X., Guo, M., Ma, J., Meng, Z., & Lu, P. (2021). An antimicrobial bio-based polymer foam from ZnO-stabilised pickering emulsion templated polymerisation. *Journal of Materials Science*, *56*(2), 1643–1657.

Tongnuanchan, P., Benjakul, S., & Prodpran, T. (2014). Structural, morphological and thermal behaviour characterisations of fish gelatin film incorporated with basil and citronella essential oils as affected by surfactants. *Food Hydrocolloids*, *41*, 33–43.

Torres, J. D., Faria, E. A., SouzaDe, J. R., & Prado, A. G. S. (2006). Preparation of photoactive chitosan-niobium (V) oxide composites for dye degradation. *Journal of Photochemistry and Photobiology A: Chemistry*, *182*(2), 202–206.

Worzakowska, M. (2017). TG/DSC/FTIR/QMS studies on the oxidative decomposition of terpene acrylate homopolymers. *Journal of Thermal Analysis and Calorimetry*, *127*(3), 2025–2035.

Yan, X., He, B., Liu, L., Qu, G., Shi, J., Hu, L., & Jiang, G. (2018). Antibacterial mechanism of silver nanoparticles in *Pseudomonas aeruginosa*: proteomics approach. *Metallomics*, *10*(4), 557–564.

Yao, Y., Ding, D., Shao, H., Peng, Q., & Huang, Y. (2017). Antibacterial activity and physical properties of fish gelatin-chitosan edible films supplemented with D-limonene. *International Journal of Polymer Science*, 2017, 1-9.

Zeng, K., Deng, Y., Ming, J., & Deng, L. (2010). Induction of disease resistance and ROS metabolism in navel oranges by chitosan. *Scientia Horticulturae*, *126*(2), 223–228.

Zhang, H., Li, R., & Liu, W. (2011). Effects of chitin and its derivative chitosan on postharvest decay of fruits: A review. *International Journal of Molecular Sciences*, *12*(2), 917–934.

CHAPTER 3

CuO nanoparticles/Indonesian cedarwood

essential oil-loaded chitosan coating film:

Characterization and antifungal improvement

against *Penicillium* spp.

3.1. Introduction

There has been special attention paid to coatings as a promising strategy to prolong the shelf life of fresh fruits through the prevention of fungal decay. This phenomenon emerged as part of the development of eco-friendly materials instead of antifungal drugs. The excessive use of antifungal drugs, which mostly fall into one of the nucleoside analogs, azoles, echinocandins, and polyenes, may be potentially be linked to increased resistance among harmful fungi (Shih et al., 2019), and at the same time being associated with health and environmental impacts.

Chitosan (poly-(β-1→4)-2-amino-2-deoxy-D-glucopyranose) is a natural, non-toxic biopolymer that is increasingly used to fabricate antimicrobial coating films (Zeng et al., 2010; Panebianco et al., 2014; Shao et al., 2015). This cationic polymer (positively charged) can actively interact with the negatively charged microbial cell surface leading to anion–cation imbalance, thus exerting disruptive effects (Martínez-Camacho et al., 2010). Beside the degree of deacetylation and pH value, the effectiveness of the antimicrobial activity levels of Chi depends on the microbial characteristics involved (Cheung et al., 2015; Hosseinnejad and Jafari, 2016). Gram-positive microorganisms are more susceptible than gram-negative due to the composition of thick peptidoglycan layer and highly negative charged, called teichoic acids, facilitating electrostatic interaction with cationic antimicrobial compound of Chi. Concerning the antifungal activity, previous work revealed that *Alternaria solani* growth was inhibited by decreasing acetylation degrees, however it was not applied for *Aspergillus niger* (Hosseinnejad and Jafari, 2016).

Early studies suggested the improved action with essential oil (EO)-loaded Chi. The synergistic antifungal against *P. digitatum* from 1% chitosan and various concentration of clove EO (0.5, 1 or 2 mL/L) was exhibited in *in vitro* assay (Shao et al., 2015). Combinations of Chi (5

and 7.5 mg/mL) and *Mentha* EO (0.15–1.25 mL/mL) could suppress the growth of *Colletotrichum* isolates (Braga et al., 2019). Furthermore, enhancement the antimicrobial properties of Chi by incorporating EO is a rapidly growing field (dos Santos et al., 2019; Lyn and Hanani, 2020). Among the EOs documented as having inhibitory actions against fungi, the use of Indonesian cedarwood essential oil (CEO)-loaded Chi has not been reported yet. CEO is commonly used as a fragrance ingredient and food additive as a flavor enhancement. Moreover, CEO has been documented as possessing antifungal activities including against *Gloeophyllum trabeum*, *Oligoporus placenta*, *Trametes versicolor*, *Coniophora puteanai Candida albicans*, and *Trichophyton mentagrophytes* (Fidah et al., 2016; Orchard et al., 2019). The antifungal potency of CEO might be related to its main constituents such as cedrol, β-cedrene, and thujopsene (Jeong et al., 2014; Powers et al., 2018). These volatile compounds interrupt the balance in the lytic and synthesis enzyme such as chitin synthase leading to the cessation of hyphal extension (Fidah et al., 2016).

In recent years, application of metal oxide nanoparticles as a means for improving antimicrobial activity has gained special attention, and such nanoparticles may be a prospective strategy employed for effective antifungal activity. There has been increasing interest in the use of copper nanoparticles (CuO), among metal-based nanoparticles, due to their beneficial characteristics including lower cost and easier availability compared with well-known silver or gold nanoparticles (Pham et al., 2019). Previous studies have described the biocompatibility and antifungal efficacy when CuO was incorporated into a biopolymer (Ghorbani et al., 2018; Muñoz-Escobar and Reyes-Lópes, 2020). Although Cu possess an important role in maintaining homeostasis of human body, high Cu intake exceeding certain limit results in toxicity of respiratory systems, gastrointestinal tract, and skin deseases (Naz et al., 2019). Another report

found that the CuO nanoparticle was more potent regarding cytotoxicity and DNA damage compared to other metal oxide particles (TiO_2, ZnO, $CuZnFe_2O_4$, Fe_3O_4, Fe_2O_3). Thus, to minimize the CuO-exposed human via the products, we considered that CuO-deposited Chi coating is only for commercial application on the surface of inedible fruit peel such as banana, avocado, melon, pineapple, papaya, mango, and citrus fruit.

Citrus, a non-climacteric fruit that has unique flavor, acidity and functional compounds, is one of the most widely produced and exported fruit genus globally. In 2016, about 124.246 thousand tonnes citrus were produced with worldwide exports of about 15.913 thousand tonnes (FAO, 2017). Orange fruits are susceptible to fungal decay and not bacteria, causing a soft rot during storage and transportation (Talibi et al., 2014). *P*. *digitatum* Saccardo and *P*. *italicum* Wehmer have been identified as the two most potential phytopathogens in citrus fruit. *P*. *digitatum*, the green mould, can account for about 90% of post-harvest total losses (Costa et al., 2019; Papoutsis et al., 2019), and *P*. *italicum*, is the responsible agent of the blue mould disease (Kanashiro et al., 2020). The wounded surface of orange fruit is more prone for infection of these diseases (Talibi et al., 2014).

There are no reports about the beneficial properties of Chi/CuO/CEO coating formulations applied on the surface of inedible citrus fruit peel. In this study, we investigated the antifungal action from double and triple antimicrobial agent based on Chi, CuO, and CEO formulations against citrus fruit fungal pathogen *in vitro* and *in vivo*, and characterized the physical, chemical, and surface properties of coating films.

3.2. Materials and methods

3.2.1. Coating film preparation

Fig. 3.1 shows the graphical scheme of coating film preparation. A Chi solution, concentration 1%, was prepared by dissolving Chi powder with a deacetylation degree of 80% (FUJIFILM Wako Pure Chemical Corporation, Japan) in 1% (w/v) aqueous acetic acid (FUJIFILM Wako Pure Chemical Corporation, Japan). The solution was heated and stirred for 5 ± 2 min until the Chi flakes were completely dissolved. The pH was adjusted to 5.8 with NaOH (FUJIFILM Wako Pure Chemical Corporation, Japan). The resulting solution was named as Chi_s. To prepare the CuO solution stock, 0.25% CuO powder, < 50 nm particle size (Sigma Aldrich, USA), was dispersed into distilled water using an sonicator (Dual Frequency, ASU-10D Series) for 60 min at frequency 43 kHz. The solution was designated as CuO_s. To prepare CEO emulsion stock, 5% Indonesian CEO, purchased from Aromindo CV, Indonesia was emulsified with the aid of 2.5% (w/v) Tween 80 (FUJIFILM Wako Pure Chemical Corporation, Japan) in distilled water using a homogenizer (T 25 digital ULTRA-TURRAX® - IKA, Germany) at 20,000 rpm for 3 min. The main components of the CEO were alpha-cedrene (15.91%), beta-cedrene (5.34%), thujopsene (14.10%), alpha-cedrol (17.62%). The emulsified solution was designated as CEO_s. To prepare the coating solutions, the prepared solutions were mixed as follows: 1) Chi_s and distilled water with ratio 8:2 (Chi treatment); 2) Chi_s, distilled water and CuO_s with ratio 8:1:1 (Chi/CuO treatment); 3) Chi_s, distilled water and CEO_s with ratio 8:1:1 (Chi/CEO treatment); and 4) 80% (w/w) Chi_s, CuO_s and CEO_s with ratio 8:1:1 (Chi/CuO/CEO treatment). These solutions were homogenized at 20,000 rpm for 3 min and subjected to analysis. Moreover, these solutions were prepared using a casting method. A 5 ml aliquot of solution was poured on a plastic plate (50 mm in diameter), dried in fan-assisted oven at 40°C for 20 h, peeled, and stored at 25°C and

50% relative humidity (RH) before testing. The concentration of Chi was selected in accordance with a preliminary antifungal test.
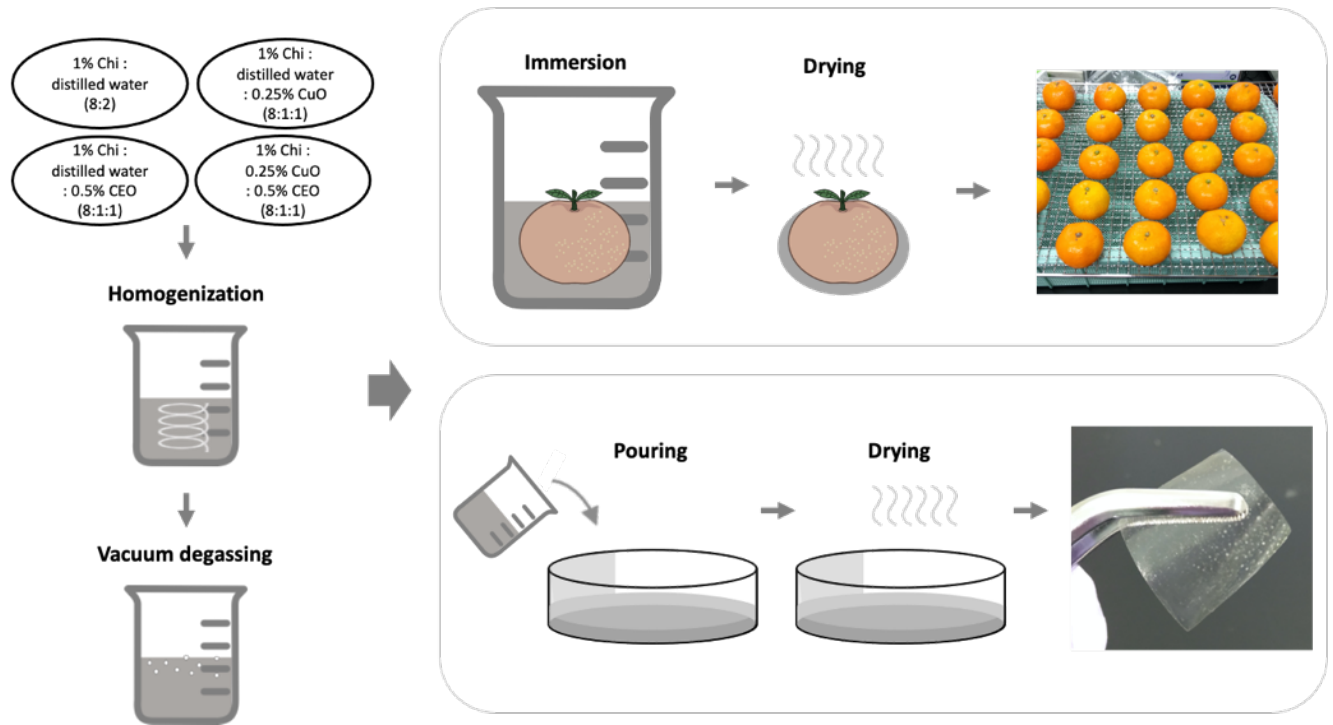
Fig. 3.1. Scheme of the procedure to prepare composite coating and film.

3.2.2. AFM

An atomic force microscope (Hitachi 5200S, Japan) was employed to visualize the grain of CuO and the surface properties of each film. The 10 μL of 0.1% CuO dispersed in acetone and each coating composite were deposited on mica and dehydrated inside the silica gel assisted desiccator for 24 h. A micro-cantilever type SI-DF20 was set prior to surface scanning at frequencies of 0.7–0.84 Hz. Roughness parameters were calculated using Equations (1) and (2) with ten replications.

$$Rq = \sqrt{\frac{1}{n} \sum_{i=1}^{n} Zi^2}$$

$$Ra = \frac{1}{n} \sum_{i=1}^{n} |Zi|$$

where Rq is root mean square mean deviation for the mean, Ra is arithmetical mean deviation from the mean, Zi is the height deviation of i-th from the heights mean, and n is the amount of data points.

3.2.3. FTIR

An FTIR spectrometer (Jasco, FTIR-620, Japan) was employed to characterize each composite and interactions among the materials. The transmittance was measured in accordance with the potassium bromide (KBr) pellet method for CuO, CEO, and the attenuated total reflectance (ATR) for the coating film samples, respectively, at wave numbers of 375–4000 cm^{-1} and 500–4000 cm^{-1}.

3.2.4. Zeta potential

About 3 mL of each coating solution was placed in a folded capillary zeta cell DTS1070 followed by measuring the zeta potential using a Zetasizer (Nano, Malvern Instruments, UK). All of the samples were analyzed using five replications.

3.2.5. Spore germination and germ tube elongation

The spore solutions were harvested from the *P. italicum* and *P. digitatum* (National Institute of Technology and Evaluation, Biological Resource Center, Tokyo, Japan) after culturing on potato dextrose agar (Nissui Pharmaceutical Co., Ltd., Japan) for 7 days. Subsequently, 2×10^5 spores/mL of spore solution was applied in the CuO solution (0.006, 0.012, 0.025, 0.05, 0.075%), CEO (0.12, 0.25, 0.5, 0.75%), coating solution and mixed with potato dextrose broth (Difco™,

USA). After incubation on a shaker (100 rpm) at 25°C for 24 h, spore germination and germ tube elongation were evaluated using a confocal laser scanning microscopy (*CLSM*) (Olympus IX71, Japan) with a 50× objective lens. Moreover, percentage inhibition (PI) was calculated as follows:

$$PI \% = \frac{A-B}{A} \times 100\%$$

where *A* is the mycelium diameter of the control and *B* is the mycelium diameter of treated samples. The measurements were done in triplicate.

3.2.6. *Membrane permeability changes*

The control and treated spore solution were incubated with shaking for 4 h at 25°C followed by staining with 50 (mg/L) propidium iodide (Sigma Aldrich, USA). Afterwards, the propidium iodide uptake was observed using a *CLSM* with excitation and emission wavelength of 543 nm and 585 nm, respectively.

3.2.7. *In vivo antifungal assays*

Tangerine and tangelo fruit varieties were purchased from the supermarket in Fukuoka, Japan. The fruit were washed with 1% sodium hypochlorite, wounded (2 mm deep) using a sterile tip for tangerine and using a corkborer (4 mm diameter and 2 mm deep) for tangelo. The 10 μL of spores (2×10^6 spores/mL) of *P. italicum* and *P. digitatum* were deposited on the lesion of tangerine and tangelo respectively. After drying, all fruit (except control) were dipped in coating solution for seconds, dried, and packed with perforated polyethylene terephthalate packaging. The lesion diameters were measured after fruit was stored at 25°C, 80% RH for 6 days. The assays were performed in triplicate.

3.2.8. Apparent viscosity

The apparent viscosity was measured using a rotational viscometer (Brookfield DV2T, USA). About 75 mL of the coating solution was prepared in a cell. A rotor speed of 50 rpm, spindle LV-01 (61), and measurement time 30 sec were set for testing in triplicate.

3.2.9. pH

The pH of each coating was measured using a pH meter (Horiba LAQUAtwin, Japan). The measurement was performed in triplicate.

3.2.10. Color

The color properties were characterized referring to the *CIELAB (Commission internationale de l'éclairage, L*, a*, and b*)* method. A thin coating film was deposited on a white standard plate and measured with a color reader (Konica Minolta CR-20, Japan). The *ΔE* (color difference) was also calculated as follows:

$$\Delta E = \sqrt{(L_0 * - L *)^2 + (a_0 * - a *)^2 + (b_0 * - b *)^2}$$

Where the L_0, a_0, b_0 are the standard white plate ($L_0* = 94.8$, $a_0* = -0.1$, and $b_0* = 4.1$), the $L*$, $a*$, $b*$ are the values of each thin coating film. The measurements in were performed in five replicates.

3.2.11. Light transmission and transparency

A sample was prepared by attaching a rectangular sample of each coating film onto the cell side. Light transmission characteristics were determined with the aid of a UV-Vis spectrophotometer (Jasco, V-530, Japan) at wavelengths of 300–800 nm in accordance with the modified method by Tongnuanchan et al. (2012). The transparency was calculated as follows:

$$Transparency = \frac{(-\log T)}{x}$$

Where *T* is the coating film transmittance at 600 nm and *x* is the coating film thickness (mm).

3.2.12. Oil droplets

The monodispersion of emulsion droplets was evaluated by referring to a previously reported method (Kingwascharapong et al., 2020). The oil phase was stained by mixing coating solution with Nile red dye (FUJIFILM Wako Pure Chemical Corporation, Japan). Subsequently, 6 μL of the stained sample was deposited on a microscope glass slide (Toshinriko, Japan) and covered with a glass coverslip (Matsunami, Japan) before observation using a *CLSM* with a 20× objective lens.

3.2.13. SEM

Prior to evaluation, the thin coating film was kept in an $Mg_2(NO_3)_2$-contained desiccator (53 ± 1% RH) at 25°C. Afterwards, the coating film was attached to a specimen stub and coated using an osmium coater. The cross-section microstructure was evaluated using a scanning electron microscope, SU3500 (Hitachi, Japan) at 15 kV.

3.2.14. Statistical analysis

The experimental data were analyzed using one-way analysis of variance (ANOVA) at *P-value* < 0.05 and DMRT post-hoc test with the aid of Statistical Package for Social Science software (SPSS 17.0, SPSS Inc., USA). Two-way ANOVA was used to assess effects of treatments (CuO and CEO) on spore germination and germ tube elongation.

3.3. Results and discussion

3.3.1. Material characteristics

CuO powder was analyzed for its 2D and 3D morphology using an AFM. As can be seen in Fig. 3.2a, small nanoclusters were easily detectable. CuO tended to have sharp features and appeared to be slender in shape with a diameter of 79–98 nm. Additionally, CuO and CEO were characterized using IR spectra with the potassium bromide (KBr) pellet technique in the range of 400–4000 cm^{-1}, as shown in Fig. 3.2b. FTIR spectra exhibited only two main vibrations, at 435 cm^{-1} and 512 cm^{-1}, which can be attributed to the vibration bond of Cu-O. These assignments were consistent with those of CuO available in the literature (Zhang et al., 2006; Azam et al., 2012). The present *FTIR* spectra of CEO was similar to previous reports (Baker et al., 2014; Kala et al., 2020). The presence of absorption bands at 1375 and 1456 cm^{-1} represented the methyl and C-H stretching band, respectively, of the terpenoid compound. The strong peak at 2930 cm^{-1} might be attributed to the C-H stretching band of fatty acids. A weak peak at approximately 2400 cm^{-1} found in CuO and CEO were possibly due to the vibrations of atmospheric CO_2 (Azam et al., 2012).

(a)
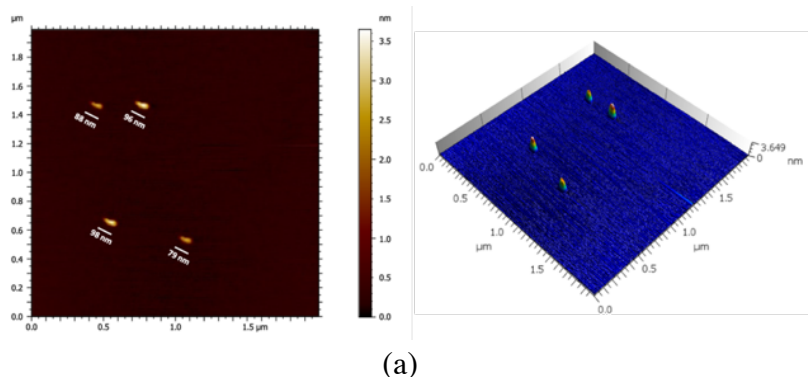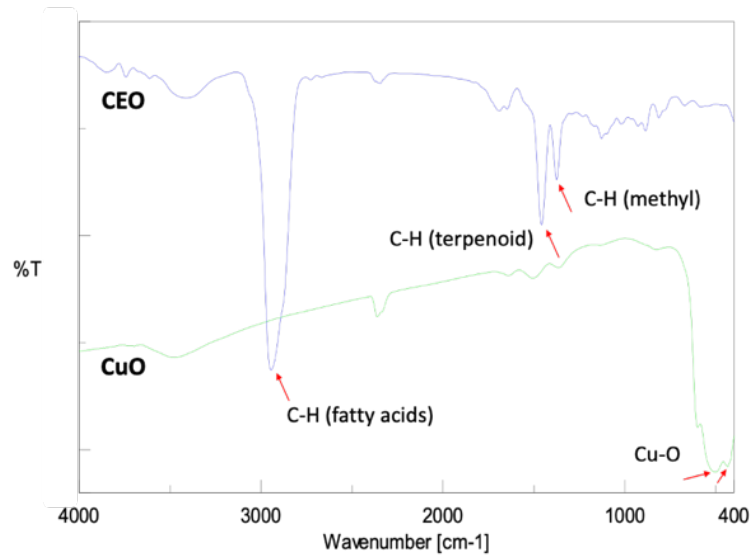
(b)
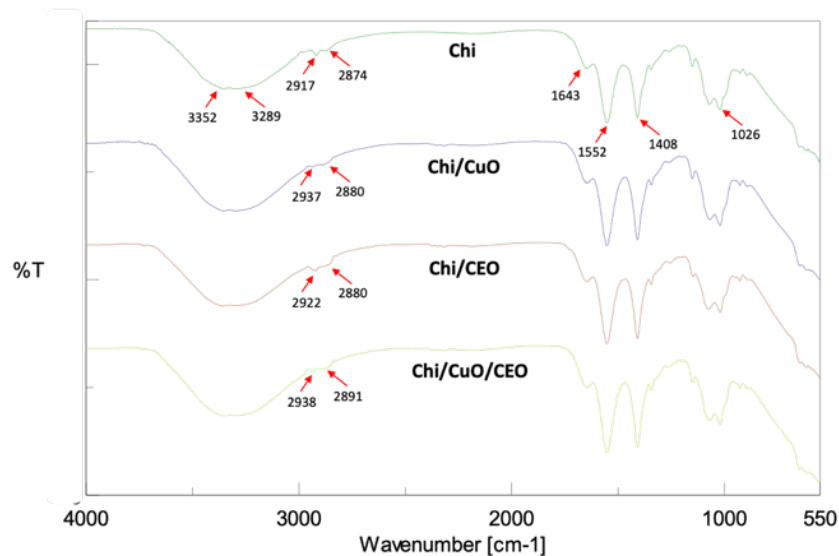
(c)

Fig. 3.2. AFM image of CuO (a), FTIR spectra of CuO and CEO (b), and FTIR spectra for coating films (c). The main IR spectrum of each sample were indicated by red arrow.

3.3.2. The effectiveness of CuO, and CEO dosage

The aim of this preliminary test was to select the optimum concentration of each material to form efficient coating films that had antifungal performance. The test was carried out using broth media. This type of assay may result in a higher accuracy among antifungal assay

techniques (Negi et al., 2012). Two-way ANOVA revealed that efficacy in spore germination and germ tube elongation differed significantly ($P < 0.05$) across the compared groups, both for *P. italicum* and *P. digitatum*. Significant differences in efficacy of CuO, and CEO dosage for 2 tested fungi were also observed *(P < 0.05)*. There was significant interaction between the given treatments and the fungal growth only for *P. digitatum*.

Table 3.1. Inhibitory effects of CuO, and CEO against *P. italicum* and *P. digitatum*

Dosage	Spore germination (%)		Germ tube elongation (*µ*m)	
	P. italicum	*P. digitatum*	*P. italicum*	*P. digitatum*
Control	97.5 ± 3.53[Aa]	98.5 ± 2.12[Aa]	160.83 ± 51.64[Aa]	238.52 ± 56.63[Aa]
CuO 0.006%	65 ± 7.07[Ab]	84.65 ± 7.56[Ab]	123.96 ± 35.21[Aa]	172.91 ± 19.71[Ab]
CuO 0.012%	12.5 ± 2.12[Ac]	54.75 ± 6.01[Ac]	25.03 ± 12.94[Bb]	85.76 ± 10.11[Ac]
CuO 0.025%	-	7.2 ± 1.69[d]	-	28.37 ± 7.62[d]
CuO 0.050%	-	-	-	-
CuO 0.075%	-	-	-	-
CEO 0.125%	93.5 ± 9.19[Aab]	97.2 ± 3.11[Aa]	176.90 ± 37.02[Aa]	204.54 ± 14.45[Aab]
CEO 0.25%	77.5 ± 3.53[Ab]	78.65 ± 1.91[Ab]	154.22 ± 48.11[Aa]	189.54 ± 8.38[Aab]
CEO 0.5%	56.5 ± 9.19[Ac]	59.35 ± 5.16[Ac]	136.23 ± 81.01[Aa]	158.67 ± 19.14[Ab]
CEO 0.75%	29.3 ± 4.66[Ad]	33.4 ± 1.27[Ad]	74.11 ± 40.14[Aa]	98.12 ± 40.77[Ac]

Different letters (small: among different treatments; capital: between *P. italicum* and *P. digitatum*) indicates statistically significant differences at *P* < 0.05.

Data shown in Table 3.1 confirms that spore germination and elongation of *Penicillium* spp. were dose dependent. The growth of spores was completely suppressed when the concentration CuO reached 0.025% and 0.050% respectively for each *P. italicum* and *P. digitatum*. A similar trend was obtained with antifungal activity of CuO against *Candida albican*, *Candida glabrata*, and *Candida tropicalis* were particle dosage dependent (Muñoz-Escobar and Lópes, 2020). Additionally, germination was also delayed when the level of CEO increased. In

order to form a compatible coating films based on 0.8% Chi, the concentration of 0.5% CEO was selected in accordance with a preliminary biofilm casting experiment. Supported by these findings, we continued our investigation by selecting coating formulation from 0.8% Chi/0.025% CuO/0.5% CEO.

3.3.3. FTIR
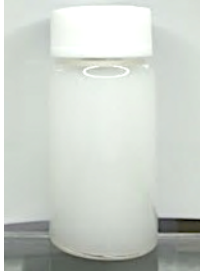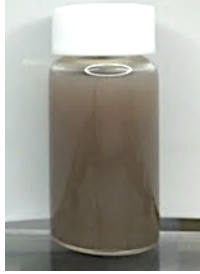
Fig. 3.2c shows *FTIR* spectra of the thin film samples. The attendance bands of Chi were present in all the samples, which were at 3289 and 3352 cm^{-1} for stretching vibrations of O–H and N–H bonds, at 1643 cm^{-1} for N–H bending (amide II), at 1552 cm^{-1} for C=O stretching (amide I), at 1408 cm^{-1} for stretching vibrations of C-N, and at 1026 cm^{-1} for stretching vibrations of C-O-C of Chi. The similar result was found by Shen and Kamdem (2015), the bands appeared at 1643 and 1552 cm^{-1} showed in a marked increase in those films containing EO compared with pure Chi. In comparison with Chi, the bands ranging from 2874 – 2891 cm^{-1}, indicating CH stretching peak, became more flattened when CuO was included. However, the addition of CEO resulted stronger intensity due to the increased in the content of ester groups from the CEO molecule. At the same time, the similar trend occurred at around 2917 - 2938 cm^{-1}. Those may be as a result of interaction between Chi and CEO through hydrogen bonding between the OH group in functional groups from oil and the NH and OH groups in Chi (Shen and Kamdem, 2015). The spectra of CuO were hard to find any characteristics both for Chi/CuO/CEO and Chi/CuO films which might as the consequence of the little chemical interaction occurred. Furthermore, the absence of CuO peaks suggested the involvement of Chi functionalities to the surface of CuO particles (Javed et al., 2021). All the changes indicated that intermolecular interaction and molecular compatibility among Chi, CuO, and CEO particularly may exist.

3.3.4. Optical properties

Visual appearance, color properties, light transmission, and either opacity or transparency, are important features of food packaging materials, because consumer's preference for food products is highly affected by optical properties (Ortega et al., 2017). The visual appearance of samples is shown in Table 3.2. It was readily observed that Chi showed clear and transparent solutions compared with the others. The turbidity of the Chi solution progressively increased when CuO, CEO, and CuO/CEO were incorporated. This was due to dispersion of the particles in solution. Furthermore, a browner color of the solution was markedly observed in the Chi solution containing CuO. This was more likely related to the natural color of CuO. Therefore, the addition of CuO, CEO and CuO/CEO played an essential role in the visual appearance of the resulting solution.

L^*, a^*, b^* values, and ΔE of the samples are presented in Table 3.2. All samples showed difference in color values ($P < 0.05$). The highest L^* was found in the Chi sample ($P < 0.05$), whereas the other solutions showed lower L^* values, particularly the solution containing CuO. Differences in L^* might be due to difference in light scattering among the samples. The a^* value of Chi/CuO, and Chi/CuO/CEO was higher than the Chi sample ($P < 0.05$) reflecting the natural color (dark brown) of CuO as seen in visual appearance. The decreases in L^* and the increases in b^*- and a^*- values of Chi containing CuO, which finally resulted in an increase in ΔE, were noticeable in Chi/CuO and Chi/CuO/CEO sample. Therefore, the incorporation of CuO had an impact on the color of the solution.

Table 3.2. Physicochemical properties of the coating and film

Characteristic	Chi	Chi/CuO	Chi/CEO	Chi/CuO/CEO
Visual appearance				
Color				
L^*	93.44 ± 0.24^a	46.32 ± 3.51^c	92.96 ± 0.21^a	51.5 ± 2.79^b
a^*	-1.28 ± 0.16^a	4.42 ± 0.24^a	-1.2 ± 0.14^a	3.78 ± 0.63^a
b^*	12.06 ± 1.73^c	15.02 ± 1.56^b	13.66 ± 1.79^{bc}	22.66 ± 1.31^a
ΔE	8.16 ± 1.56^b	49.94 ± 2.78^a	9.80 ± 1.58^b	47.27 ± 2.76^a
Light transmission at various wavelength (%)				
300	31.51 ± 0.50^a	1.75 ± 0.14^c	6.93 ± 0.34^b	0.35 ± 0.22^d
350	48.12 ± 1.42^a	10.58 ± 0.02^c	15.1 ± 0.13^b	0.87 ± 0.31^d
450	75.95 ± 0.11^a	23.62 ± 0.01^c	28.76 ± 0.02^b	15.84 ± 0.01^d
600	79.57 ± 0.08^a	34.81 ± 0.01^c	32.28 ± 0.02^b	29.52 ± 0.02^d
800	77.68 ± 0.08^a	59.82 ± 0.01^c	35.59 ± 0.01^b	43.08 ± 0.02^d
Transparency	1.71 ± 0.01^d	7.63 ± 0.01^a	6.13 ± 0.01^c	6.97 ± 0.01^b
Apparent viscosity (cP)	22.68 ± 0.16^c	26.04 ± 0.59^b	26.88 ± 0.09^a	26.44 ± 0.24^{ab}
pH	5.65 ± 0.02^a	5.65 ± 0.01^a	5.62 ± 0.01^a	5.63 ± 0.01^a
Zeta potential (mV)	$+47.71 \pm 1.51^a$	$+48.66 \pm 1.03^a$	$+28.92 \pm 2.82^b$	$+22.94 \pm 1.01^c$
Roughness (nm)				
Ra	5.55 ± 1.08^a	3.92 ± 4.01^{ab}	2.14 ± 0.44^b	3.85 ± 3.43^{ab}
Rq	6.95 ± 1.55^a	2.85 ± 1.26^b	2.56 ± 0.47^b	2.65 ± 2.36^b

Different letters indicates statistical significant differences at $P < 0.05$.

The addition of oil and nanoparticles influenced the transparency and light transmission. As given in Table 3.2, the neat Chi film showed very high transmittance. However, a dramatic

decrease was exhibited in the transmittance value at various UV and visible wavelengths, when CEO was added. Yao et al. (2017) explained that it was attributed to the presence of oil droplets in polymer film leading to scattering of the light, and finally the opacity increased. It could be assumed that CEO-loaded Chi film had higher barrier properties for UV and visible light. Furthermore, a significant decrease in light transmission and transparency were also demonstrated by incorporating CuO. This was due to the natural properties of CuO, which might facilitate the diffuse reflection of light. In addition, a decrease in transmittance value was attributed to a consequence of the crystalline structure of metallic nanoparticles (Vejdan et al., 2016). A similar downward trend was documented by Vejdan et al. (2016) when gelatin/agar film incorporated TiO_2 nanoparticles.

3.3.5. *Apparent viscosity*

The apparent viscosity of the coating solutions is given in Table 3.2 and ranged from 22.68 to 26.88 cP and increased significantly, compared with Chi alone, by the incorporation of CuO and CEO. When oil was added to an oil-in-water emulsion system, the viscosity of the solution tended to increase (Bonilla et al., 2012). Another mechanism was possibly due to the ability of Chi matrix in stabilizing oil droplets by amphiphilic action. Moreover, the increase in apparent viscosity was significantly ($P < 0.05$) affected by loading of CuO, which was in agreement with a previous study (Namburu et al., 2007). However, the intermolecular interaction between the OH group from oil and the NH and OH groups in Chi through hydrogen bonding might be interrupted by the presence of CuO. *FTIR* analysis (Fig. 3.2) verified that the interaction of Chi functionalities to the surface of CuO particles may exist causing a slightly drop of the viscosity of Chi/CuO/CEO compared to Chi/CEO coating solution.

3.3.6. pH and zeta potential

The pHs of coating solution are shown in Table 3.2. No difference in those samples ($P >$ 0.05) was observed. It was confirmed that CuO and CEO did not affect pH of solutions. The microbial inhibitory properties of Chi based coating is higher at low pH (below 6) due to the ionized of amino groups. The effects of different formulations on zeta potential are summarized in Table 3.2. Zeta potential refers to the density of the surface charge and is influenced by the composition of the particles and the suspension in which they are dispersed (Al-Kassas et al., 2016). The zeta potential of Chi and Chi/CuO was +47.71 ± 1.51 and +48.66 ± 1.03 mV, respectively, which means that they may be stable for a prolonged time. Generally, the zeta potential of the solution is over +30 mV or below -30 mV, resulting in a physically stable solution due to electrostatic repulsion (Chu et al., 2020). The opposite behavior when the zeta potential of the solution is in the range of +30 mV and −30 mV, the aggregation of particles will be occurring (Carneiro-da-Cunha et al., 2011). The results are in agreement with the value obtained by previous researchers who reported that zeta potential of Chi solutions were ranging between +31.6 and +63.5 mV (Vargas et al., 2009; Carneiro-da-Cunha et al., 2011). Generally, the presence of nanoparticles in Chi solution may enhance the solution stability due to the accumulation of positively charged between nanoparticles and Chi (Du et al., 2009). The incorporation of CEO into Chi solutions led to a decrease in zeta-potential when compared with Chi and Chi/CuO. This can be explained by the reduction in electrostatic repulsion caused by the positive charge of the amino group of Chi was occupied and partially neutralized by the carboxylate group of the EO (Vargas et al., 2009).

3.3.7. Oil droplets

Oil droplets formed in the coating solution were visualized using fluorescence microscopy. This method was important to confirm easily and clearly the distribution of dispersed phase (oil) in the emulsion system of the coating solution. Bright field and fluorescence images of each coating stained with Nile red dye are presented qualitatively in Fig. 3.3. Lipid droplets contained in Chi/CEO and Chi/CuO/CEO samples exhibited red color indicating that an oil-in-water emulsion type existed. However, the smaller size of oil droplet was not clearly distinguished in the image. Colucci et al. (2020) explained that using the fluorescence method the dispersed phase was not clearly perceptible once it had sizes lower than 2μm.
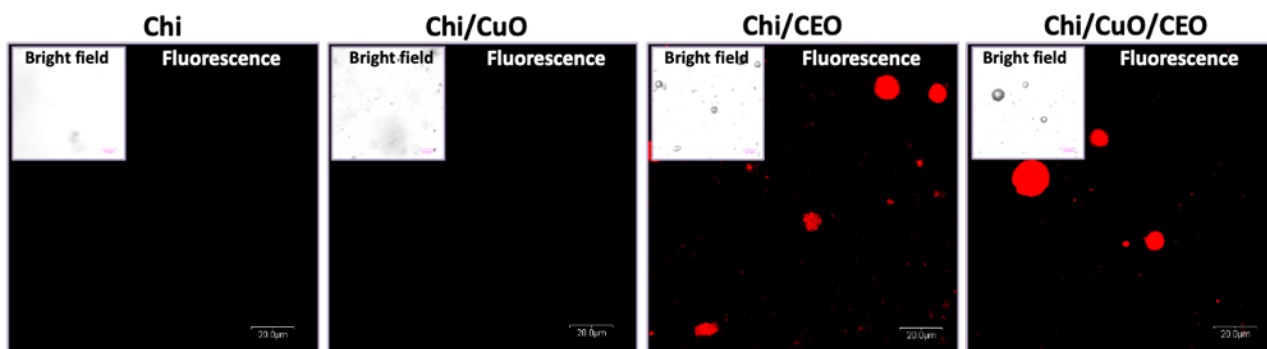
Fig. 3.3. CLSM photographs to confirm distribution and emulsion droplets of CEO.

3.3.8. AFM

The surface topography of the films affected by the incorporation of CuO and CEO were determined using *AFM*, as displayed in Fig 3.4. The *AFM* image (3D) clearly showed different morphologies in each dried coating solution. Spherical shaped structures distributed in Chi/CuO and Chi/CuO/CEO samples indicated individual particles of CuO. However, less frequent nanoclusters in Chi/CuO/CEO samples were found, which might be due to the physical effect of

the emulsifier and oil. Surprisingly, there was a tendency for a decreasing *Ra* value and significantly so for *Rq* value after CuO addition into Chi. Although it was not clearly explained, a previous study reported that a film without the addition of other components tended to possess *Z* agglomerates allowing a rougher surface (Escamilla-García et al., 2017). The CEO-loaded Chi film displayed a smoother surface with homogeneous oil droplets dispersed uniformly resulting in *Ra* and *Rq* values that were significantly ($P < 0.05$) lower compared with pure Chi. The physical interaction between biopolymer and the liquid state of CEO molecules might contribute to make a smoother surface. This result was in agreement with an earlier study that homogeneous oil droplets occurred after drying leading them to fill in the irregularities on the film surface (Atarés et al., 2010). Further explanation was noted by Jahed et al. (2017), in which the stabilizing effect of emulsifier and oil was responsible and resulting in the formation of a smoother film surface.
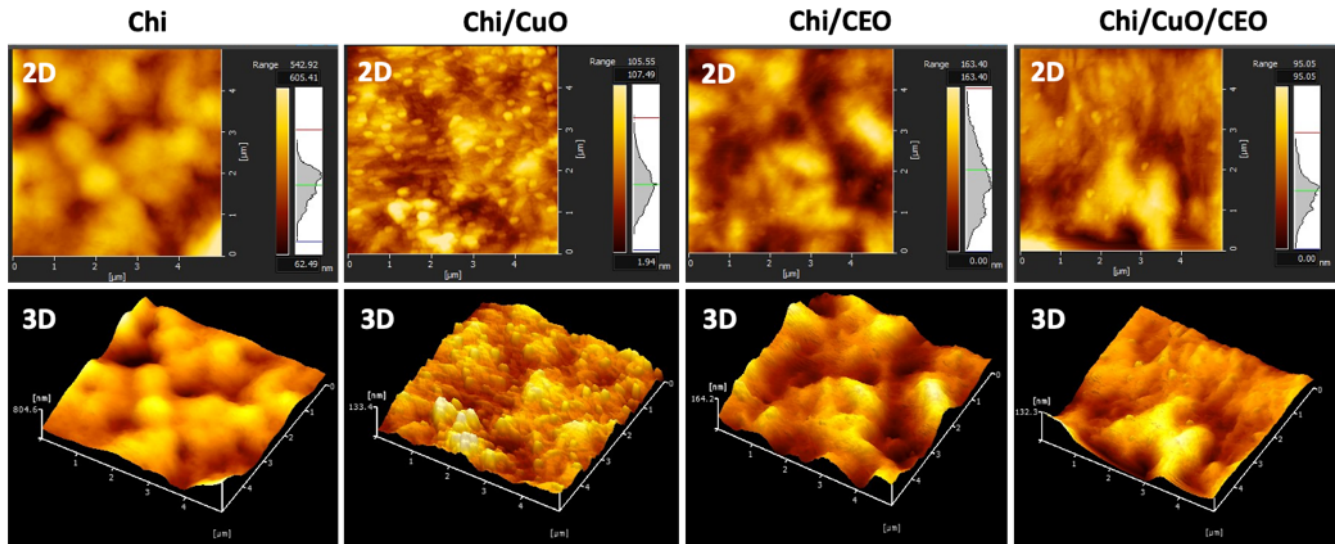
Fig. 3.4. *AFM* topography images.

3.3.9. SEM

SEM image characteristics of the cross-section of films are visualized in Fig. 3.5. The microstructure was qualitatively analyzed to explain the role both CuO and CEO in the structure of the Chi matrix. At a magnification 3000×, pure Chi and composite Chi/CuO films were relatively homogenous and with continuous structures. However, although the Chi/CuO film was relatively compact, a fragile appearance and slight disruption were observed, which might be due to the sample preparation process. When CEO was added, oval-shaped droplets of oil of various sizes were distributed across the film, as exhibited in the Chi/CEO and Chi/CuO/CEO films. Although flocculation and coalescence commonly occurred during the drying step of the film (Peng and Li., 2013), no destabilization phenomena of the emulsion system were indicated in this study. When the magnification was increased (25,000×), the CuO-loaded film images showed the presence of some CuO nanoclusters, indicating that CuO were successfully incorporated into the matrix of film with Chi/CuO and Chi/CuO/CEO. Those presence of CuO nanocluster indicated the biocompatibility of CuO-incorporated Chi biopolymer and increased the antifungal action of Chi based film which is discussed in the next chapter.
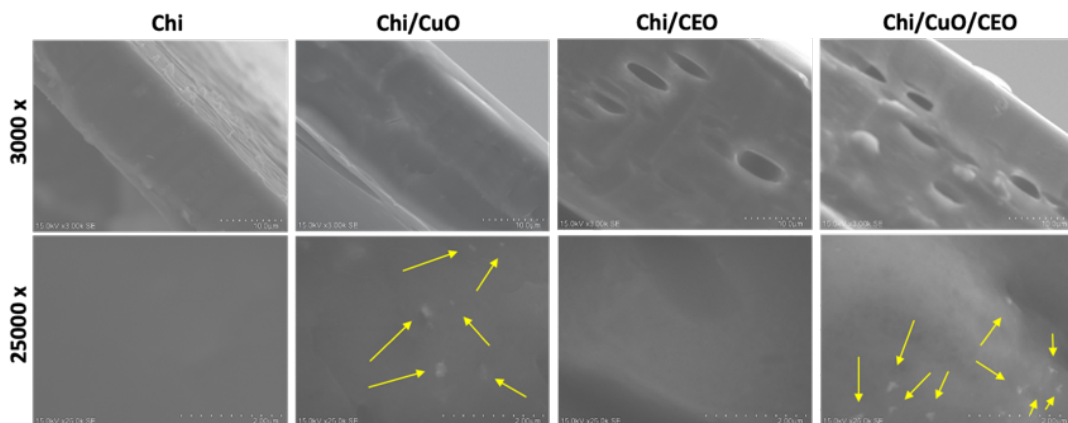
Fig. 3.5. Longitudinal cross section of *SEM i*mages. CuO nanoclusters were indicated by yellow arrow.

3.3.10. Effect of coating treatment on spore germination

The spore germination of *Penicillium* spp. in broth medium were controlled in response to the treatment with Chi/CuO/CEO, as demonstrated in Fig. 3.6. The small black spots, other than spores, seen in Chi/CuO and Chi/CuO/CEO samples indicated the agglomeration of individual CuO. Moreover, there were small droplets of dispersed CEO present in Chi/CEO and Chi/CuO/CEO. Spores readily germinated in the absence of coating treatment. In general, *P. digitatum* was more resistant for all of treatments than *P. italicum*. Spores readily germinated in the absence of coating treatment. No germinated spores were seen in the treated spore of *P. italicum*. The results indicated that Chi coating restricted the growth of spore significantly ($P < 0.05$) compared with the control. Improvement occurred when Chi was combined with CuO and CEO, the germinated spore of *P. digitatum* decreased significantly ($P < 0.05$). However, in this assay, the addition of CuO and CEO did not show a synergistic benefit for *P. italicum* compared with single CuO or CEO into Chi matrix. Surprisingly, the inhibition of mycelial growth when treated with CEO was slightly more effective than with CuO in combination with Chi, which was indirectly different to the earlier data (Table 3.1). The Chi/CuO-microbial penetration was probably lower compared with single CuO, resulting a lower efficacy, which was also noted in a previous report by Negi et al. (2012).
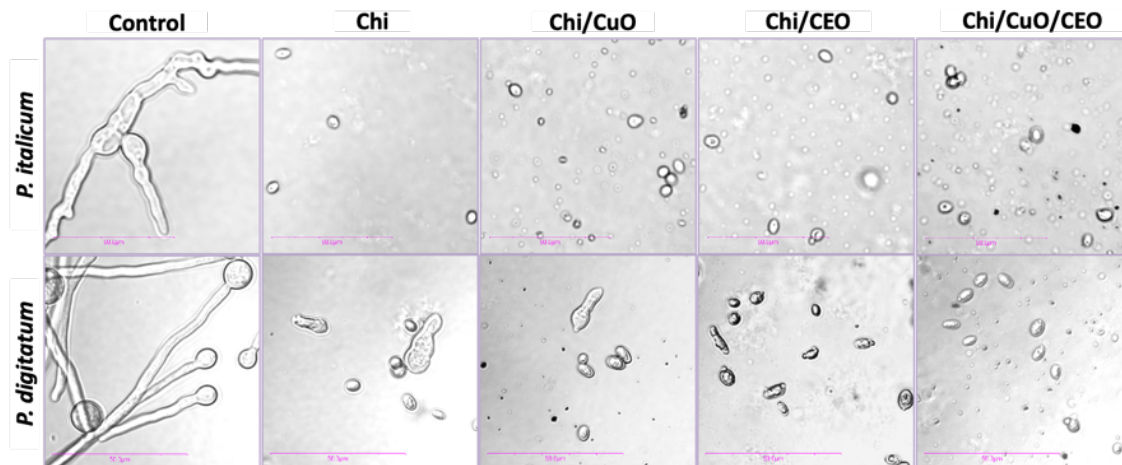
(a)
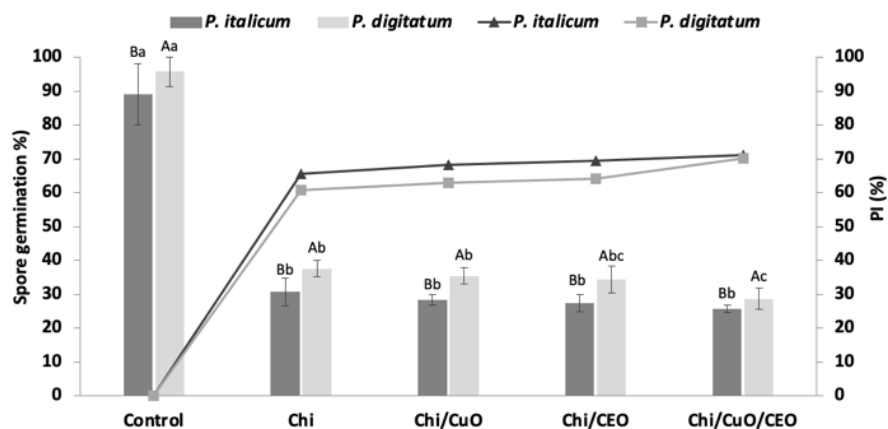
(b)

Fig. 3.6. Analysis for spore germination visually (a), and statistically (b). Different letters (small: among different treatments; capital: between *P. italicum* and *P. digitatum*) indicates statistically significant differences at $P < 0.05$.

3.3.11. *Membrane integrity of spores treated with coating solution*

This indicated that fungal spore germination was suppressed by coating solution treatment. Further investigation was carried out using a propidium iodide staining test to evaluate the loss of membrane integrity in *P. italicum* and *P. digitatum*. Propidium iodide can bind to

DNA in the fungi resulting in a specific color of fluorescence. The stain was unable of penetrating into healthy spores because of the membrane barrier (membrane impermeable dye) (Suzuki et al., 1997). Fig. 3.7 shows that no dye was observed in the absence of treatment, while the exposed spores were quite easily stained. Spores treated with Chi combined with CuO/CEO demonstrated a higher level of colored spore visually compared with Chi alone, representing better antifungal abilities. The result indicated that coating treatments interrupted the membrane integrity, resulting in metabolic disruption and the death of fungi, which were identified by green fluorescence.
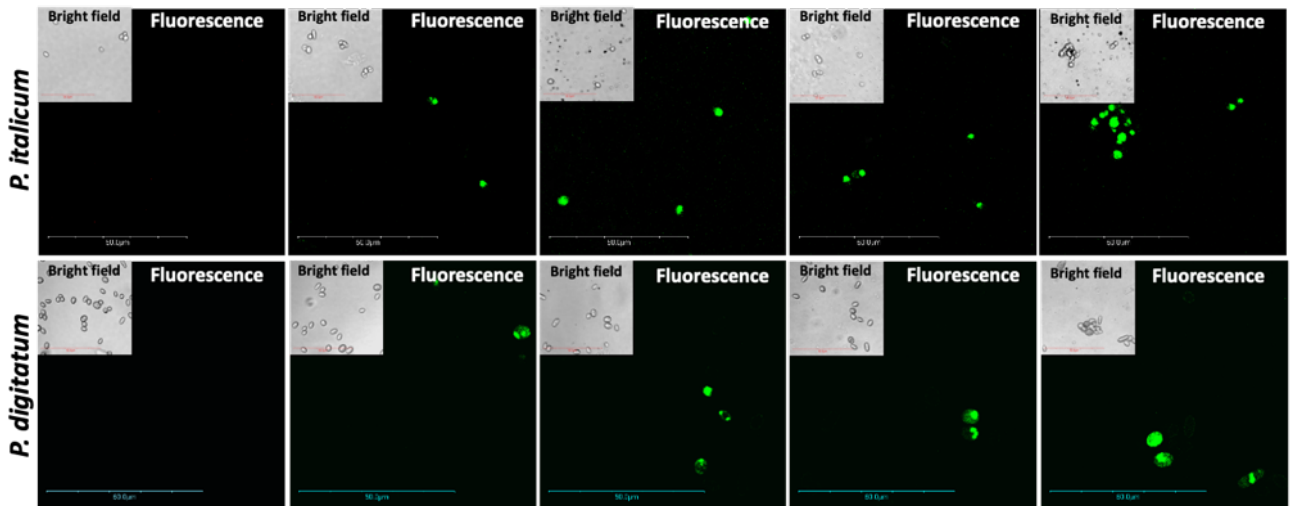
Fig. 3.7. Membrane integrity of *Penicillium* spp. Scale bars = 50 μm.

3.3.12. Efficacy of coating treatment in controlling mold infected in citrus fruit (in vivo)

Further investigation of the antifungal action of the coatings against *Penicillium* spp. was carried out using an in vivo test. Fig. 3.8a demonstrates visually that the symptoms and growth of blue mold on infected fruit increased during storage. Among the samples, extensive hyphae on control fruit appeared in the end of the storage period (day 6) with a diameter of 47.93 ± 2.53 mm for *P. italicum* and 35.05 ± 0.92 mm for *P. digitatum*. Hyphal fragments of *P. digitatum* was

more clearly seen than *P. italicum* on untreated citrus. The hyphal fragments were also observed

on fruit treated with Chi coating; however, the diameter was lower by 8.80 ± 6.28% and 26.04 ±

1.74% for each *P. italicum* and *P. digitatum* in comparison with the untreated sample.

Furthermore, even though almost no hyphae appeared visually on the surface of Chi/CuO treated

fruit; however, lesions occurred with a diameter of 32.03 ± 2.23 mm (PI = 32.97 ± 6.96%) and

19.03 ± 1.11 mm (PI = 45.68 ± 3.21%) on tangerine and tangelo respectively, which were

significantly lower than for Chi-treated fruit. Minor symptoms decreased significantly for

Chi/CEO-treated tangerines, with a diameter of 23.88 ± 3.32 mm (PI = 50.01 ± 7.86%). Fruits

showed the lowest fungal diameter and the highest inhibition when they were coated with

Chi/CuO/CEO. No fruit lesion extension occurred with this combination of Chi/CuO/CEO. It can

be assumed that at the end of storage, only Chi/CuO/CEO-coated fruit showed visual

acceptability. Likewise, by evaluating cross-section of coated fruit, fungal decay demonstrated a

deeper penetration in untreated samples than the coated fruits, and no fungal symptoms were

observed in Chi/CuO/CEO -coated tangerines. Overall, the combination of CuO and CEO

collaborated in increasing the antifungal action of Chi, as confirmed using the *in vivo* test. It

might be associated with the dissolution characteristics of the CuO due to environmental pH

(Table 3.2). Previous work found that at lower pH (<6), the concentration of dissolved Cu^{2+} ions

was higher than at pH 6–8 (Ko and Lee, 2010; Khan et al., 2019). Although the specific

mechanism has not been comprehensively documented, previous studies suggested that

microbial susceptibility to nanoparticles was more potent compared with their ions (Yan et al.,

2018). The hydrophobicity of CEO might increase at lower pH leading to dissolution of the

membrane lipids of the microorganisms (Negi, 2012; Navarro-Cruz et al., 2018). The synergistic

effect of CuO and CEO was showed in the in vivo test, which may significantly ($P < 0.05$)

inhibit fungal growth compared with Chi/CEO. The antifungal action of CuO probably involved more effective penetration when it was coated in the form of a solid than in a liquid phase (in *in vitro* test).
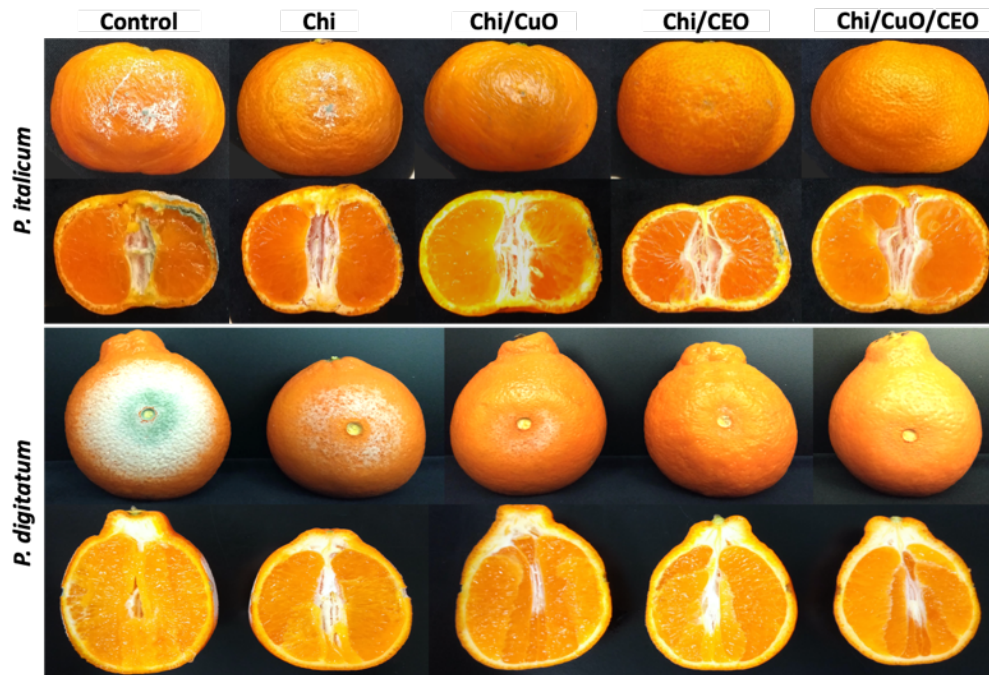
(a)
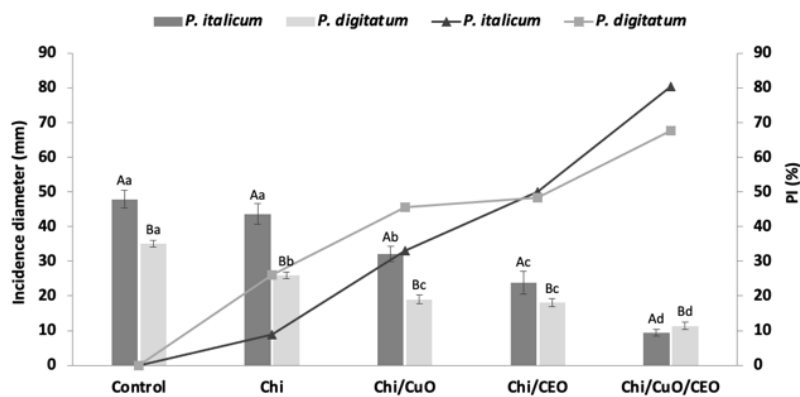
(b)

Fig. 3.8. Efficacy of various coating treatment on disease severity caused by *Penicillium* spp. visually (a) and statistically (b). Different letters (small: among different treatments; capital: between *P. italicum* and *P. digitatum*) indicates statistically significant differences at *P* < 0.05.

3.4. References

Al-kassas, R., Wen, J., Cheng, A. E., Kim, A. M., Sze, S., Liu, M., & Yu, J. (2016). Transdermal delivery of propranolol hydrochloride through chitosan nanoparticles dispersed in mucoadhesive gel. *Carbohydrate Polymers*, 153, 176–186.

Atarés, L., Bonilla, J., & Chiralt, A. (2010). Characterization of sodium caseinate-based edible films incorporated with cinnamon or ginger essential oils. *Journal of Food Engineering,* 100, 678–687.

Azam, A., Ahmed, A. S., Oves, M., Khan, M., & Memic. A. (2012). Size-dependent antimicrobial properties of CuO nanoparticles against Gram-positive and -negative bacterial strains. *International Journal of Nanomedicine*, 7, 3527-3535.

Baker, M. J., Trevisan, J., Bassan, P., Bhargava, R., Butler, H. J., Dorling, K. M., Fielden, P. R., Fogarty, S. W., Fullwood, N. J., Heys, K. A., Hughes, C., Lasch, P., Martin-Hirsch, P. L., Obinaju, B., Sockalingum, G. D., Sulé-Suso, J., Strong, R. J., Walsh, M. J., Wood, B. R., Martin, F. L. (2014). Using Fourier transform IR spectroscopy to analyze biological materials. *Nature Protocols*, 9, 1771–1791.

Bonilla, J., Atarés, L., Vargas, M., & Chiralt, A. (2012). Effect of essential oils and homogenization conditions on properties of chitosan-based films. *Food Hydrocolloids*, 26, 9–16.

Braga, P., Alencar, G., Alves, S., Fechine, J., Anderson, W., Paz, M., Câmara, S., Leite, E., & Souza, D. (2019). Application of coatings formed by chitosan and *Mentha* essential oils to control anthracnose caused by *Colletotrichum gloesporioides* and *C . brevisporum* in papaya (Carica papaya L .) fruit. *International Journal of Biological Macromolecules*, 139, 631–639.

Carneiro-da-Cunha, M. G., Cerqueira, M. A., Souza, B. W. S., Teixeira, J. A., & Vicente, A. A. (2011). Influence of concentration , ionic strength and pH on zeta potential and mean hydrodynamic diameter of edible polysaccharide solutions envisaged for multinanolayered films production. *Carbohydrate Polymers*, 85, 522–528.

Cheung, R. C. F., Ng, T. B., Wong, J. H., & Chan, W. Y. (2015). Chitosan: An update on potential biomedical and pharmaceutical applications. *Marine Drugs*, 13, 5156-5186.

Chu, Y., Gao, C., Liu, X., Zhang, N., Xu, T., Feng, X., Yang, Y., Shen, X., & Tang, X. (2020). LWT - Food Science and Technology Improvement of storage quality of strawberries by pullulan coatings incorporated with cinnamon essential oil nanoemulsion. *LWT - Food Science and Technology*, 122, 1-8.

Colucci, G., Santamaria-Echart, A., Silva, S. C., Fernandes, I. P. M., Sipoli, C. C., & Barreiro, M. F. (2020). Development of water-in-oil emulsions as delivery vehicles and testing with a natural antimicrobial extract. *Molecules*, 25, 5–7.

Costa, J. H., Wassano, C. I., Angolini, C. F. F., Scherlach, K., Hertweck, C., & Fill, T. P. (2019). Antifungal potential of secondary metabolites involved in the interaction between citrus pathogens. *Scientific Reports*, 9, 18647.

dos Santos, E. P., Nicácio, P. H. M., Barbosa, F. C., da Silva, H. N., Andrade, A. L. S., Fook, M. V. L., Silva, S. M. D. L., & Leite, I. F. (2019). Chitosan / essential oils formulations for potential use as wound dressing:physical and antimicrobial properties. *Materials*, 12, 1–21.

Du, W., Niu, S., Xu, Y., Xu, Z., & Fan, C. (2009). Antibacterial activity of chitosan tripolyphosphate nanoparticles loaded with various metal ions. *Carbohydrate Polymers*, 75, 385–389.

Escamilla-García, M., Calderón-Domínguez, G., Chanona-Pérez, J. J., Mendoza-Madrigal, A. G., Di Pierro, P., García-Almendárez, B. E., Amaro-Reyes, A., & Regalado-González, C. (2017). Physical, structural, barrier, and antifungal characterization of chitosan-zein edible films with added essential oils. *International Journal of Molecular Sciences,* 18.

FAO. 2016. Citrus fruit Fresh and processed statistical bulletin 2016. Available at http://www.fao.org/economic/est/est-commodities/citrus-fruit/en/ (accessed June 2, 20120).

Fidah, A., Salhi, N., Rahouti, M., Kabouchi, B., Ziani, M., Aberchane, M., & Famiri, A. (2016). Natural durability of cedrus atlantica wood related to the bioactivity of its essential oil against wood decaying fungi. *Maderas. Ciencia y tecnología,* 18, 567–576.

Ghorbani, H. R., Alizadeh, V., Mehr, F. P., Jafarpourgolroudbary, H., Erfan, K., & Yenageh, S. S. (2018). Preparation of polyurethane / CuO coating film and the study of antifungal activity. *Progress in Organic Coatings*, 123, 322–325.

Lyn, F. H., & Hanani, Z. A. N. (2020). Effect of lemongrass *(cymbopogon citratus)* essential oil on the properties of chitosan films for active packaging. *Journal of Packaging Technology and Research*, 4, 33–44.

Hosseinnejad, M., & Jafari, S. M. (2016). Evaluation of different factors affecting antimicrobial properties of chitosan. *International Journal of Biological Macromolecules*, 85, 467–475.

Jahed, E., Khaledabad, M. A., Bari, M. R., & Almasi, H. (2017). Effect of cellulose and lignocellulose nanofibers on the properties of *Origanum vulgare* ssp. *gracile* essential oil-loaded chitosan films. *Reactive and Functional Polymers*, 117, 70-80.

Javed, R., Rais, F., Kaleem, M., Jamil, B., Ahmad, M. A., Yu, T., Qureshi, S. W., & Ao, Q. (2021). Chitosan capping of CuO nanoparticles: Facile chemical preparation, biological

analysis, and applications in dentistry. *International Journal of Biological Macromolecules*, 167, 1452–1467.

Jeong, H.-U., Kwon, S.-S., Kong, T. Y., Kim, J. H., & Lee, H. S. (2014). Inhibitory effects of cedrol, β-cedrene, and thujopsene on cytochrome P450 enzyme activities in human liver microsomes. *Journal of Toxicology and Environmental Health, Part A*, 77, 1522–1532.

Kala, S., Sogan, N., Naik, S. N., Agarwal, A., & Kumar, J. (2020). Impregnation of pectin-cedarwood essential oil nanocapsules onto mini cotton bag improves larvicidal performances. *Scientific Reports*, 10, 1–12.

Kanashiro, A., M., Akiyama, D. Y., Kupper, K. C., & Fill, T. P. (2020). *Penicillium italicum*: An underexplored postharvest pathogen. *Frontiers in Microbiology*, 11, 606852.

Khan, R., Inam, M. A., Zam, S. Z., Akram, M., Shin, S., & Yeom, I. T. (2019). Coagulation and dissolution of CuO nanoparticles in the presence of dissolved organic matter under different pH values. *Sustainability*, 11, 2825.

Kingwascharapong, P., Arisa, K., Karnjanapratum, S., Tanaka, F., & Tanaka, F. (2020). Effect of gelatin-based coating containing frog skin oil on the quality of persimmon and its characteristics. *Scientia Horticulturae*, 260, 1-9.

Ko, C. K., & Lee, W. G. (2010). Effects of pH variation in aqueous solutions on dissolution of copper oxide. *Surface and Interface Analysis*, 42, 1128–1130.

Martínez-Camacho, A. P., Cortez-Rocha, M. O., Ezquerra-Brauer, J. M., Graciano-Verdugo, A. Z., Rodriguez-Félix, F., Castillo-Ortega, M. M., Yépiz-Gómez, M. S., & Plascencia-Jatomea, M. (2010). Chitosan composite films: Thermal, structural, mechanical and antifungal properties. *Carbohydrate Polymers*, 82, 305–315.

Namburu, P. K., Kulkarni, D. P., Misra, D., & Das, D. K. (2007). Viscosity of copper oxide nanoparticles dispersed in ethylene glycol and water mixture. *Experimental Thermal and Fluid Science*, 32, 397–402.

Navarro-Cruz, R., Ochoa-velasco, C. E., Caballero-alvarez, F. J., & Lazcano-hern, M. A. (2018). Effect of pH and mexican oregano (*Lippia berlandieri* Schauer) essential oil added to carboxymethyl cellulose and starch edible films on *Listeria monocytogenes* and *Staphylococcus aureus*. *Journal of Food Quality*. 2018, 1-6.

Naz, S., Gul, A., & Zia, M. (2020). Toxicity of copper oxide nanoparticles: A review study. *IET Nanobiotechnology*, 14, 1–13.

Negi, P. S. (2012). Plant extracts for the control of bacterial growth : Efficacy, stability and safety issues for food application. *International Journal of Food Microbiology*, 156, 7–17.

Orchard, A., Vuuren, S. F. Van, & Viljoen, A. M. (2019). Commercial essential oil combinations against topical fungal pathogens. *NPC Natural Product Communications*, 14, 151–158.

Ortega, F., Giannuzzi, L., Arce, V. B., & García, M. A. (2017). Active composite starch fi lms containing green synthetized silver nanoparticles. *Food Hydrocolloids*, 70, 152–162.

Papoutsis, K., Mathioudakis, M. M., Hasperué, J. H., & Ziogas, V. (2019). Nonchemical treatments for preventing the postharvest fungal rotting of citrus caused by *Penicillium digitatum* (Green Mold) and *Penicillium italicum* (Blue Mold). *Trends in Food Science & Technology*, 86, 479–491.

Panebianco, S., Vitale, A., Platania, C., Restuccia, C., Polizzi, G., & Cirvilleri, G. (2014). Postharvest efficacy of resistance inducers for the control of green mold on important Sicilian citrus varieties. *Journal of Plant Diseases and Protection*, 121, 177–183.

Peng, Y., & Li, Y. (2014). Combined effects of two kinds of essential oils on physical, mechanical and structural properties of chitosan films. *Food Hydrocolloids*, 36, 287–293.

Pham, N., Duong, M., Le, M., Hoang, H. A., & Pham, L. (2019). Preparation and characterization of antifungal colloidal copper nanoparticles and their antifungal activity against *Fusarium oxysporum* and *Phytophthora capsici*. *Comptes Rendus Chimie*, 22, 786–793.

Powers, C. N., Osier, J. L., Mcfeeters, R. L., Brazell, C. B., Olsen, E. L., Moriarity, D. M., Satyal, P., & Setzer, W. N. (2018). Antifungal and cytotoxic activities of sixty commercially - available essential oils. *Molecules,* 23, 1-13.

Muñoz-Escobar, A., & Reyes-Lópes, S. Y. (2020). Antifungal susceptibility of *Candida* species to copper oxide nanoparticles on polycaprolactone fibers (PCL-CuONPs). *Plos-One,* 15, 1–12.

Shao, X., Cao, B., Xu, F., Xie, S., Yu, D., & Wang, H. (2015). Effect of postharvest application of chitosan combined with clove oil against citrus green mold. *Postharvest Biology and Technology*, 99, 37–43.

Shen, Z., & Kamdem, D. P. (2015). Development and characterization of biodegradable chitosan films containing two essential oils. *International Journal of Biological Macromolecules*, 74, 289–296.

Shih, P., Liao, Y., Tseng, Y., Deng, F., & Lin, C. (2019). A potential antifungal effect of chitosan against *Candida albicans* is mediated via the inhibition of SAGA complex component expression and the subsequent alteration of cell surface integrity. *Frontiers in Microbiology,* 10, 1–14.

Suzuki, T., Fujikura, K., Higashiyama, T., & Takata, K. (1997). DNA staining for fluorescence and laser confocal microscopy. *Journal of Histochemistry and Cytochemistry*, 45, 49–53.

Talibi, I., Boubaker, H., Boudyach, E. H., & Aoumar, A. A. B. (2014). Alternative methods for the control of postharvest citrus diseases. *Journal of Applied Microbiology*, 117, 1–17.

Tongnuanchan, P., Benjakul, S., & Prodpran, T. (2012). Properties and antioxidant activity of fish skin gelatin film incorporated with citrus essential oils. *Food Chemistry*, 134, 1571–1579.

Vargas, M., Albors, A., Chiralt, A., & Gonzáles-Martínez, C. (2009). Characterization of chitosan – oleic acid composite films. *Food Hydrocolloids*, 23, 536–547.

Vejdan, A., Ojagh, S. M., Adeli, A., & Abdollahi, M. (2016). Effect of TiO_2 nanoparticles on the physico-mechanical and ultraviolet light barrier properties of fish gelatin/agar bilayer film. *LWT - Food Science and Technology*, 71, 88–95.

Yan, X., He, B., Liu, L., Qu, G., Shi, J., Hu, L., & Jiang, G. (2018). Antibacterial mechanism of silver nanoparticles in *Pseudomonas aeruginosa*: proteomics approach. *Metallomics,* 10, 557–564.

Yao, Y., Ding, D., Shao, H., Peng, Q., & Huang, Y. (2017). Antibacterial activity and physical properties of fish gelatin-chitosan edible films supplemented with D-Limonene. *International Journal of Polymer Science*, 2017, 1-9.

Zeng, K., Deng, Y., Ming, J., & Deng, L. (2010). Induction of disease resistance and ROS metabolism in navel oranges by chitosan. *Scientia Horticulturae*, 126, 223–228.

Zhang, Y. C., Tang, J. Y., Wang, G. L., Zhang, M., & Hu, X. Y. (2006). Facile synthesis of submicron Cu 2 O and CuO crystallites from a solid metallorganic molecular precursor. *Journal of Crystal Growth*, 294, 278–282.

CHAPTER 4

Antifungal features and properties of

chitosan/sandalwood oil Pickering emulsion

coating stabilized by appropriate cellulose

nanofiber dosage for fresh fruit application

4.1. Introduction

In recent years, due to growing environmental concerns, edible films and coatings have attracted interest in place of petroleum-based packaging. To achieve satisfactory characteristics, it is required that the selected biomaterials can form continuous network structures during the film-forming process. Among edible film-making materials (polysaccharides, proteins, and lipids), chitosan (Chi) has been receiving increasing research attention due to its favorable properties including biocompatibility and antimicrobial action (Shahidi et al., 1999; Coma et al., 2003). Despite the benefits have been demonstrated by Chi-based films and coatings, the use of pure Chi had a relatively limited antifungal activity (Kong et al., 2010). Efforts to overcome the Chi limitations, particularly antimicrobial improvements are ongoing (Elsabee et al., 2013).

Reports have documented improved methods in order to enhance Chi performance including by: oil incorporation (Shi et al., 2016; Deng et al., 2018); crosslinking (Alhwaige et al. 2013; Yeng et al., 2013); and blending with gelatin, quinoa protein, tara gum, and zein (Kong et al., 2010; Rivero et al., 2009; Medina et al., 2019; Antoniou et al., 2015). Incorporation of essential oil (EO) has gained considerable interest due to its efficacy in increasing the antimicrobial performance of Chi-based films and coatings (Valenzuela et al., 2013; Yuan et al., 2016). Indonesian sandalwood essential oil (SEO), extracted from *Santalum album* originating from the Papua area contains potential active compounds, such as α- and β-santalol. Earlier reports revealed the antifungal potency of SEO against *Trichophyton mentagrophytes* (Inouye et al., 2006), *Microsporum canis* (Nardoni et al., 2015), and *Trichophyton rubrum* (Kim et al., 2017). Furthermore, SEO, which is commonly utilized as a food flavoring and adjuvant, is permitted for use in food applications by the United States Food and Drug Administration (FDA),

Flavor and Extract Manufacturers Association (FEMA), and the Council of Europe (CoE) (Burdock and Carabin, 2008).

The development of essential oil-loaded biopolymer still remains a challenge due to its hydrophobic nature and volatility which reduce the stability and biological activity. The oil droplet size and distribution along longitudinal and transverse sections led to a reduction in the distance as a consequence of water evaporation via flocculation and/or coalescence pathways (Wang et al., 2013). To overcome these limitations, a proper emulsion technique is essential. Pickering emulsion offers a prospective method to enhance the stability of the emulsion system by utilizing solid particles instead of surfactants (Shi et al., 2016; Zou et al., 2019; Souza et al., 2021). The solid particles play a role in preventing the collision and aggregation of emulsion droplets by accumulation at the oil–water interface. Furthermore, that stability mechanism resulted in tight packing of irreversibly adsorbed particles at the interface thus reducing the diffusion surface area of lipid droplets (Liu et al., 2019). The use of polysaccharide-based emulsifiers such as nanocellulose has been gaining interest due to their prospective features including hydrophobicity, high adsorption capacity, biodegradability, and biocompatibility. An appealing aspect of nanocellulose is its anisotropic fiber structure, allowing for stabilization of the oil–water interface at very low loading levels (Lu et al., 2021; Seo et al., 2021).

In terms of preparation and application of nanocellulose-stabilized emulsions on fresh fruit commodities, only limited studies have been reported. Deng et al. (2018) found that the use of 0.1% cellulose nanocrystal, 3% oleic acid, and 2% Chi coating significantly ($P < 0.05$) delayed ripening and reduced senescent scalding of 'Bartlett' pears compared with Semperfresh™ coating during 3 months of storage (Deng et al., 2018). Jung and his coworkers (2020) investigated effect of Pickering emulsion coating of Bartlett' pears coated with 1% oleic

acid, 0.1% cellulose nanocrystal, and 2% Chi was suggested for delaying ripening and superficial scalding of 'fruit during the long-term cold storage (Jung et al., 2020). However, these studies provided no information on fruit disease inhibition offered by the emulsified coating, such as antifungal properties. In fact, fungi cause decay in a wide range of fruit commodities.

Unfortunately, regardless of cellulose having a positive effect on the emulsion stabilizer, fungi possess some capacity to degrade cellulose resulting in a chain of glucose units that can be used for energy. Fungi use extracellular enzymes, cellulases, to break down cellulose into smaller chains, including cellobiose or glucose allowing for uptake across cell walls and use for metabolism (Edwards et al., 2002; Lynd et al., 2002). Therefore, determining the appropriate concentration of cellulose nanofibers (CNFs) is necessary to produce the functional properties-improved coating film without reducing the antifungal feature from Chi/SEO composite coating. The objectives of this work were to: 1) develop an emulsified coating film formulation based on Chi and SEO using a Pickering emulsion approach with an appropriate level of CNF as a stabilizer, 2) study and compare the antifungal features against *Botrytis cinerea* and *Penicillium digitatum* and film properties of Chi, Chi/SEO, and Chi/SEOpick.

4.2. Materials and methods

4.2.1. *Materials*

Chitosan (Chi), Tween 80, and glacial acetic acid were obtained from FUJIFILM Wako Pure Chemical Corporation, Japan. CNF powder, made from wood-derived fiber, was obtained from Nippon Paper Industries Co., Ltd, Japan. That CNF was chemically treated by 2,2,6,6-tetramethylpiperidine-1-oxyl (TEMPO) catalytic oxidation method. Papua sandalwood essential oil (SEO) was obtained from Aromindo CV, Indonesia, with the two main contents, α-santalol

(19.36%) and β-santalol (16.48%), identified using a gas chromatography (GC)-mass spectrometer (Shimadzu QP 2010 Plus, Japan) equipped with capillary column of 0.25 mm i.d., length 30 m, film thickness 0.25 μm (DB-5MS column, J. & W. Scientific, USA).

4.2.2. *Preparation of SEO Pickering emulsions and coating*

The stabilized Pickering emulsion agent stock (CNF$_s$) was prepared by dispersing CNFs at various concentrations into distilled water using high speed stirring at 15,000 rpm for 1 min with a high-speed homogenizer (T 25 digital ULTRA-TURRAX® - IKA, Germany). At the same time, the SEO stock (SEO$_s$) solution was prepared using same procedure. Then, CNF$_s$, SEO$_s$, and distilled water were homogenized at 15,000 rpm for 5 min with a high-speed homogenizer to produce emulsion containing 0.5% SEO and various concentration of CNFs (0, 0.006%, 0.012%, 0.038%, 0.063%, 0.088%, 0.11%, 0.14%, 0.16%, 0.19%, 0.21%, 0.24%, 0.27%, 0.29%, and 0.31%). The emulsion containing 0.25% surfactant Tween 80 was used as a positive control representing a regular emulsion.

The stabilized Pickering emulsion coating film (Chi-SEOpick) was prepared by mixing SEO$_s$ (0.5%), and CNFs (0.24%) at 15,000 rpm for 3 min to form solid particles-stabilized SEO at the oil/water interface. The stabilized SEO droplets were inserted into the main matrix, Chi solution, using a homogenizer at 15,000 rpm for 2 min, then degassed in a vacuum oven (ADP300, Yamato Scientific Co, Ltd, Japan). Chi solution was prepared by gelatinizing Chi powder in glacial acetic acid solution (1% v/v) followed by adding 2 N NaOH solution until pH 6. For some analyses, the thin films were produced using the casting method on a silicon molds plate (8 × 8 cm), dried at 40°C for 15 h and peeled.

4.2.3. AFM

The CNF morphology and the coating roughness were measured using AFM (Hitachi 5200S, Japan) equipped with the Nano Navi Application program, operating in dynamic force mode. Respectively, 3 μL of CNF solution (0.01% CNF in distilled water) and 10 μL of coating solution were dripped onto freshly precleaned mica, and dried and stored in a silica gel-containing desiccator for 24 h before imaging. Samples were scanned in noncontact mode using a sharpened cantilever type SI-DF20, scanning frequency 0.7–0.84 Hz, and scanning area 2 μm $\times$ 2 μm. Roughness characteristics including root mean square deviation from the mean (Rq) and arithmetical mean deviation from the mean (Ra) were examined using ten replicates and calculated as follows:

$$Rq = \sqrt{\frac{1}{n} \sum_{i=1}^{n} Zi^2}$$

$$Ra = \frac{1}{n} \sum_{i=1}^{n} |Zi|$$

where Zi was the height deviation of i-th and n was the total of data points.

4.2.4. Emulsion stability and creaming behavior

The emulsion stability of the coating solutions were determined visually referring to the photographed images taken after 10 min, 14 and 30 days of storage in room temperature. The percentage of creaming index was calculated following the method from Wand and Hauzei (2016).

$$CI = \frac{HS}{HE} x100\%$$

where HS is the height of the emulsion layer, HE is the total height of the coating solution.

4.2.5. The microstructure and droplet size of Pickering emulsion layer

The oil droplet and layer of the Pickering emulsion were observed using CLSM with 20× objective lens (Olympus IX71, Japan). The top layer of the emulsion samples was stained with Nile red (FUJIFILM Wako Pure Chemical Corporation, Japan) solution (1 mg/mL in ethanol) to indicate the oil phase. CNFs were dyed with 0.1% acridine orange (FUJIFILM Wako Pure Chemical Corporation, Japan) before emulsion preparation. Then, 6 μL of each dyed sample was dropped gently onto a glass slide (Toshinriko, Japan) and covered with a thin coverslip (thickness ≈ 170 μm) (Matsunami, Japan). The mean of diameter of oil droplet size in the Pickering emulsions was measured with the aid of ImageJ software from 30 of individual droplets.

4.2.6. Antifungal assays

The agar dilution technique was used to test in vitro antifungal activities. Solid media was firstly prepared by mixing each coating solution and potato dextrose agar at a ratio of 1:1 and poured into sterilized petri dishes. After solidification, the 7-mm-agar disc with *P. digitatum* and *B. cinerea* mycelium, were placed on the center of each petri dish. Then they were incubated at 25°C and the diameter of the colony zone was measured after 5 days.

The antifungal action was also determined using a spore germination test. The spore solution 5×10^6 spores/mL of *P. digitatum* or *B. cinerea* from the National Institute of Technology and Evaluation, Biological Resource Center, Tokyo, Japan was mixed with distilled water (untreated sample) or coating solution, and potato dextrose broth (Difco™, USA) with a ratio 1:1:1. Fungal spores will break dormancy and begin to germinate once exposed to favorable

conditions. The germinated spore was evaluated under CLSM with a 50× objective lens after shaking-incubated for 24 hours, 100 rpm at room temperature.

$$Spore\ germination\ \% = \frac{Germinated\ spores}{Total\ spores} x\ 100\%$$

where the total spores of each observation were around 200-250 spores. The result was analyzed from triplicate observations.

The in vivo test was determined by observing the lesion diameter on tangerine and apple fruits. Fruits used in the protocol comply with relevant institutional, national, and international guidelines and legislation. Fresh fruits, purchased from local supermarket in Fukuoka, Japan, were washed into 1% sodium hypochlorite solution for 10 min followed by air drying. Each fruit was wounded using a sterile corkborer (4 mm diameter and 2 mm deep) in the central region. About 10 μL of the spore solution was deposited in each wound. After air drying for 5 h, the whole surfaces of fruits were sprayed evenly on each side (±2 mL/fruit) with distilled water (control) or coating solution, which was allowed to dry. Untreated and coated fruits were then kept at 25°C and 90% RH for 5 days. The percentage inhibition (PI) was also calculated for all antifungal assays.

$$PI\ \% = \frac{A-B}{A} x\ 100\%$$

where A is the maximum of the germinated spore (untreated sample) or lesion diameters and B is the germinated spore or lesion diameter obtained from each coating treatment. The result was analyzed from triplicate measurements.

4.2.7. Membrane integrity

Membrane integrity of *B. cinerea* and *P. digitatum* was evaluated by observing the uptake of propidium iodide (Sigma Aldrich, USA). The spore solutions were mixed with distilled

water (untreated) or coating solution followed by shaking-incubation for 4 hours, at 100 rpm, and at room temperature. Then, the samples were stained with 50 (mg L^{-1}) propidium iodide and examined using a CLSM with excitation and emission wavelengths of 543 nm and 585 nm. The dead cells were indicated by propidium iodide fluorescent staining.

Percentage of staining % $= \frac{Stained\ spores}{Total\ spores} x$ 100%

where the total spores of each observation were around 150-200 spores. The result was analyzed from triplicate observations.

4.2.8. *Color properties*

The film specimens were prepared on a standard white plate, followed by a color reader (Konica Minolta CR-20, Japan) measurement on five different spots per sample. The *CIE L*, a*, b** color method was used to measure *L** (lightness), *a** (green to red), and *b** (blue to yellow) values of the coating films. These values were further processed to obtained *ΔE** (color difference) value.

ΔE* $= \sqrt{(L_0 * -L *)^2 + (a_0 * -a *)^2 + (b_0 * -b *)^2}$

where $L_0, a_0,$ and b_0 come from a standard white plate, and the *L*, a*,* and *b** come from the values of the films.

4.2.9. *Light transmission and opacity*

Each thin film was firstly shaped into a rectangle. It was further attached on the cell side of a cuvette and the light transmission was read using a UV-Vis spectrophotometer (Jasco, V-530, Japan) at wavelength ranges of 200–800 nm. The opacity was determined using the following equation:

$$Opacity = \frac{(A600)}{x}$$

where *A600* is the absorbance at 600 nm and *x* is the film thickness (mm). Triplicate measurements were performed for each film specimen.

4.2.10. Mechanical properties

The coating films were cut into a 1 × 5 cm rectangle, and the thickness of the film was measured at five different positions. The coating films were further attached into grip pairs of the motorized force test stand (Shimpo, FGS-50E-L) equipped with digital force gauge (Shimpo FGPX-50). The initial gap separation was set to 30 mm, then stretched by moving the grip with a speed of 60 mm/s until breaking. The triplicate measurements were performed. Values for tensile strength and elongation were calculated using the following equations:

$$Tensile\ strength\ (MPa) = \frac{Fmax}{A}$$

where *Fmax* represents the max load (N) used to pull the film and *A* is the cross sectional area (m^2) of the film.

$$Elongation\ \% = \frac{Imax}{Io} x\ 100$$

where *Imax* represents the film elongation (mm) at that moment of rupture and *Io* is the original grip length (mm) of the film.

4.2.11. SEM

Thin coating films were pre-conditioned in a desiccator containing saturated salt of $Mg_2(NO_3)_2$, at 18 ± 2°C. The film specimens were placed on a specimen stub and coated in vacuum conditions with the aid of an osmium coater. Then, cross-section images were captured using a scanning electron microscope (SU3500, Hitachi, Japan) at 15 kV.

4.2.12. Statistical analysis

The experimental data were analyzed through analysis of variance (ANOVA) at a significance level of P-value < 0.05. Post hoc testing was performed using Duncan's multiple range test (DMRT) with the aid of Statistical Package for Social Science software (SPSS 17.0, SPSS Inc., USA).

4.3. Results and discussion

4.3.1. Materials characterization

AFM images were taken to confirm the morphology and dimensions in the CNF suspension, as shown in Fig. 4.1. CNFs exhibited a typical rod-like structure, and agglomeration between individual cellulose fibrils occurred in some regions. CNFs possess a diameter in the nanometer scale and length in the micrometer scale and have both crystalline and amorphous sections (Kafy et al., 2017). In this study, the width of CNFs was approximately 13.04–40.08 nm, with an average of 24.86 ± 10.01 nm. Heterogenous sizes were shown for the length of individual CNFs. Although the length of CNFs cannot be estimated properly from AFM, it may be considered that the length of CNFs was in the micrometer scale.
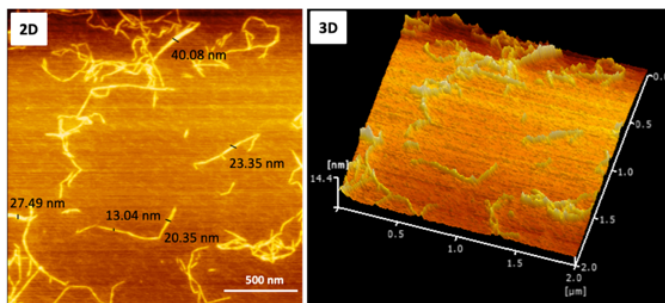

Fig. 4.1. AFM images represent the morphology of two- and three-dimensional of CNF.

4.3.2. Emulsion stability and creaming behavior

In this section, oil-in-water type emulsions were prepared by dispersing various levels of CNFs into aqueous solutions of Chi-SEO. Preliminary test was performed for emulsion stability and creaming behavior in selecting the optimum concentration of CNFs for further development of the coating film. Fig. 4.2a shows images of the emulsion samples at 10 min, and 14 and 30 days after preparation and with storage at ambient temperature. It was divided these into several groups according to the typical stability of each emulsion, and we named these groups I, II, III, and IV. Group I exhibited a creaming index of the emulsion in the absence of CNFs (0% CNFs), which did not affect emulsion stability leading to the formation of a cream layer upon storage (negative control). Group II showed a creaming index of emulsion mixtures in the presence of CNFs (0.006–0.21%). In this group, we determined that when CNFs were added, the emulsification capacity was improved, indicating that CNFs played an essential role in stabilization of the emulsion, as shown after 10 min of storage (Fig. 4.2b). Even though the creaming index was gradually augmented with increasing CNF concentration, the emulsion was not stable and clearly separated in two different phases, as demonstrated at 14 days (Fig. 4.2b). Group III demonstrates the creaming index of emulsion mixtures in the presence 0.24–0.31% CNF, demonstrating the absence of creaming after the storage period because of the emulsion-stabilizing effect of CNFs in the emulsion system. The ability of emulsion stabilization of Group III was the same as Group IV, which formed a regular emulsion (positive control). Considering the above results, we assumed that the use of 0.24% CNFs (from group III) was preferable from the stabilization improvement and economic point of view. Previous work investigated the stability mechanism of cellulose and found that cellulose adsorbed at the oil–water interface induced attraction and aggregation phenomena under the interfacial disturbance, as confirmed

with the interfacial rheological properties (Li et al., 2018). An improved stability mechanism was also proposed, which was related to the coverage effect from CNF–carboxymethyl CS complexes, allowing irreversible adsorption on a beeswax–water interface preventing coalescence or creaming as a result of the dense three-dimensional network (Xie et al., 2020).
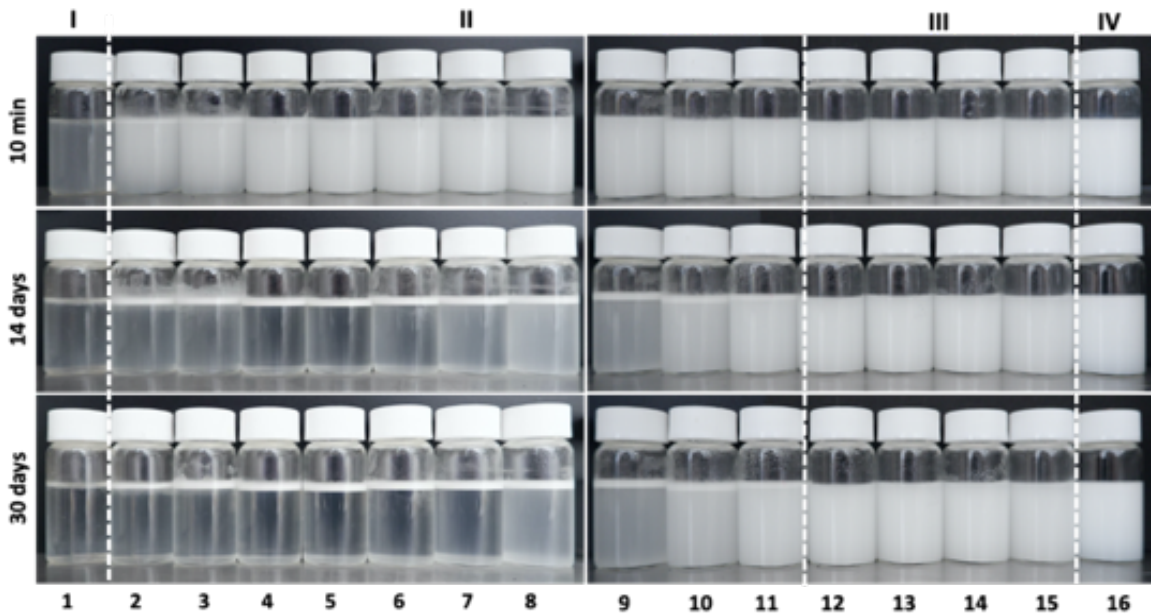
(a)
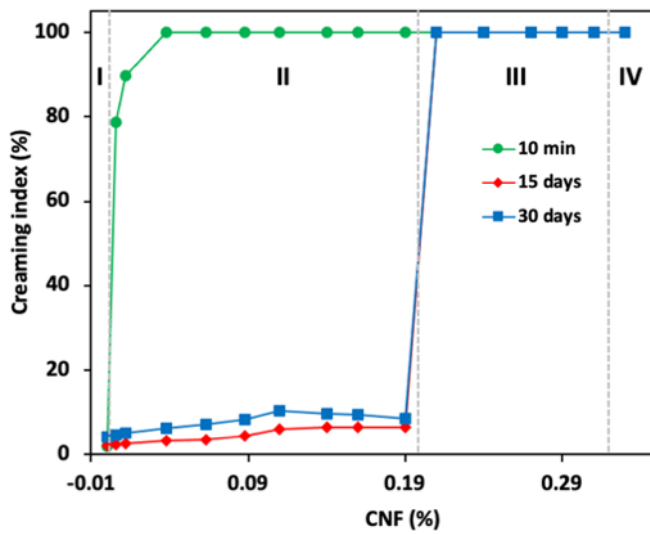
(b)
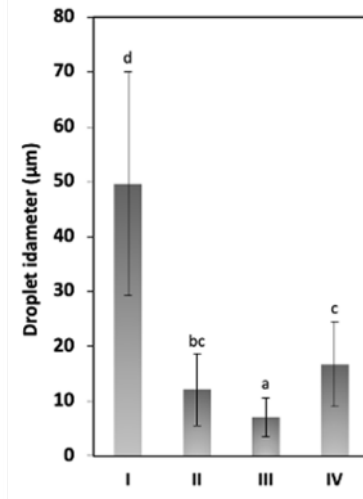
(c)
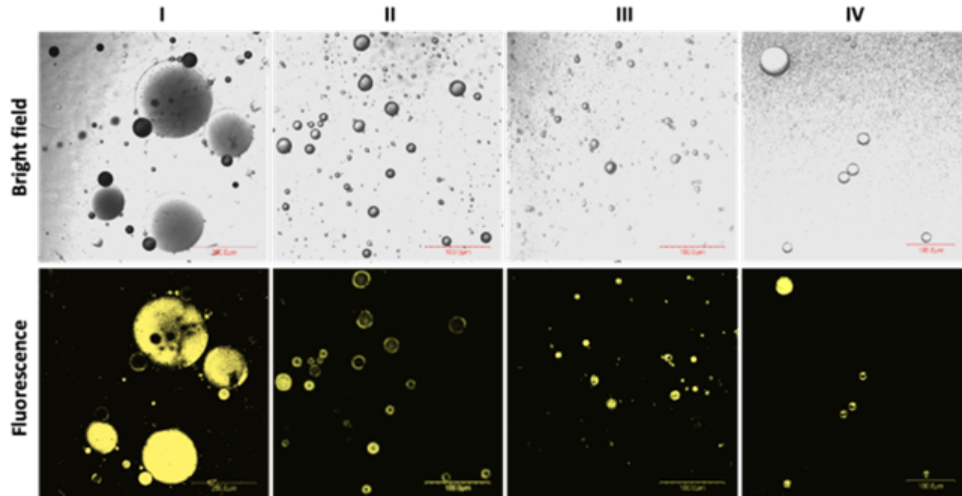
(d)
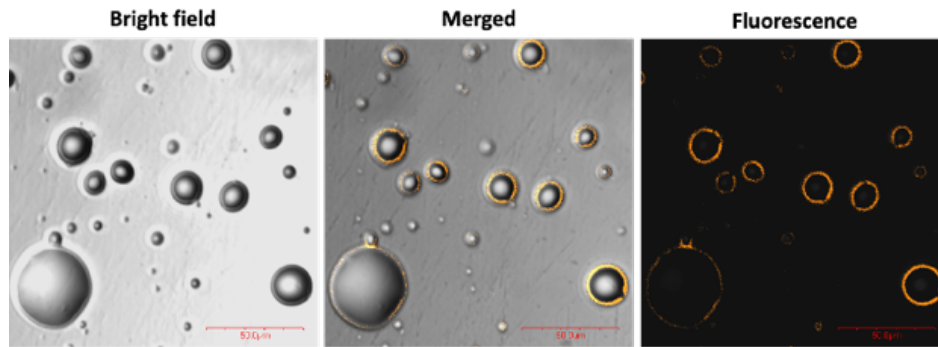
(e)

Fig. 4.2. a) Visual appearance of CNF-stabilized Pickering emulsions containing 0.5% SEO and CNF at various concentration of: $0, 0.006, 0.012, 0.038, 0.063, 0.088, 0.11, 0.14, 0.16, 0.19, 0.21, 0.24, 0.27, 0.29, 0.31\%$ (from left to right, 1-15), and regular emulsion (16), and (b) their creaming index properties. (c) droplet size distribution of emulsion, (d) confocal images of emulsion at day 7 after preparation, and (e) CNF-stabilized Pickering emulsion. The CNF was stained with acridine orange. Different letters indicate statistically significant differences at $P < 0.05$.

4.3.3. *Morphology and droplet size*

The microstructure of emulsified coating samples was investigated using confocal laser scanning microscopy (CLSM) obtained from the top creaming layers of the emulsion system. Obviously, the emulsion droplets were distributed in the CLSM photograph, the droplets had a spherical shape with various particle sizes ranging from 7.02 to 49.63 μm (Fig. 4.2c). Fig. 4.2d shows that with increasing contents of CNFs, the droplets size gradually decreased compared with both negative and positive control emulsions. Notably, the oil droplet size in group III was more homogeneously distributed and significantly ($P < 0.05$) lower that regular emulsion. It indicated that CNFs had an important role in preventing the collision and aggregation of emulsion droplets by their accumulation at the oil–water interface. Again, the above results suggested that the incorporation of 0.24% CNFs may be an ideal stabilizer candidate to maintain demulsification of the coating film solution.

4.3.4. *The morphological structure of Pickering emulsion stabilized by CNFs*

CLSM was used to further understand the deeper morphological structure of Pickering emulsions and the location of CNFs in the emulsion system. Morphology monitoring using CLSM revealed that orange fluorescence indicating acridine orange stained-CNFs lay at the surface of the dispersed phase, thereby stabilizing the oil droplets. As seen in Fig. 4.2e in bright field mode, the distribution of spherical droplets of SEO was clearly captured. When monitored using merged mode, orange fluorescence from acridine orange stained-CNFs lay in the surface of the dispersed phase. In the fluorescence image, orange circles around spherical droplets were more clearly observed at SEO–water boundaries. This use of CLSM to confirm the template of the Pickering emulsion agent was also reported for zein particles stained with Nile blue A (Shi et

al., 2016), CNFs and nanocrystals stained with calcofluor white (Bai et al., 2018), and nanocellulose stained with acridine orange (Fujisawa et al., 2021).

4.3.5. *Effect of coating treatment on mycelial growth inhibition*

B. cinerea and *P. digitatum* are regarded as the most important fresh fruit fungal pathogens; therefore, in this study the inhibition of fungal growth was tested. The mycelial growth and extension of *P. digitatum* and *B. cinerea* in solid medium were controlled in response to the coating treatment, as demonstrated in Fig. 4.3.
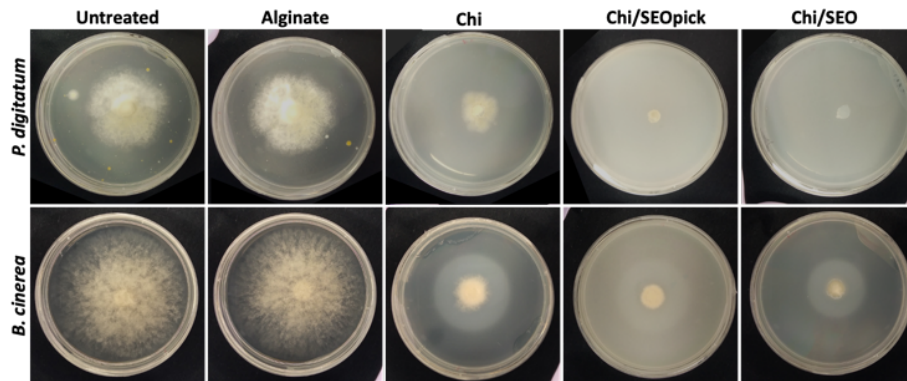
(a)
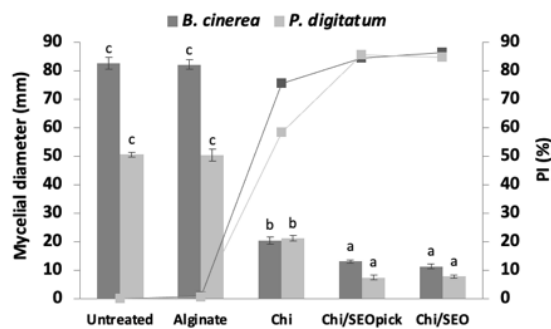
(b)

Fig. 4.3. Influence of coating treatment on mycelial growth inhibition visually (a) and statistically (b) in the day 5. Different letters indicate statistically significant differences among different treatments at $P < 0.05$.

The results indicated that coating restricted the spread of mycelia significantly ($P < 0.05$) compared with the untreated and alginate representing the common commercial edible coating . Improvement occurred when Chi was combined with SEO, mycelium extension decreased significantly ($P < 0.05$) at the end of incubation. There was no significant difference ($P > 0.05$) when the CNFs was loaded.

4.3.6. *Effect of coating treatment on fungal growth*

Visually, *B. cinerea* spores were more susceptible in the presence of coating solution than those of *P. digitatum* (Fig. 4.4a). All spores germinated easily when the coating treatment was absent. No completely germinated spores were observed among the treated spores of *B. cinerea*, even though some Chi-treated spores were seen starting to germinate, as indicated by swelling of the spores. A spore was categorized as germinated when the longest germ tube length was equal to or greater than the largest dimension of the swollen spore (Dantigny et al., 2006). It can assume that the use of Chi alone without the addition of EO was sufficient to suppress *B. cinerea* spore growth. However, it was slightly different compared to the mycelial growth inhibition. The Chi-microbial penetration was probably lower compared with the liquid phase, resulting a lower efficacy (Fig. 4.3). Proposed mechanisms have been documented to explain the antifungal performance of Chi, including: electrostatic interactions between positively charged Chi molecules and negatively charged fungal cell walls resulting in ionic imbalance (Liu et al., 2007; Jayaraj et al., 2009); intracellular interactivity of Chi and DNA allowing the disruption of mRNA and protein synthesis (Avadi et al., 2005; Zhang et al. 2011); and the chelating ability of Chi for metals that are essential as microbial nutrients (Torres et al., 2006; Jiang et al., 2012).

(a)

(b)

(c)

(d)   (e)
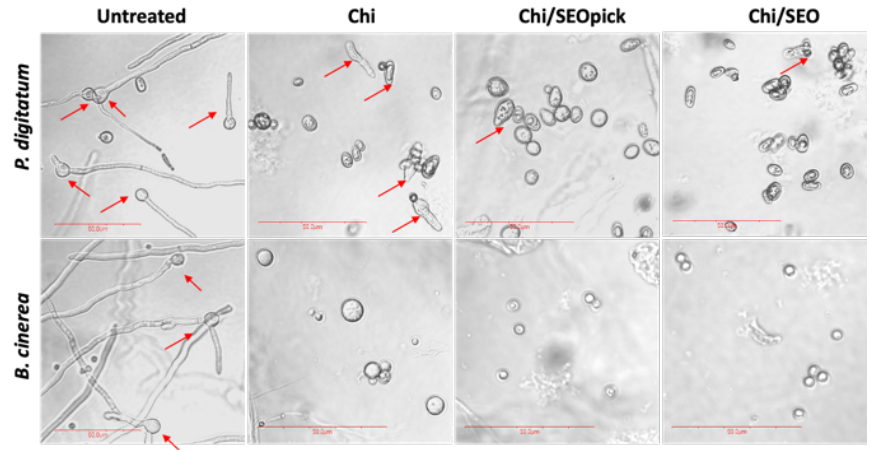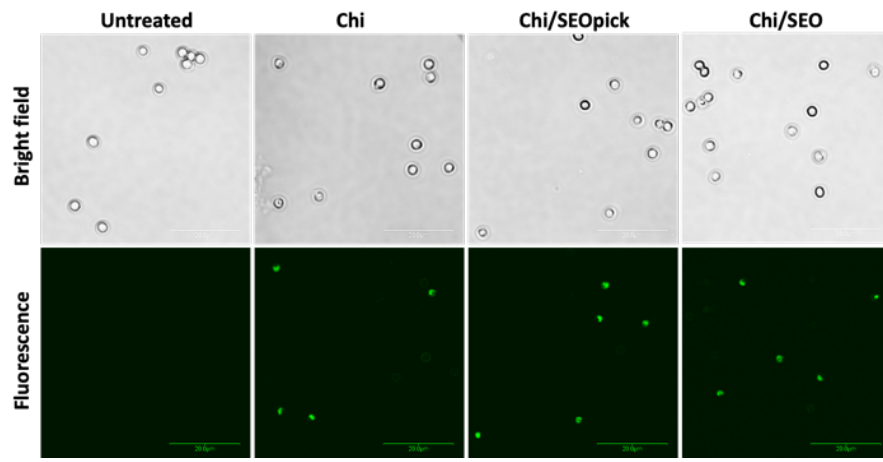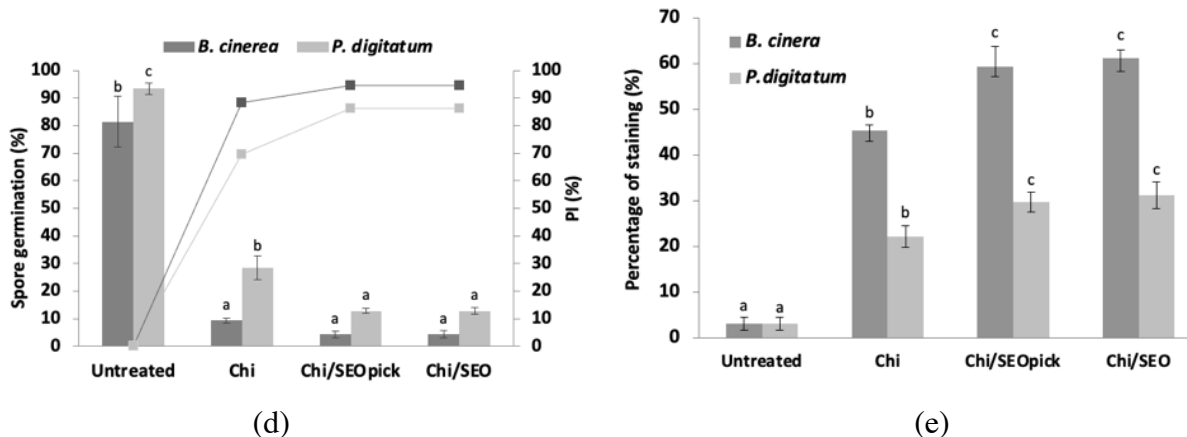
Fig. 4.4. Effect of coating treatment for the decrease in spore survival of *P. digitatum* and

B.cinerea visually (a) and statistically (d). Detection of membrane integrity visually of

P.digitatum (b), *B. cinerea* (c), and statistically (e). Different letters indicate statistically

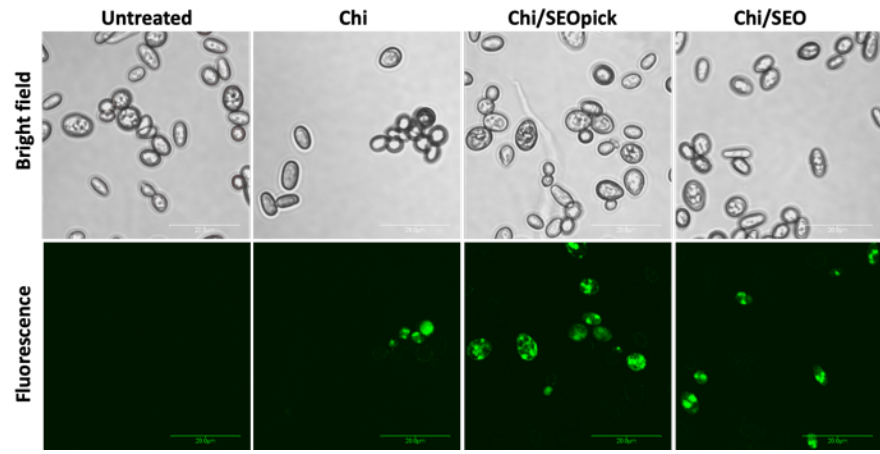significant differences among different treatments at $P < 0.05$.

Unlike spores of *B. cinerea*, some spores of *P. digitatum* were able to germinate, as indicated with red arrows, and the number was reduced with the incorporation of SEO into Chi, indicating higher inhibition. Statistically, comparing with untreated spores, the inhibition of spore germination of *B. cinerea* treated with Chi increased dramatically by 88.32% (Fig. 4.4d). No difference in spore survival inhibition was seen when Chi was augmented with SEO and CNFs. In the case of *P. digitatum*, Chi-coating treatment also effectively reduced percentage of spore germination from 93.5% (untreated) to 28.41% (Chi treated), with percentage inhibition (*PI*) a value 69.55%. Furthermore, SEO-containing Chi showed synergistically improved antifungal performance that inhibited the growth of *P. digitatum* spores with 12.87% germination and a *PI* value 86.24%. There was no significant difference ($P > 0.05$) when the Pickering emulsion agent, CNFs, was added. Similar findings have been reported when lemongrass or clove EO was entrapped in Chi (Shao et al., 2015). The active components, α- and β-santalol, are believed to be potent antifungal agents contained in SEO. These sesquiterpenoid compounds

may disturb fungal cell wall synthesis and have been confirmed by the occurrence of abnormal swelling and curling of terminal hyphae of test fungi (Kim et al., 2017). Notably, no difference was found when a Pickering emulsion agent, CNFs, was added. Naturally, cellulose can be used by fungi for energy. Chains of glucose units obtained from cellulose degradation using extracellular cellulases is taken up across the fungal cell wall and metabolized (Lynd et al., 2002; Edwards et al., 2008; Treserder et al., 2015). There are two proposed possibilities associated with these phenomena, (1) the use of CNFs in this study was at appropriate concentration as a Pickering agent without reducing the antifungal features of the Chi-SEO composite coating, and (2) CNFs may inhibit the loss of SEO by protecting the oil droplets from environmental exposure.

4.3.7. *Effects of coating on fungal membrane permeability*

A propidium iodide staining test was used to better confirm the effects of coating treatment for the loss of membrane integrity in fungal spores. Propidium iodide can penetrate dead cells with damaged plasma membranes, resulting fluorescent staining (Jiamprasertboon et al., 2019; Kringel et al., 2020). As a result, untreated spores were not stained, indicating that they were healthy spores (Fig. 4.4b,c), whereas coating-treated spores were readily stained, and a significant difference demonstrated ($P < 0.05$) compared with the control (untreated). This method is applicable for all type of spores (*P*. *digitatum* and *B*. *cinerea*). A significant increase ($P < 0.05$) in the percentage of stained cells with green fluorescence occurred when they were treated with Chi/SEO or Chi/SEOpick coatings (Fig. 4.4e) in comparison with Chi treatments, indicating a better antifungal action. Because propidium iodide is membrane impermeable, the results (Figure 4.4b,c) implied that membrane integrity was interfered with by coating treatment, which led to metabolic disruption and the death of fungi.

4.3.8. Antifungal performance of coating on tangerine and apple fruit in vivo

To confirm the antifungal efficacy of the coating treatment, in vivo tests on tangerine and apple fruit that had been artificially contaminated with *P. digitatum* and *B. cinerea*, respectively, were carried out. *B. cinerea* is a ubiquitous microorganism that is the main cause of postharvest disease, thereby causing considerable losses in harvested fruit. Green mold *P. digitatum* is well known as a pathogen inflicting major postharvest disease on citrus fruits and for being resistant to different fungicides (Grande-Tovar et al., 2018). During storage for 5 days, all fruits exhibited similar trends of decay, in which is mold symptoms and growth increased (Fig. 4.5a,b). Until day 2 of storage, no mycelial expansion appeared on uncoated (control) and coated fruits, indicating a lag phase of mold. On day 4, lesion diameter increased drastically on the surface of fruit, ranging from 22.26 to 39.49 mm and from 7.63 to 10.55 mm on tangerine and apple, respectively (Fig. 4.5c,d). The hyphal expansion of *P. digitatum* was delayed significantly ($P < 0.05$) by Chi coating treatment with a *PI* value 27.71% higher than the control. The inhibition effect of Chi also occurred for *B. cinerea* by 13.68% compared with untreated fruit. Furthermore, SEO-containing Chi showed synergistically improved antifungal activity in vivo with *PI* values of 37.21% and 43.61% for Chi-SEO- and Chi-SEOpick-coated tangerines.
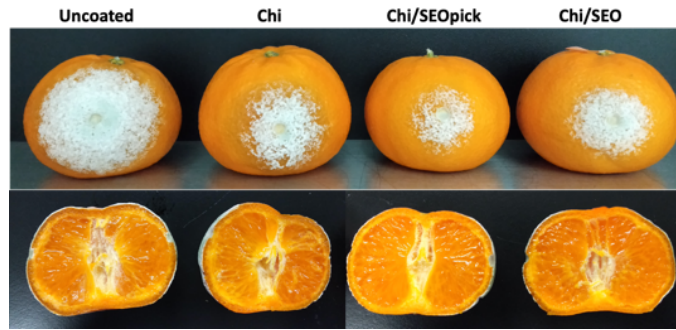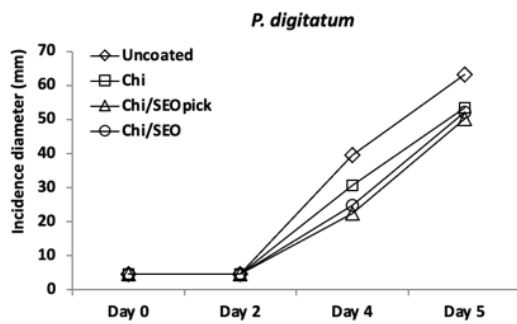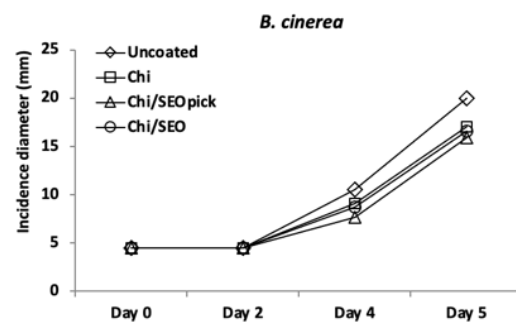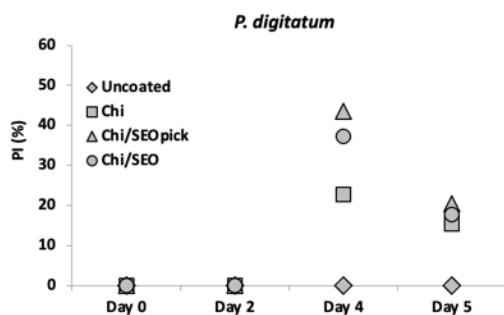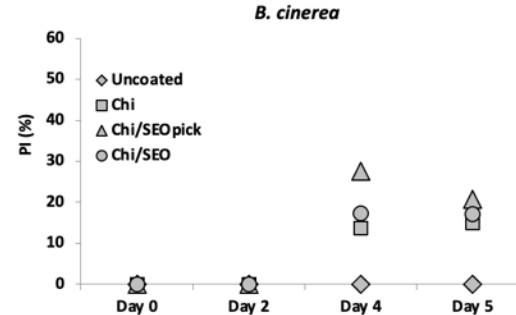
Fig. 4.5. Efficacy of various coating treatment against *P. digitatum* and *B.cinerea* disease severity. (a, b) visual appearance of representative sample and (c, d) statistical analysis.

The result was slightly different for *B. cinerea*-infected fruit, with no improvement in the inhibition of lesion extension by coating treatment between Chi and Chi-SEO except after the inclusion of Pickering emulsion with CNFs. The trend in mycelial expansion diameter steadily increased until the final day of storage (day 5). Surprisingly, the *PI* values for *P. digitatum* and *B. cinerea* growth on day 5 were lower than on day 4 (Fig. 4.5e,f). Through observation of cross-sections of infected tangerines, the penetration growth of internal fungal decay showed similar appearances for all samples. Decay with *B. cinerea* showed higher penetration in control fruit than Chi, Chi-SEO-coated apples, and the growth of internal decay of Chi-SEOpick-coated fruit was the lowest. The result reflected a coherent efficacy profile from the results of spore germination (Fig. 4.4). Again, there was clear evidence of the appropriate level of CNFs as a Pickering agent and the improvement of functional properties in this study, suggesting that the components have an effective antifungal action. There was a surprising finding that the PI values at day 5 were lower than at day 4. This might be ascribed to the availability of intrinsic carbon in plant hosts (Ji et al., 2018). On the final storage day, a higher number of carbon source may be available in coated fruits, whereas molds have exceeded the adaptation phase in the host environment. This lesion incidence also has implications for fruit internal decay.

4.3.9. *Color properties*

In practice, film coatings are applied either directly onto the surface of food forming a thin layer film or as a stand-alone wrapping material; therefore, the color properties of the thin film (*L**, *a**, *b**) and *ΔE** were characterized. As presented in Table 5.1, the *a** value was negative for all films and decreased significantly (*P* < 0.05) with the addition of CNFs. The *b** value (blue-yellow color), which varied from 6.94 to 15.22, indicating a slight yellowish color to the films, increased with the addition of SEO and CNFs (*P* < 0.05). The *L** value decreased

slightly due to the incorporation of SEO and CNFs into the Chi film ($P < 0.05$). It was documented that EO or cellulose-enriched edible film may enhance the brightness visually, indicated by lower $L*$ value and greater $\Delta E*$ value (Shankar and Rim, 2016; Yao et al., 2017), in which our results were consistent with this phenomenon. Overall, the value of ($L*$, $a*$, $b*$) and $\Delta E*$ were altered by the addition of SEO and CNF into CS films. Based on the results for $\Delta E*$, people were able to easily perceive a visual color difference with the prepared coating films. A literature noted that at the limit of $\Delta E* = 2$, the human eye is not able to distinguish the color of each coating film with the naked eye (Luzi et al., 2017).

Table 4.1. Characteristics of developed films

Characteristic	Chi	Chi/SEOpick	Chi/SEO
$L*$	98.2 ± 0.32[c]	96.52 ± 0.36[a]	97.18 ± 0.22[b]
$a*$	-0.12 ± 0.18[b]	-0.7 ± 0.16[a]	-0.14 ± 0.05[b]
$b*$	6.94 ± 0.72[a]	15.22 ± 0.84[c]	9.8 ± 1.29[b]
$\Delta E*$	3.02 ± 0.65[a]	11.48 ± 0.75[c]	6.03 ± 1.12[b]
Tensile strength (MPa)	9.02 ± 0.73[a]	12.41 ± 1.74[b]	10.18 ± 1.29[a]
Elongation (%)	33.02 ± 4.47[a]	31.42 ± 2.19[a]	39.01 ± 4.18[b]
Ra	4.07 ± 2.20	5.44 ± 1.08	4.26 ± 1.99
Rq	4.47 ± 2.77	6.86 ± 1.21	5.47 ± 2.61

Different letters indicate statistically significant differences at $P < 0.05$. CS: chitosan, CS-SEOpick: chitosan-sandalwood oil Pickering emulsion, CS-SEO: chitosan-sandalwood oil regular emulsion films.

4.3.10. *Light transmittance and opacity*

The light transmission parameter reflects the barrier ability of the developed film against UV and visible light. It is one of the essential features associated with the potency of a coating film is its ability to inhibit the oxidation of lipids, pigments, proteins, or vitamins in packed foods (Haghighi et al., 2021). The Chi film showed the highest clarity with transmittance

between 82.84% and 87.59% in the visible wavelengths. Compared to Chi alone, Chi-SEO had a 18.22 ± 0.61% lower transmittance at all visible light wavelengths; therefore, significantly higher opacity was exhibited (Figure 4.6b,c). Moreover, sweating-out of SEO, indicated with a yellow arrow, from the inside to the surface of the Chi-SEO film was seen clearly with the naked eye (Fig. 4.6a). The highest reduction in light transmission was demonstrated with Chi-SEOpick with lower transmittance values of 78.91 ± 0.34% and 74.21 ± 0.31% compared with Chi and Chi-SEO, respectively. Consequently, the opacity value was dramatically decreased. The average thickness of Chi was 0.038 ± 0.004 mm, and the addition of SEO increased this value to a significant extent ($P < 0.05$). Chi-SEOpick showed the highest thickness at an average value of 0.09 ± 0.01 mm.

(a)

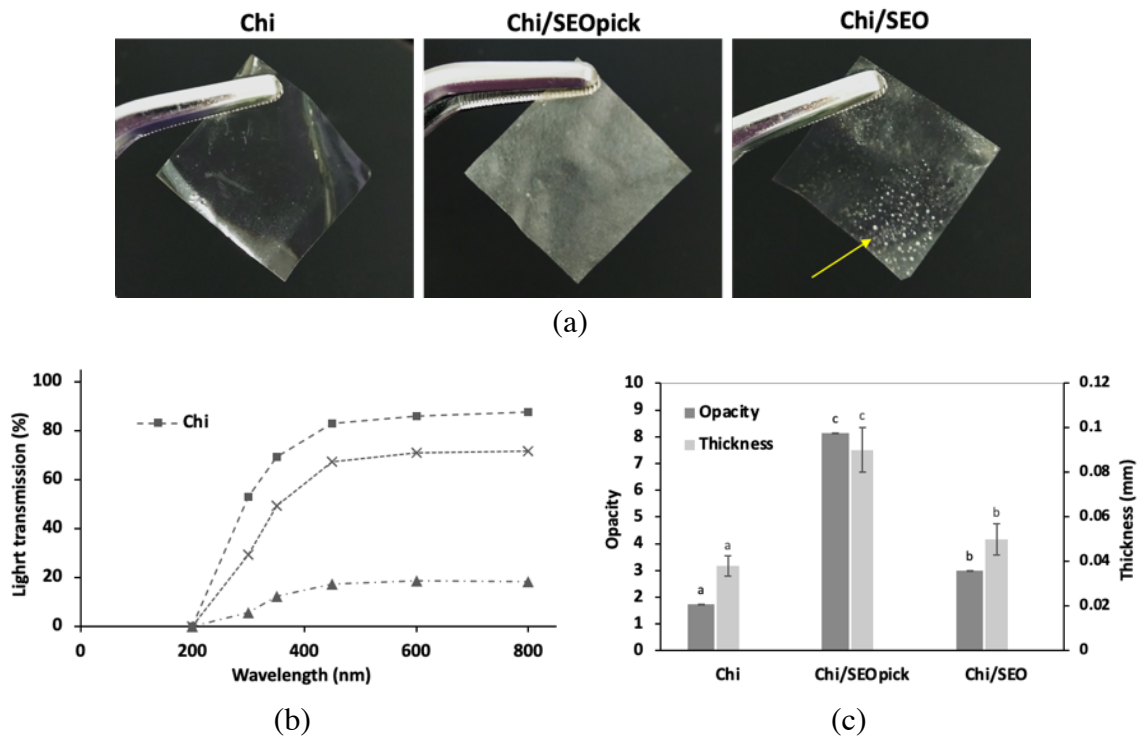(b)   (c)

Fig. 4.6. Visual photographs of coating film appearance (a) and its optical properties; light transmittance (b) and opacity and thickness for thin coating film (c). Different letters indicate statistically significant differences at $P < 0.05$.

The incorporation of SEO and/or CNFs decreased Chi transmittance throughout the visible light range, consequently higher opacity was exhibited. Earlier study explained that higher opacity was due to the presence of oil droplets in the film matrix that scattered the transmitted light (Yao et al., 2017). Moreover, sweating-out (exudation) of SEO from the biopolymer matrix film onto the surface may also contribute to the decreasing transparency value of the Chi-SEO composite film. The intermolecular interactions between SEO and water or biopolymer matrix mediated by Tween 80 were diminished as the water content decreased during film formation (drying process). Thereby, the dispersed phase (oil) was not immobilized, leading to migration to the surface of the film. In the case of CNF-stabilized film, it is likely that CNF addition affected the internal and surface structure, and efficiently blocked the visible spectrum. The enhancement of the opacity of edible films was positively correlated with the addition of CNF which lead to light scattering (Zhang et al., 2021). All coating films showed lower light transmission values with UV light than in the visible light spectrum, with a similar trend except at 200 nm. From this result, it can be assumed that the Chi-SEOpick film had higher barrier properties for UV and visible light. Moreover, the thickness of a film is a predominant factor affecting the optical characteristics (Fig. 4.6c). The changes in thickness were probably due to an increase in the total solid content of the films.

4.3.11. Mechanical properties

The use of CNF as a Pickering emulsion agent increased the tensile strength of the films. The tensile strength of film was enhanced significantly ($P < 0.05$) from 9.02 ± 0.73 MPa and 10.17 ± 1.29 MPa for Chi and Chi-SEO films up to 12.41 ± 1.74 MPa (Table 5.1). The elongation of Chi films ($33 \pm 0.73\%$), indicating the flexibility of the films, was not altered by the addition of CNFs ($31.4 \pm 1.74\%$). However, significant ($P < 0.05$) enhancement of the

elongation value was found when 0.5% SEO was added. Not only due to the geometry and rigidity of the nano-filler but also the enhancement in tensile strength was also associated with the formation of a stiff continuous network of CNFs linked through hydrogen bonding (Samir et al., 2004). In addition, nano-sized cellulose can readily form hydrogen bonds with the surrounding molecules, leading to strong interactions even at low concentration as a result of the large aspect ratio and ability to form interconnected network structures (Abdul Khalil et al., 2016; Cheng et al., 2019). However, another study investigated whether the reinforcing efficacy of CNFs declined when crystalline nanocellulose was incorporated into alginate and pectin at higher concentration (>5% w/w on solid polymer) due to the agglomeration and non-uniform dispersion of the filler (Abdollahi et al., 2013). The level of CNF used in this study was assumed to be in the optimum concentration range for the filler in improving the tensile strength of the coating film. There were no significant changes of Chi elongation due to the addition of CNFs. In this investigation, the emulsified films had higher elongation, and this was in agreement with other investigations (dos Santos et al., 2019; da Silva et al., 2020). This behavior may be attributed with a sufficient level essential oil resulting in a synergistic impact of the plasticizer and SEO. Essential oil can perform as a plasticizer agent allowing greater mobility and flexibility in the polymer chain (dos Santos et al., 2019).

4.3.12. Surface morphology

AFM analysis is a powerful method to analyze the occurrence of slight changes in the surface of films as a consequence of filler material incorporation both qualitatively and quantitatively (Yekta et al., 2020). As seen in Fig. 4.7a, although no significant differences were demonstrated ($P > 0.05$), there was a tendency from an increasingly smooth surface in Chi film with average *Ra* and *Rq* values of 4.07 ± 2.20 and 4.47 ± 2.77 nm, respectively. The surface was

rougher, $Ra = 4.26 \pm 1.99$ nm and $Rq = 5.47 \pm 2.61$ nm, when SEO droplets were inserted into the Chi matrix. A less smooth surface, $Ra = 5.54 \pm 1.08$ nm and $Rq = 6.86 \pm 1.21$ nm, appeared with the addition CNFs as a Pickering emulsion agent. Reduced smoothness of the Chi coating surface after the addition of SEO might be ascribed to lipid aggregation and/or creaming phenomena. Furthermore, these phenomena were exacerbated by an evaporation step during film formation, thereby the level of irregularities on the films' surfaces increased (Ma et al., 2012). This was confirmed visually by 2D and 3D topography image and line profiles which oil aggregates are exist forming several spherical uplands structure. A previous study also found an increase in terms of film roughness because of the incorporation of oregano oil into gelatin-chitosan blend film (Hosseini et al., 2013). Furthermore, the roughness value also increased with the incorporation of CNFs. An earlier study proposed that nanocellulose might be aggregated, implying the higher roughness of the film through the formation of uplands in the surface (Saxena et al., 2009). This trend was in good agreement with another report which observed the agglomeration of cellulose nanocrystals in the pectin matrix (Chaichi et al., 2017). However, as seen in Fig. 4.7a, CNFs were dispersed uniformly on the surface of the Chi-SEO composite films assuming a good matrix-CNF interaction and confirming the improvement in mechanical properties (tensile strength). A slight increase and insignificant difference in roughness implies the ideal concentration of CNFs used in this study without prejudice from its main function as an emulsifier.

4.3.13. SEM

Cross-section analysis was performed to observe the microstructural arrangement of the films and to confirm the distribution of SEO droplets and CNF entrapped in the biopolymer. Chi film obtained without CNF or SEO displayed a compact, continuous, and homogenous

microstructure, without cracks, and almost no obvious separation was detected, showed in Fig. 4.7b. There were two slight cavity-like structures found (indicated by yellow arrows), which were probably caused by the sample preparation procedure. The incorporation of SEO resulted in an amorphous structure, with vacuoles and pores distributed along the cross-section surface of Chi/SEOpick and Chi/SEO. Notably, the dispersion of SEO developed with Pickering emulsion caused a decrease in the discontinuities and droplet size and an increase the droplet distribution in the cross-sections of films, as indicated with a yellow circle. The discontinuities demonstrated in SEO-loaded films may be associated with SEO microdrop. Similar findings in the presence of the oil micro-droplets of the hazelnut meal protein matrix, observed with the cross-section of a film (Gul et al., 2018). Furthermore, the SEO droplets obtained in this study showed a shrinkage-like shape of an oval structure (Fig. 4.7b). The existence of these types of pore droplets might correspond to a consequence of the drying process and the density of the coating film matrix (Salgado et al., 2013; Gul et al., 2018). A decrease in discontinuities and droplet size and an increase in droplet distribution was found in Chi-SEOpick film. This phenomenon possibly corresponded to the occurrence of flocculation and coagulation from the dispersed phase in Chi-SEO. The emulsion system in Chi-SEOpick was believed to have a higher physical stability compared with the regular emulsion mediated by surfactant (Chi-SEO). This suggested that the presence of CNFs may have fully covered the oil droplets allowing the prevention of oil droplet coalescence. The lower size of cellulose was noted to be more easily adsorbed onto the oil–water interface, hence facilitating the higher stability of oil in water emulsion formation (Liu et al., 2019). These stabilization mechanisms not only minimized the evaporation of SEO during the drying process but also protected against the oxidation of SEO.
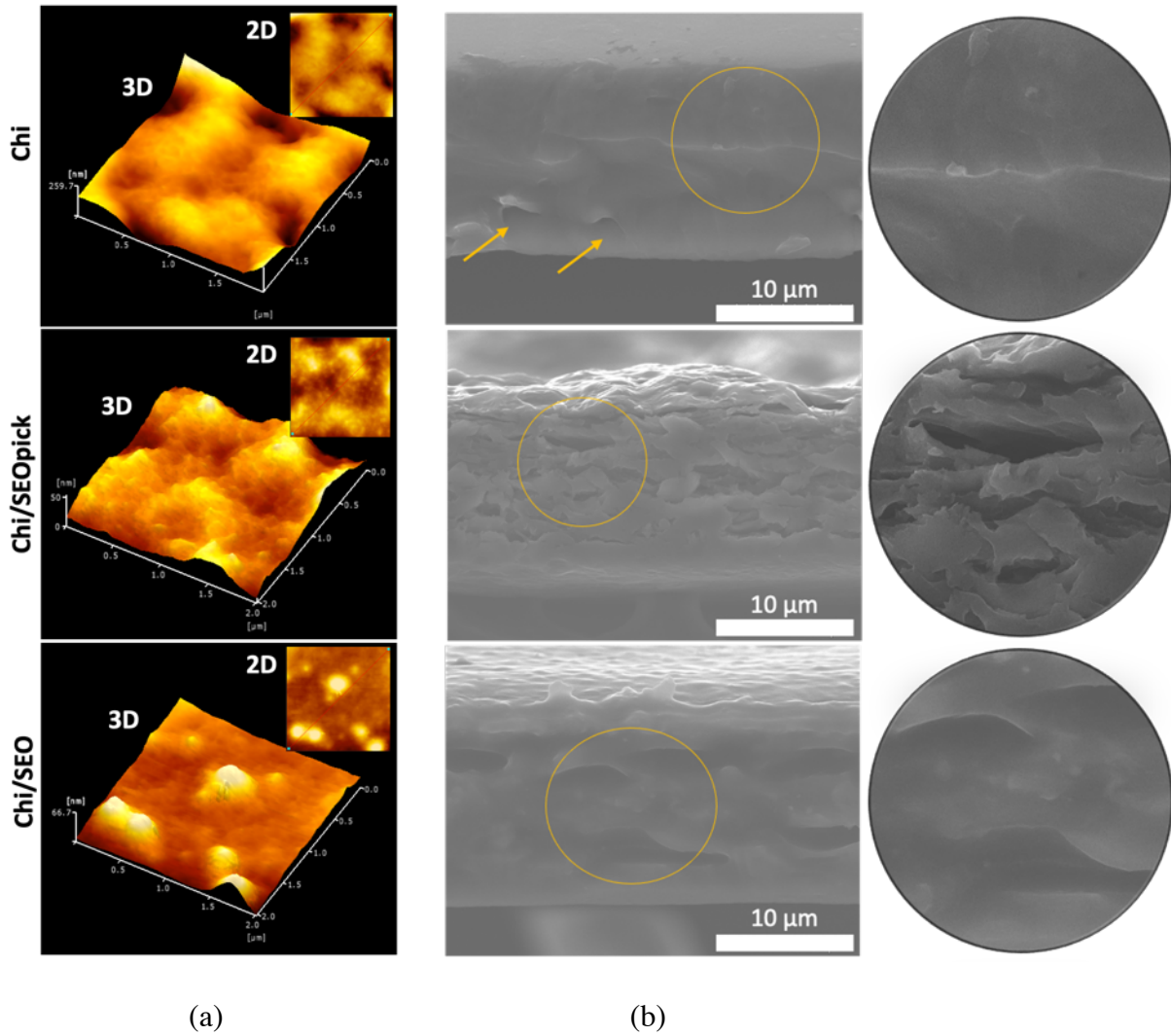
(a)　　　　　　　　　　　　(b)

Fig. 4.7. (a) AFM topographic image and (b) SEM longitudinal cross section image.

4.4. References

Abdollahi, M., Alboofetileh, M., Behrooz, R., Rezaei, M., & Miraki, R. (2013). Reducing water sensitivity of alginate bio-nanocomposite film using cellulose nanoparticles. *International Journal of Biological Macromolecules*, *54*(1), 166–173.

Abdul Khalil, H. P. S., Saurabh, C. K., Adnan, A. S., Nurul Fazita, M. R., Syakir, M. I., Davoudpour, Y., Rafatullah, M., Abdullah, C. K., Haafiz, M. K. M., & Dungani, R. (2016). A review on chitosan-cellulose blends and nanocellulose reinforced chitosan biocomposites: Properties and their applications. *Carbohydrate Polymers*, *150*, 216–226.

Aguayo, M. G., Pérez, A. F., Reyes, G., Oviedo, C., Gacitúa, W., Gonzalez, R., & Uyarte, O. (2018). Isolation and characterization of cellulose nanocrystals from rejected fibers originated in the Kraft Pulping process. *Polymers*, *10*(10).

Alhwaige, A. A., Agag, T., Ishida, H., & Qutubuddin, S. (2013). Biobased chitosan/polybenzoxazine cross-linked films: Preparation in aqueous media and synergistic improvements in thermal and mechanical properties. *Biomacromolecules*, *14*(6), 1806–1815.

Antoniou, J., Liu, F., Majeed, H., & Zhong, F. (2015). Characterization of tara gum edible films incorporated with bulk chitosan and chitosan nanoparticles: A comparative study. *Food Hydrocolloids*, *44*, 309–319.

Avadi, M. R., Jalali, A., Mir Mohammad Sadeghi, A., Shamimi, K., Bayati, K. H., Nahid, E., Dehpour, A. R., & Rafiee-Tehrani, M. (2005). Diethyl methyl chitosan as an intestinal paracellular enhancer: *Ex vivo* and *in vivo* studies. *International Journal of Pharmaceutics*, *293*(1–2), 83–89.

Azizi Samir, M. A. S., Alloin, F., Sanchez, J. Y., & Dufresne, A. (2004). Cellulose nanocrystals reinforced poly(oxyethylene). *Polymer*, *45*(12), 4149–4157.

Bai, L., Huan, S., Xiang, W., & Rojas, O. J. (2018). Pickering emulsions by combining cellulose nanofibrils and nanocrystals: Phase behavior and depletion stabilization. *Green Chemistry*, *20*(7), 1571–1582.

Burdock, G. A., & Carabin, I. G. (2008). Safety assessment of sandalwood oil (*Santalum album* L.). *Food and Chemical Toxicology*, *46*(2), 421–432.

Chaichi, M., Hashemi, M., Badii, F., & Mohammadi, A. (2017). Preparation and characterization of a novel bionanocomposite edible film based on pectin and crystalline nanocellulose. *Carbohydrate Polymers*, *157*, 167–175.

Cheng, K. C., Huang, C. F., Wei, Y., & Hsu, S. hui. (2019). Novel chitosan–cellulose nanofiber self-healing hydrogels to correlate self-healing properties of hydrogels with neural regeneration effects. *NPG Asia Materials*, *11*(1).

Coma, V., Deschamps, A., & Martial-Gros, A. (2003). Bioactive packaging materials from edible chitosan polymer - antimicrobial activity assessment on dairy-related contaminants. *Journal of Food Science*, *68*(9), 2788–2792.

Dantigny, P., Bensoussan, M., Vasseur, V., Lebrihi, A., Buchet, C., Ismaili-Alaoui, M., Devlieghere, F., & Roussos, S. (2006). Standardisation of methods for assessing mould germination: A workshop report. *International Journal of Food Microbiology*, *108*(2), 286–291.

da Silva, A. O, Cortez-Vega, W. R., Prentice, C., & Fonseca, G. G. (2020). Development and characterization of biopolymer films based on bocaiuva (Acromonia aculeata) flour. *International Journal of Biological Macromolecules*, *155*, 1157–1168.

Deng, Z., Jung, J., Simonsen, J., & Zhao, Y. (2018). Cellulose nanocrystals Pickering emulsion incorporated chitosan coatings for improving storability of postharvest Bartlett pears (*Pyrus communis*) during long-term cold storage. *Food Hydrocolloids*, *84*, 229–237.

Edwards, I. P., Upchurch, R. A., & Zak, D. R. (2008). Isolation of fungal cellobiohydrolase I genes from sporocarps and forest soils by PCR. *Applied and Environmental Microbiology*, *74*(11), 3481–3489.

Elsabee, M. Z., & Abdou, E. S. (2013). Chitosan based edible films and coatings: A review. *Materials Science and Engineering C*, *33*(4), 1819–1841.

Fujisawa, S. (2021). Material design of nanocellulose/polymer composites via Pickering emulsion templating. *Polymer Journal*, *53*(1), 103–109.

Grande-Tovar, C. D., Chaves-Lopez, C., Serio, A., Rossi, C., & Paparella, A. (2018). Chitosan coatings enriched with essential oils: Effects on fungi involve in fruit decay and mechanisms of action. *Trends in Food Science and Technology*, *78*, 61–71.

Gul, O., Saricaoglu, F. T., Besir, A., Atalar, I., & Yazici, F. (2018). Effect of ultrasound treatment on the properties of nano-emulsion films obtained from hazelnut meal protein and clove essential oil. *Ultrasonics Sonochemistry*, *41*, 466–474.

Haghighi, H., Gullo, M., La China, S., Pfeifer, F., Siesler, H. W., Licciardello, F., & Pulvirenti, A. (2021). Characterization of bio-nanocomposite films based on gelatin/polyvinyl alcohol blend reinforced with bacterial cellulose nanowhiskers for food packaging applications. *Food Hydrocolloids*, *113*, 106454.

Hosseini, S. F., Zandi, M., Rezaei, M., & Farahmandghavi, F. (2013). Two-step method for encapsulation of oregano essential oil in chitosan nanoparticles: Preparation, characterization and in vitro release study. *Carbohydrate Polymers*, *95*(1), 50–56.

Inouye, S., Uchida, K., & Abe, S. (2006). Vapor activity of 72 essential oils against a Trichophyton mentagrophytes. *Journal of Infection and Chemotherapy*, *12*(4), 210–216.

Jayaraj, J., Rahman, M., Wan, A., & Punja, Z. K. (2009). Enhanced resistance to foliar fungal pathogens in carrot by application of elicitors. *Annals of Applied Biology*, *155*(1), 71–80.

Ji, D., Chen, T., Ma, D., Liu, J., Xu, Y., & Tian, S. (2018). Inhibitory effects of methyl thujate on mycelial growth of Botrytis cinerea and possible mechanisms. *Postharvest Biology and Technology*, *142*(December 2017), 46–54.

Jiang, R., Zhu, H., Yao, J., Fu, Y., & Guan, Y. (2012). Chitosan hydrogel films as a template for mild biosynthesis of CdS quantum dots with highly efficient photocatalytic activity. *Applied Surface Science*, *258*(8), 3513–3518.

Jung, J., Deng, Z., & Zhao, Y. (2020). Mechanisms and performance of cellulose nanocrystals Pickering emulsion chitosan coatings for reducing ethylene production and physiological disorders in postharvest 'Bartlett' pears (*Pyrus communis* L.) during cold storage. *Food Chemistry*, *309*, 125693.

Kafy, A., Kim, H. C., Zhai, L., Kim, J. W., Hai, L. Van, Kang, T. J., & Kim, J. (2017). Cellulose long fibers fabricated from cellulose nanofibers and its strong and tough characteristics. *Scientific Reports*, *7*(1), 1–8.

Kim, T. H., Hatano, T., Okamoto, K., Yoshida, T., Kanzaki, H., Arita, M., & Ito, H. (2017). Antifungal and Ichthyotoxic Sesquiterpenoids from Santalum album Heartwood. *Molecules (Basel, Switzerland)*, *22*(7), 1–8.

Kong, M., Chen, X. G., Xing, K., & Park, H. J. (2010). Antimicrobial properties of chitosan and mode of action: A state of the art review. *International Journal of Food Microbiology*, *144*(1), 51–63.

Li, P., Sirviö, J. A., Haapala, A., Khakalo, A., & Liimatainen, H. (2019). Anti-oxidative and UV-absorbing biohybrid film of cellulose nanofibrils and tannin extract. *Food Hydrocolloids*, *92*(December 2018), 208–217.

Li, Z., Wu, H., Yang, M., Xu, D., Chen, J., Feng, H., Lu, Y., Zhang, L., Yu, Y., & Kang, W. (2018). Stability mechanism of O/W Pickering emulsions stabilized with regenerated cellulose. *Carbohydrate Polymers*, *181*, 224–233.

Liu, B., Zhu, Y., Tian, J., Guan, T., Li, D., Bao, C., Norde, W., Wen, P., & Li, Y. (2019). Inhibition of oil digestion in Pickering emulsions stabilized by oxidized cellulose nanofibrils for low-calorie food design. *RSC Advances*, *9*(26), 14966–14973.

Liu, J., Tian, S., Meng, X., & Xu, Y. (2007). Effects of chitosan on control of postharvest diseases and physiological responses of tomato fruit. *Postharvest Biology and Technology*, *44*(3), 300–306.

Lu, Y., Li, J., Ge, L., Xie, W., & Wu, D. (2021). Pickering emulsion stabilized with fibrous nanocelluloses: Insight into fiber flexibility-emulsifying capacity relations. *Carbohydrate Polymers*, *255*.

Luzi, F., Fortunati, E., Giovanale, G., Mazzaglia, A., Torre, L., & Balestra, G. M. (2017). Cellulose nanocrystals from Actinidia deliciosa pruning residues combined with carvacrol in PVA_CH films with antioxidant/antimicrobial properties for packaging applications. *International Journal of Biological Macromolecules*, *104*, 43–55.

Lynd, L. R., Weimer, P. J., Zyl, W. H. Van, & Isak, S. (2002). Microbial cellulose utilization : fundamentals and biotechnology. *Microbiology and Molecular Biology Reviews*, *66*(3), 506–577.

Ma, W., Tang, C. H., Yin, S. W., Yang, X. Q., Wang, Q., Liu, F., & Wei, Z. H. (2012). Characterization of gelatin-based edible films incorporated with olive oil. *Food Research International*, *49*(1), 572–579.

Maryam Adilah, Z. A., Jamilah, B., & Nur Hanani, Z. A. (2018). Functional and antioxidant properties of protein-based films incorporated with mango kernel extract for active packaging. *Food Hydrocolloids*, *74*, 207–218.

Medina, E., Caro, N., Abugoch, L., Gamboa, A., Díaz-Dosque, M., & Tapia, C. (2019). Chitosan thymol nanoparticles improve the antimicrobial effect and the water vapour barrier of chitosan-quinoa protein films. *Journal of Food Engineering*, *240*, 191–198.

Mohammadi, A., Hashemi, M., & Hosseini, S. M. (2016). Integration between chitosan and Zataria multiflora or Cinnamomum zeylanicum essential oil for controlling Phytophthora drechsleri, the causal agent of cucumber fruit rot. *LWT - Food Science and Technology*, *65*, 349–356.

Nardoni, S., Giovanelli, S., Pistelli, L., Mugnaini, L., Profili, G., Pisseri, F., & Mancianti, F. (2015). In vitro activity of twenty commercially available, plant-derived essential oils against selected dermatophyte species. *Natural Product Communications*, *10*(8), 1473–1478.

Rivero, S., García, M. A., & Pinotti, A. (2009). Composite and bi-layer films based on gelatin and chitosan. *Journal of Food Engineering*, *90*(4), 531–539.

Salgado, P. R., López-Caballero, M. E., Gómez-Guillén, M. C., Mauri, A. N., & Montero, M. P. (2013). Sunflower protein films incorporated with clove essential oil have potential application for the preservation of fish patties. *Food Hydrocolloids*, *33*(1), 74–84.

Saxena, A., Elder, T. J., Pan, S., & Ragauskas, A. J. (2009). Novel nanocellulosic xylan composite film. *Composites Part B: Engineering*, *40*(8), 727–730.

Seo, S.-M., Lee, J.-W., Shin, J., Tak, J.-H., Hyun, J., & Park, I.-K. (2021). Development of cellulose nanocrystal-stabilized Pickering emulsions of massoia and nutmeg essential oils for the control of *Aedes albopictus*. *Scientific Reports*, *11*(1), 1–12.

Shahidi, F., Arachchi, J. K. V., & Jeon, Y. J. (1999). Food applications of chitin and chitosans. *Trends in Food Science and Technology*, *10*(2), 37–51.

Shankar, S., & Rhim, J. W. (2016). Preparation of nanocellulose from micro-crystalline cellulose: The effect on the performance and properties of agar-based composite films. *Carbohydrate Polymers*, *135*, 18–26.

Shao, X., Cao, B., Xu, F., Xie, S., Yu, D., & Wang, H. (2015). Effect of postharvest application of chitosan combined with clove oil against citrus green mold. *Postharvest Biology and Technology*, *99*, 37–43.

Shi, W. J., Tang, C. H., Yin, S. W., Yin, Y., Yang, X. Q., Wu, L. Y., & Zhao, Z. G. (2016). Development and characterization of novel chitosan emulsion films via pickering emulsions incorporation approach. *Food Hydrocolloids*, *52*, 253–264.

Souza, A. G., Ferreira, R. R., Paula, L. C., Mitra, S. K., & Rosa, D. S. (2021). Starch-based films enriched with nanocellulose-stabilized Pickering emulsions containing different essential oils for possible applications in food packaging. *Food Packaging and Shelf Life*, *27*, 100615.

Torres, J. D., Faria, E. A., SouzaDe, J. R., & Prado, A. G. S. (2006). Preparation of photoactive chitosan-niobium (V) oxide composites for dye degradation. *Journal of Photochemistry and Photobiology A: Chemistry*, *182*(2), 202–206.

Treseder, K. K., & Lennon, J. T. (2015). Fungal traits that drive ecosystem dynamics on land. *Microbiology and Molecular Biology Reviews*, *79*(2), 243–262.

Valenzuela, C., Abugoch, L., & Tapia, C. (2013). Quinoa protein-chitosan-sunflower oil edible film: Mechanical, barrier and structural properties. *LWT - Food Science and Technology*, *50*(2), 531–537.

Wang, L. J., Yin, Y. C., Yin, S. W., Yang, X. Q., Shi, W. J., Tang, C. H., & Wang, J. M. (2013). Development of novel zein-sodium caseinate nanoparticle (ZP)-stabilized emulsion films for improved water barrier properties via emulsion/solvent evaporation. *Journal of Agricultural and Food Chemistry*, *61*(46), 11089–11097.

Wang, X. Y., & Heuzey, M. C. (2016). Chitosan-Based Conventional and Pickering Emulsions with Long-Term Stability. *Langmuir*, *32*(4), 929–936.

Wu, X., Zhang, L., Zhang, X., Zhu, Y., Wu, Y., Li, Y., Li, B., Liu, S., Zhao, J., & Ma, Z. (2017). Ethyl cellulose nanodispersions as stabilizers for oil in water Pickering emulsions. *Scientific Reports*, *7*(1), 1–10.

Xing, Y., Xu, Q., Yang, S. X., Chen, C., Tang, Y., Sun, S., Zhang, L., Che, Z., & Li, X. (2016). Preservation mechanism of chitosan-based coating with cinnamon oil for fruits storage based on sensor data. *Sensors*, *16*(7).

Xu, Y., Chu, Y., Feng, X., Gao, C., Wu, D., Cheng, W., Meng, L., Zhang, Y., & Tang, X. (2020). Effects of zein stabilized clove essential oil Pickering emulsion on the structure and properties of chitosan-based edible films. *International Journal of Biological Macromolecules*, *156*, 111–119.

Yao, Y., Ding, D., Shao, H., Peng, Q., & Huang, Y. (2017). Antibacterial activity and physical properties of fish gelatin-chitosan edible films supplemented with *D-Limonene*. *International Journal of Polymer Science*, *2017*.

Yekta, R., Mirmoghtadaie, L., Hosseini, H., Norouzbeigi, S., Hosseini, S. M., & Shojaee-Aliabadi, S. (2020). Development and characterization of a novel edible film based on Althaea rosea flower gum: Investigating the reinforcing effects of bacterial nanocrystalline cellulose. *International Journal of Biological Macromolecules*, *158*, 327–337.

Yeng, C. M., Husseinsyah, S., & Ting, S. S. (2013). Chitosan/corn cob biocomposite films by cross-linking with glutaraldehyde. *BioResources*, *8*(2), 2910–2923.

Yuan, G., Chen, X., & Li, D. (2016). Chitosan films and coatings containing essential oils: The antioxidant and antimicrobial activity, and application in food systems. *Food Research International*, *89*, 117–128.

Zhang, H., Li, R., & Liu, W. (2011). Effects of chitin and its derivative chitosan on postharvest decay of fruits: A review. *International Journal of Molecular Sciences*, *12*(2), 917–934.

Zhang, W., Zhang, Y., Cao, J., & Jiang, W. (2021). Improving the performance of edible food packaging films by using nanocellulose as an additive. *International Journal of Biological Macromolecules*, *166*, 288–296.

Zou, T., Sipponen, M. H., & Österberg, M. (2019). Natural shape-retaining microcapsules with shells made of chitosan-coated colloidal lignin particles. *Frontiers in Chemistry*, *7*, 1–12.

CHAPTER 5

CONCLUSIONS AND FUTURE WORKS

5.1. Conclusions

This thesis described the development and application of novel emulsified nanocomposite coating film on fresh fruits. This work was focused on the following objectives:

1) Application of edible coatings comprised of Chi/ZNP/SEO composites against *P. italicum* and its physico-chemical characterization.

2) Investigation of the antifungal action from double and triple antimicrobial agent based on Chi, CuO, and CEO formulations against citrus fruit fungal pathogen *in vitro* and *in vivo*, and characterized the physical, chemical, and surface properties of coating films.

3) Development of emulsified coating film formulation based on Chi and SEO using a Pickering emulsion approach with an appropriate level of CNF as a stabilizer, and investigation on the antifungal features against *Botrytis cinerea* and *Penicillium digitatum* and film properties of Chi, Chi/SEO, and Chi/SEOpick.

The general conclusions of this present study were summarized as follows:

1) Novel composites from formulations of 0.8% Chi blended with 0.025% ZNP and/or 0.5% SEO have been successfully developed, as confirmed with FTIR, CLSM, and SEM

analysis. These materials can additively improve antifungal features that inhibited *P. italicum* compared with Chi-based coating from the evidence of inhibition of mycelial growth and spore germination, as well as the effect on membrane damage. Furthermore, it was confirmed by coating application on tangerines and successfully protected fruit from fungal decay. This study also found that the incorporation of ZNPs significantly ($P < 0.05$) increased the pH and light transmission at UV and visible wavelength, which means that it could reduce the opacity compared with the Chi based coating. Furthermore, our results showed that the addition of SEO significantly ($P < 0.05$) influenced the Chi coating characteristics by increasing the apparent viscosity, ΔE, and transparency of the coating, and decreasing the zeta potential, light transmission, and roughness. Based on the overall results, it was concluded that the best performance was achieved with 0.8% Chi/0.025% ZNP/0.5% SEO, which may improve antifungal action against *P. italicum* with highest inhibitions of 85.91% (*in vitro*) and 79.86% (*in vivo*). It was characterized using apparent viscosity 34.74 cP, *pH* 5.78, zeta potential +29.70 mV, color difference 14.55, transparency 1.39, *Ra* 4.36 nm, and *Rq* 3.37 nm.

2) Novel composite coating formulations using 0.8% Chi/0.025% CuO/0.5% CEO were developed. This work suggested that the presence of CuO and CEO modified the characteristics of pure Chi coating solutions, which was confirmed by the alteration in light transmission, transparency, apparent viscosity, and roughness. The physical stability of the coating solution and colour changed dramatically as a consequence of the presence of CEO and CuO, respectively, as indicated by the zeta potential and ΔE value. This work also revealed that the addition of CuO and CEO had great potential as antifungal improvement agents for pure Chi-film-forming solution. The addition of CEO and CuO

to the Chi coating solution showed the best inhibition effect in suppressing *Penicillium* spp. growth, as confirmed using an in vivo test. The loss of membrane integrity of spores as a consequence of antifungal action was shown using fluorescent microscopy. Additional studies should be performed, particularly for sensory acceptability, to confirm the potential of this novel active coating in maintaining the quality of postharvest commodities.

3) Novel composite coating formulations using 0.8% Chi/0.5% SEO/0.24% CNF were developed. The incorporation of 0.24% CNF as a stabilizer agent into chitosan/sandalwood oil Pickering emulsion coating was found to improve the performance of antifungal activity synergistically confirmed with in vitro and in vivo assays. This work also revealed that the addition of CNF had potential to improve the functional properties such as light transmission at UV and visible light wavelengths and tensile strength.

5.2. Future works

Application of edible film and coating have been gained attention in the field of food science and technology in the last decades. This upward trend is influenced by increasing customer awareness on natural, healthy, and safe food produce from the excessive use of chemical preservatives. The concern about environmentally problem instead of antimicrobial drugs also affects the increasing of the use eco-friendly materials. Furthermore, the limited use of conventional plastic has been regulated by government policies. The novel formulations, mentioned above, are considered as alternatives to fulfill those reasons, particularly in the terms of maintaining the quality and extending the shelf life of fresh fruit from fungal decay. Additional investigation are needed, particularly for physico-chemical characteristics and

sensory acceptability, to confirm the potential of these novel active coatings in maintaining the quality of fresh fruit commodities. Also, additional research developments should focus on improvements to the technology transformation from a laboratory scale to a commercial scale process using continuous coating and casting equipments.